ANALYSIS OF FLUID FLOW AND LOSSES IN REGENERATIVE FLOW COMPRESSORS USING CFD

A THESIS

BY

Kassa Teferi

Submitted to the School of Graduate Studies

Addis Ababa University

In Partial Fulfillment of the Requirement for the Degree of

Masters of Science in Mechanical Engineering

(With Specialization in Thermal Engineering)

ADVISOR: Dr. - Ing. Edessa Dribsa

April, 2008

ADDIS ABABA UNIVERSITY

FACULTY OF TECHNOLOGY

SCHOOL OF GRADUATE STUDIES

"ANALYSIS OF FLUID FLOW AND LOSSES IN REGENERATIVE FLOW COMPRESSORS USING CFD"

By

Kassa Teferi

Approved by Board of Examiners

Ato Hamsasew Moges	
Chairman, Department Graduate committee	Signature
Dr. - Ing Edessa Dribsa	
Advisor	Signature
Dr. - Ing Demiss Alemu	
Internal Examiner	Signature
Dr. Tesfaye Dama	
External Examiner	Signature

ACKNOWLEDGEMENT

First I thank God for giving me strength to finish my work and also the work described would not have been possible with out the valuable assistance of many people. I would like to express my deepest gratitude to my thesis advisor, Dr. - Ing. Edessa Dribsa, for his skillful guidance, encouragement, enormous patience and willing attitude throughout the course of this research.

I would also like to thank my friends, and specially Ato Yonas Theshome, for his support in giving me important research papers, journals and in sharing of his ideas. I also want to appreciate all of my instructors / colleague in the Department of Mechanical Engineering, Addis Ababa University for their continuous encouragement.

Finally, I would like to thank my family for the unending confidence, constant support and endless love.

ABSTRACT

Regenerative flow compressors are rotodynamic machines capable of producing high heads at very low flow rates. With comparable tip speed, they can produce heads equivalent to that of several centrifugal stages from a single rotor. They have found many applications for duties requiring high heads at low flow rates but the compression process is usually with very low efficiency which is their major drawback.

Even though there are several factors that can be considered to improve the efficiency of these machines in this thesis various models will be developed with different blade and flow channel geometries to investigate their effect on performance.

Details of CFD analysis on the models of the compressor, using a commercial software "FLUENT", will be presented. And based on simulation results of the different models a blade and channel geometry that gives significant improvement on performance will be suggested.

Title **Page No.**

Acknowledgement.....I

Abstract…. .....……II

Table of Contents.....…III

List of Figures.....VII

List of Tables.....…...XIV

CHAPTER ONE

INTRODUCTION

1.1 Classifications of compressors.……..……..1

1.2 Turbocompressors……...3

1.3 Regenerative Flow Compressors……...……..4

1.4 Objective of the thesis.……....5

1.5 Methodology……6

1.6 Outline of the thesis…...……..7

CHAPTER TWO

DESIGN AND OPERATIONAL FEATURES OF REGENERATIVE TURBOMACHINES

2.1 Essential components of Regenerative Turbomachine……...……9

2.1.1 Impeller……..…….……...…...10

2.1.1.1 Impeller blades.....…….....11

2.1.2 Inlet and Exit Ports……..……..…….……..…...…..14

2.1.3 Stripper.……..…….…….....14

2.1.4 Flow Channel.....……..……..…….…14

2.2 Working Principle …….....…….....……...…....15

2.3 Performance characteristic s of RFC…….……....……...……...17

2.4 Comparison of Centrifugal and Regenerative Flow Compressors.....…….…….....18

2.5 Applications of Regenerative Flow Compressors ……...…….20

CHAPTER THREE

LITERATURE REVIEW

3.1 Introduction……...……..…….……...23

3.2 Theoretical Models ……...…..……..……..……...….23

3.3 Experimental Work …....……..…….……....……25

3.4 Losses in Regenerative Turbomachines.....……..……..26

3.5 Impeller Blades Profile...…...……....…….……..……..27

3.6 CFD Work ……...……..…….……..……..28

CHAPTER FOUR

ANALYSIS OF RFC USING FLUENT

4.1 Introduction…….…….….30

4.2 Compressible flow theory…….……30

4.3 Flows in Rotating (Moving) Frame of Reference...…….…….32

4.4 Governing Equations…….…….…....33

4.4.1 The Mass Conservation Equation…..…..…..…….33

4.4.2 Momentum Conservation Equation.....……....…….33

4.4.3 The Energy Equation…….……....35

4.5 Governing Equations in a Rotating Reference Frame……...36

4.6 Turbulent Flow Models….....39

4.6.1 Transport Equations for the Realizable k-ε Model…….40

4.7 Numerical Computation.....….....42

4.7. 1 Pressure-Based Segregated Algorithm……...43

4.7. 2 Discretization Technique in FLUENT……....44

4.7.2.1 Solving the Linear System…….……46

4.7.2.2 Spatial Discretization……..…...47

4.7.2.3 Evaluation of Gradients and Derivatives……...…...48

4.7.2.4 Implicit Linearization……..……..……49

4.7.2.5 Pressure Interpolation and Pressure-Velocity Coupling…..…....50

4.7.2.6 Density Interpolation Schemes……..……..…….53

4.7.2.7 Under-Relaxation……..……..……..53

4.8 Multigrid Method.....54
4.8.1 The Need for Multigrid.....54
4.8.2 Algebraic Multigrid (AMG).....55
4.9 Standard Wall Functions.....56

CHAPTER FIVE

RFC MODIFICATION AND SIMULATION PROCEDURES

5.1 Introduction.....62
5.2 Non-dimensional Design Parameters.....63
5.3 Base Regenerative Flow Compressor.....66
5.3.1 Dimensions of the Base Machine.....67
5.3.2 Operation points of the Base Machine.....69
5.3.3 Performance Characteristics of the Base Machine.....70
5.4 Modification of the Base RFC.....72
5.4.1 Major Losses in RFC.....72
5.4.2 Modification of the basic Geometries.....74
5.5 Basic Steps for CFD Analysis.....79
5.5.1 Preprocessing of Simulation.....81
5.5.1.1 Preprocessing in GAMBIT.....81
5.5.1.2 Preprocessing in FLUENT.....85
5.5.2 Processing in FLUENT.....91
5.5.2.1 Setting of Solution controls.....92
5.5.2.2 Selecting Solution monitors.....93
5.5.2.3 Solution Computing.....96
5.5.3 Post processing in FLUENT.....96

CHAPTER SIX

RESULTS AND DISCUSION

6.1 Introduction.....98
6.2 Results of CFD Analysis.....99
6.2.1 Graphical Displays.....99

6.2.2 Numerical Results.....110
6.3 Evaluation of Design Parameters.....111
6.4 Validation.....115
6.5 Results of Modifications done to Improve Performance 115
6.5.1 Effect of changing Flow Channel and Impeller Profile.....115
6.5.2 Effect of changing Blade Angles.....116
6.5.3 Effect of adding a Core.....117
6.5.4 Effect of changing the Working Fluid.....118

CHAPTER SEVEN

CONCLUSION AND RECOMMENDATIONS

7.1 Conclusion.....119
7.2 Recommendations.....120

REFERENCES.....122

APPENDIX.....123

1. Output results for model RFCR-90.....123
2. Output results for model RFCS-135.....125
3. Output results for model RFCA-135.....127
4. Output results for model RFCA-145.....130
5. Output results for model RFCA-150.....132
6. Output results for model RFCA-160.....135
7. Output results for model RFCA-180.....137
8. Output results for model RFCSE-145.....140
9. Output results for model RFCNGA-145.....142
10. Output results for model RFCCA-145.....145

List of figures

Title **Page No.**

Figure 1.1: Classifications of Compressors.....2

Figure 2.1: A Regenerative Turbomachine....……..…...8

Figure 2.2: A Regenerative Turbomachine with magnified fluid flow between blades…….....9

Figure 2.3: Schematic diagram of a Regenerative Turbomachine….....9

Figure 2.4: Section A-A enlarged.……...…….…… .10

Figure 2.5: Section B-B enlarged…….....…….…….. ...10

Figure 2.6: Regenerative Turbomachines blades with radial and non-radial profiles…….12

Figure 2.7: Regenerative Turbomachine blades with semi-circular profiles….…….....13

Figure 2.8: Regenerative Turbomachine blades with aerofoil profile and having a core……13

Figure 2.9: Tangential pressure variation in a Regenerative Turbomachine….....16

Figure 2.10: Performance characteristics of Regenerative Turbomachine.....18

Figure 4.1: Stationary and Rotating Reference Frames.....…….…...36

Figure 4.2: Overview of the Pressure-Based Solution Methods…….....44

Figure 4.3: Control volume used to illustrate discretization of a scalar transport equation.....46

Figure 5.1: Schematic of blade and channel geometry for Single stage RFC……..…68

Figure 5.2: Pressure ratio Vs Specific mass flow rate at various tip Mach number……....71

Figure5.3: Isothermal efficiency Vs Specific mass flow rate at various tip Mach number….71

Figure 5.4: Modified schematic of flow channel and impeller geometry.....….....75

Figure 5.5: Blade variations with blade angle - β and velocity triangles on the cross section of the flow field.....……..76

Figure 5.6: Modified schematic geometry with Core.....77

Figure 5.7 Basic Program Structure….....80

Figure 5.8: Numerical model of Regenerative Flow Compressor….....84

Figure 5.9: Scaled residuals at the final iterations for Model RFCA-145.....93

Figure 5.10: Convergence history of total pressure at exit port for Model RFCA-145.....94

Figure 5.11: Convergence history of mass flow rate at exit port for Model RFCA-145.....95

Figure 6.1: Plot of total pressure contours over the entire flow field for model RFCR-90 (*at design point running speed, 28910 rpm*).....99

Figure 6.2: Plot of total pressure contours over the entire flow field for model RFCA-145 (*at design point running speed, 28910 rpm*).....100

Figure 6.3: Plot of density contours over the entire flow field for model RFCA-145 (*at design point running speed, 28910 rpm*).....101

Figure 6.4: Plot of a particle path line from inlet to exit port for Model RFCA-145 (*at starting running speed, 2891 rpm*).....102

Figure 6.5: Detail view of plot of a particle path line from inlet to exit port for Model RFCA-145 (*at starting running speed, 2891 rpm*).....103

Figure 6.6: Plot of Isothermal power gained by a particle along its path line from inlet to exit port for Model RFCR-90 (*at starting running speed, 2891 rpm*).....104

Figure 6.7: Plot of Isothermal power gained by a particle along its path line from inlet to exit port for Model RFCA-145 (*at starting running speed, 2891 rpm*).....105

Figure 6.8: Plot of Isothermal power gained by a particle along its path line from inlet to exit port for Model RFCA-145 (*at the second running speed, 5782 rpm*).....105

Figure 6.9: Plot of Isothermal power gained by a particle along its path line from inlet to exit port for Model RFCA-145 (*at the third running speed, 8673 rpm*).....106

Figure 6.10: Plot of Isothermal power gained by a particle along its path line from inlet to exit port for Model RFCA-145 (*at the fourth running speed, 11564 rpm*).....106

Figure 6.11: Plot of Isothermal power gained by a particle along its path line from inlet to exit port for Model RFCA-145 (*at running speed, 20237 rpm*)……107

Figure 6.12: Plot of Isothermal power gained by a particle along its path line from inlet to exit port for Model RFCA-145 (*at the design point speed, 28910 rpm*).....108

Figure 6.13: Plot of relative velocity vectors on a cross-sectional surface in the flow field for Model RFCR-90 (*at the design point running speed, 28910 rpm*).....109

Figure 6.14: Plot of relative velocity vectors on a cross-sectional surface in the flow field for Model RFCA-145 (*at the design point running speed, 28910 rpm*).....109

Figure 6.15: Plot of a particle path line from inlet to exit port for Model RFCCA-145 (*at starting running speed, 2891 rpm*).....117

Figure 6.16: Plot of total pressure contours over the entire flow field for model RFCCA-145 (*at design point running speed, 28910 rpm*).....118

Figure 6.17: Plot of total pressure contours over the entire flow field for Model RFCR-90.....123

Figure 6.18: Plot of density contours over the entire flow field for Model RFCR-90.....123

Figure 6.19: Plot of relative velocity vectors on a cross-sectional surface in the flow field for Model RFCR-90.....124

Figure 6.20: Plot of Isothermal power gained by a particle along its path line from inlet to exit port for Model RFCR-90.....124

Figure 6.21: Plot of total pressure contours over the entire flow field for Model RFCS-135.....125

Figure 6.22 Plot of density contours over the entire flow field for Model RFCS-135.....125

Figure 6.23: Plot of a particle path line from inlet to exit port for Model RFCS-135(*at starting running speed, 2891 rpm*).....126

Figure 6.24: Plot of Isothermal power gained by a particle along its path line from inlet to exit port for Model RFCS-135.....126

Figure 6.25: Plot of relative velocity vectors on a cross-sectional surface in the flow field for Model RFCS-135.....127

Figure 6.26: Plot of total pressure contours over the entire flow field for Model RFCA-135.....127

Figure 6.27: Plot of density contours over the entire flow field for Model RFCA-135.....128

Figure 6.28: Plot of a particle path line from inlet to exit port for Model RFCA-135 (*at starting running speed, 2891 rpm*).....128

Figure 6.29: Plot of Isothermal power gained by a particle along its path line from inlet to exit port for Model RFCA-135.....129

Figure 6.30: Plot of relative velocity vectors on a cross-sectional surface in the flow field for Model RFCA-135.....129

Figure 6.31: Plot of total pressure contours over the entire flow field for Model RFCA-145.....130

Figure 6.32: Plot of density contours over the entire flow field for Model RFCA-145.....130

Figure 6.33: Plot of a particle path line from inlet to exit port for Model RFCA-145 (*at starting running speed, 2891 rpm*).....131
Figure 6.34: Plot of Isothermal power gained by a particle along its path line from inlet to exit port for Model RFCA-145 131
Figure 6.35: Plot of relative velocity vectors on a cross-sectional surface in the flow field for Model RFCA-145.....132
Figure 6.36: Plot of total pressure contours over the entire flow field for Model RFCA-150.....132
Figure 6.37: Plot of density contours over the entire flow field for Model RFCA-150.....133
Figure 6.38: Plot of a particle path line from inlet to exit port for Model RFCA-150 (*at starting running speed, 2891 rpm*).....133
Figure 6.39: Plot of Isothermal power gained by a particle along its path line from inlet to exit port for Model RFCA-150 134
Figure 6.40: Plot of relative velocity vectors on a cross-sectional surface in the flow field for Model RFCA-150.....134
Figure 6.41: Plot of total pressure contours over the entire flow field for Model RFCA-160.....135
Figure 6.42: Plot of density contours over the entire flow field for Model RFCA-160.....135
Figure 6.43: Plot of a particle path line from inlet to exit port for Model RFCA-160 (*at starting running speed, 2891 rpm*).....136
Figure 6.44: Plot of Isothermal power gained by a particle along its path line from inlet to exit port for Model RFCA-160.....136

Figure 6.45: Plot of relative velocity vectors on a cross-sectional surface in the flow field for Model RFCA-160.....137
Figure 6.46: Plot of total pressure contours over the entire flow field for Model RFCA-180.....137
Figure 6.47: Plot of density contours over the entire flow field for Model RFCA-180.....138
Figure 6.48: Plot of a particle path line from inlet to exit port for Model RFCA-180 (*at starting running speed, 2891 rpm*).....138
Figure 6.49: Plot of Isothermal power gained by a particle along its path line from inlet to exit port for Model RFCA-180.....139
Figure 6.50: Plot of relative velocity vectors on a cross-sectional surface in the flow field for Model RFCA-180.....139
Figure 6.51: Plot of total pressure contours over the entire flow field for Model RFCSEA-145.....140
Figure 6.52: Plot of density contours over the entire flow field for Model RFCSEA-145.....140
Figure 6.53: Plot of a particle path line from inlet to exit port for Model RFCSEA-145 (*at starting running speed, 2891 rpm*).....141
Figure 6.54: Plot of Isothermal power gained by a particle along its path line from inlet to exit port for Model RFCSEA-145.....141
Figure 6.55: Plot of relative velocity vectors on a cross-sectional surface in the flow field for Model RFCSEA-145.....142
Figure 6.56: Plot of total pressure contours over the entire flow field for Model RFCNGA-145.....142

Figure 6.57: Plot of density contours over the entire flow field for
Model RFCNGA-145.....143
Figure 6.58: Plot of a particle path line from inlet to exit port for Model RFCNGA-145
(*at starting running speed, 2891 rpm*).....143
Figure 6.59: Plot of Isothermal power gained by a particle along its path line from inlet
to exit port for Model RFCNGA-145.....144
Figure 6.60: Plot of relative velocity vectors on a cross-sectional surface in the flow field for
Model RFCNGA-145.....144
Figure 6.61: Plot of total pressure contours over the entire flow field for
Model RFCCA-145.....145
Figure 6.62: Plot of density contours over the entire flow field for
Model RFCCA-145.....145
Figure 6.63: Plot of a particle path line from inlet to exit port for Model RFCCA-145
(*at starting running speed, 2891 rpm*).....146
Figure 6.64: Plot of Isothermal power gained by a particle along its path line from inlet
to exit port for Model RFCCA-145.....146
Figure 6.65: Plot of relative velocity vectors on a cross-sectional surface in the flow field for
Model RFCCA-145.....147

List of Tables

Title **Page No.**

Table 5.1: Non-dimensionalized geometric data's for configuration 4 (***S4***)…….....68

Table 5.2: Geometric data's calculated for ***S4***….....69

Table 5.3: Material Properties...….....89

Table 6.1: Numerical inputs and results of CFD analysis for RFC Models.....113

CHAPTER ONE

INTRODUCTION

A compressor is a mechanical device that increases the pressure (or enthalpy) of a gas. The pressure (or enthalpy) of the gas is increased by reducing the gas specific volume during its passage through the compressor. There are various types of compressors used in different sectors because of indefinite range of service requirements. Before a compressor type is selected for a particular application certain basic information related to its performance requirements should be at hand. This includes: pressure ratio, flow rate, efficiencies desired and some other special characteristics. One can then consider the type of machine desired from a range of types of compressors available.

In following sections of this chapter, different types of compressors, the basic characteristics of regenerative flow compressor, the objective of this thesis, methodology used and the outline of the thesis will be presented.

1.1 Classification of Compressors

Compressors are classified in to two basic types depending on how the mechanical elements act on the fluid to be compressed. These are positive displacement compressors and continuous flow compressors, as shown in Figure 1.1 [4].

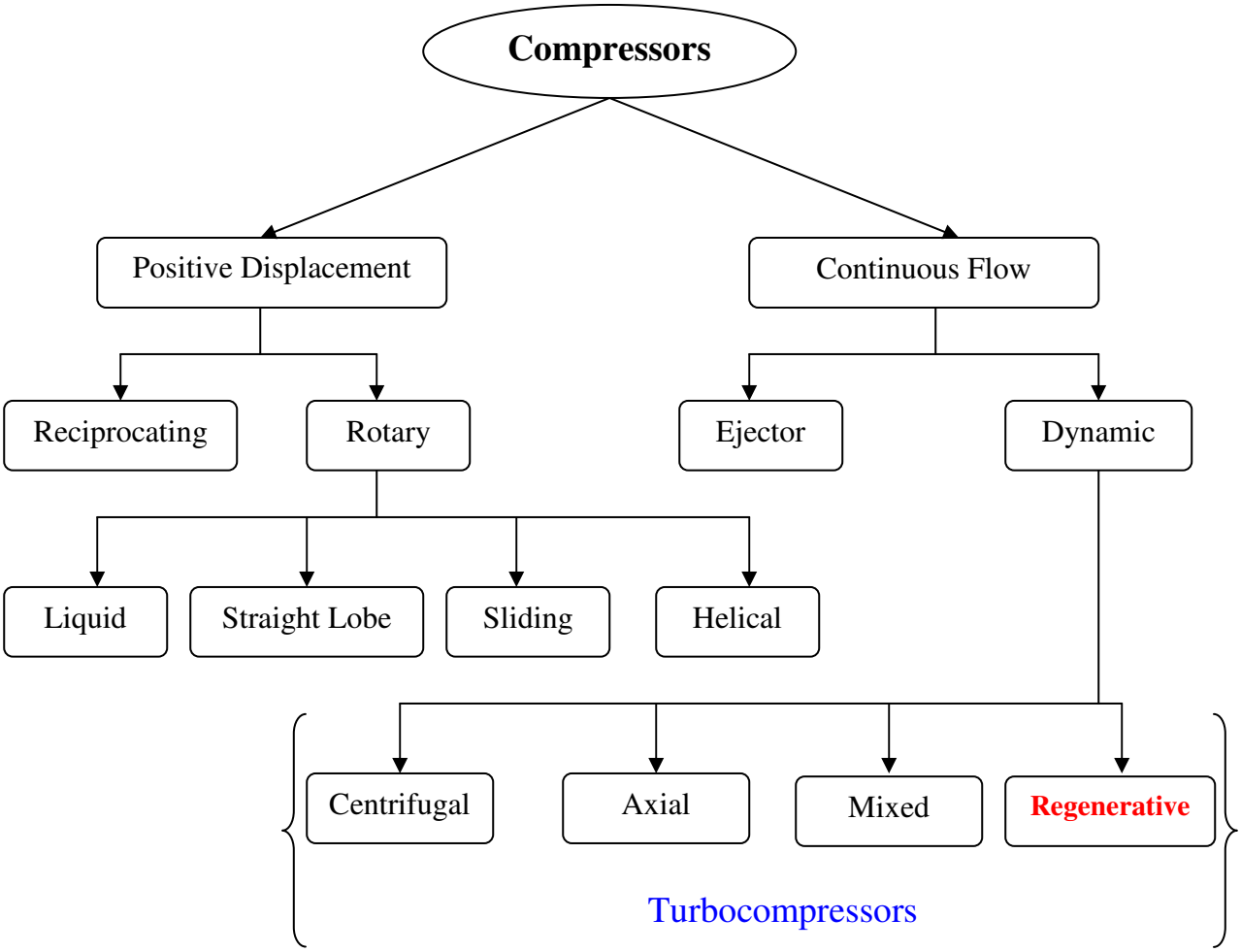

Figure 1.1: Classifications of Compressors (Raheel [4])

In positive displacement compressors a certain amount of gas is contained in a compression chamber, and the volume in which it resides is mechanically decreased. This situation causes a corresponding increase in the pressure before it is released. There may be variations in the discharge pressure of the gas flow, but basically the flow of gas stays relatively constant provided that a continuous speed is maintained. These compressors are available as reciprocating and rotary types.

Reciprocating compressors use a piston driven by a crankshaft. They can be driven by electric motors or internal combustion engines. They reduce the volume in the cylinder occupied by the gas, compressing it to a higher pressure.

Rotary screw compressors work on the principle of gas filling the void between two helical mated screws and their housing. As the two helical screws are turned, the volume is reduced resulting in an increase of gas pressure. Most rotary screw compressors inject oil into the bearing and compression area. The reasons are for cooling, lubrication and creating a seal between screws and the housing wall to reduce internal leakage. After the compression cycle, the oil and gas must be separated before the gas can be used by the system. Rotary screw compressors have low initial cost, compact size, low weight and are easy to maintain.

In continuous flow compressors the fluid is accelerated to a high velocity (kinetic energy) and this velocity energy is changed into pressure energy by decelerating the gas in the discharge volutes or diffusers. The continuous flow compressors are categorized into ejector and dynamic type compressors. The dynamic compressors are subdivided into axial, centrifugal, mixed type and regenerative compressors. These four categories are also called Turbocompressors.

1.2 Turbocompressors

Turbocompressors are classified by the predominant direction of flow path through the device relative to the rotating shaft. When the meridian flow path is axial, the compressors are called an axial-flow compressor. The flow enters and leaves the impeller of the compressor in the axial direction. Axial-flow compressor uses cascade of blades to progressively compress the working fluid. And the deceleration takes place in the stator blade

passages. These compressors are used where there is a requirement for a high flows or a compact design.

If the flow is predominantly radial they are called radial or centrifugal compressors. In centrifugal compressors the flow leaves the compressor in a direction perpendicular to the axis of the rotating shaft. Centrifugal compressors use a vaned rotating disk or impeller in a shaped housing to force the gas to the rim of the impeller, increasing the velocity of the gas. A diffuser (divergent duct) section converts the velocity energy to pressure energy. They are primarily used for continuous, stationary service in industries such as oil refineries, chemical and petrochemical plants and natural gas processing plants.

The third category is called the mixed flow compressors in which the flow path is a combination of axial and radial flows. Mixed flow compressors have impellers which combine the characteristics of both axial and centrifugal compressors.

1.3 Regenerative Flow Compressors (RFC)

The regenerative flow compressor (RFC) is a turbomachine that permits a head equivalent to that of several stages of a traditional machine of comparable tip speed, but at low flow rate. The flow through the rotor of this machine is helical superimposed on tangential flow through its annular / flow channel and hence the fluid passes through the vanes a number of times. This repetitive action of the impeller blades on the fluid, in effect, “multistaging” accounts for a high head per stage.

A regenerative flow compressor has a similar performance characteristic to those of a positive displacement turbomachines for duties requiring a high head at low flow rate, but the isothermal efficiency of RFC is usually less than 50 %. The low efficiency arises from

various losses which are directly related to the geometry and operating principle of the machine. These are turbulence and friction losses, shock loss, the carry-over of the liquid through the stripper seal and the leakage through the clearance spaces and they will be discussed in detail in chapter five.

Despite this, RFC machines have found a wide application in chemical, petroleum, food staff and nuclear industries. This is because of their simplicity, absence of wear, oil free operation and no surge or stall instability as compared to a comparable positive displacement turbomachine. Earlier the benefits of RFC were not well studied and supported, but through time many researches were conducted and several papers have been published with the aim of improving the performance of this machine due to their advantage in different sectors.

The need for this thesis then arises from this fact i.e. RFCs have wide advantage in different sectors, but the low efficiency is the usual problem. Actually alleviating or minimizing the losses means increasing the performance of the compressor. Even though the determining factors for enhancing the performance of RFC are many, this thesis focuses on changing basic geometries to improve the performance of the machine.

1.4 Objective of the Thesis

The objective of this thesis is to improve the performance of a regenerative flow compressor by studying the fluid flow for varies channel and vane geometries using CFD coded software, FLUENT. The specific objectives are to study the effect of different geometries on the performance of the machine and to discuss the different losses based on the modified geometries. The other intention is to introduce and motivate CFD analysis to get a better insight of a complicated flow patterns in regenerative turbomachines, so that it can serve as

reference for those interested to work on regenerative turbomachines using commercially available CFD software's.

1.5 Methodology

A CFD coded software called FLUENT is chosen for this project because of the ease with which the analyzed model can be created and because the software allows users to modify the code for special analysis conditions through the use of user subroutines. FLUENT code uses the finite-volume method to solve the momentum and energy equations of the flow. CFD offers advantages over experimental systems for simulating fluid flows and this technique is finding increased acceptance for the study of fluid flows. It is attractive to industry since it is more cost-effective than physical testing. This obviously drives the researcher to use CFD coded software to tackle the problem.

A single stage RFCs tested by Capstone Turbine Corporation [4] are used as a base to develop different models with modified geometry and their simulation results will be compared with the experimental data's. These RFCs are employed for the compression of a low pressure natural gas for C30 microturbine system. But the required pressure is achieved with an isothermal efficiency in the range of 8 - 20 % at the operation point. These efficiency values are very low and there is significant room for improvement.

The working conditions (i.e. speed, inlet and discharge pressure) are kept the same for each simulation. And at last the output results are analyzed and interpreted to give some design recommendation.

1.6 Outline of Thesis

This thesis has seven chapters and it starts with a detail discussion of fundamentals, hypothesis of operation and applications of regenerative turobmachines in chapter 2. Chapter 3 deals with previous research work done on regenerative turbomachines. The literature survey presented in chapter 3 consists of published theoretical models, experimental investigations, blade designs, loss analysis and CFD work performed on regenerative turbomachines. Chapter 4 describes basic assumptions, governing equations and the numerical computation scheme, that is CFD analysis using FLUENT. Chapter 5 deals with the procedures of flow simulation through RFC which includes building geometry with varying flow channel and blade profiles and mesh generation in GAMBIT and problem set up for the numerical computation in FLUENT. The analysis and interpretation of the results is discussed in Chapter 6 by using graphical displays and empirical reporting of results. In the last chapter conclusions are drawn based on results obtained and some recommendations are given in regard to the long-term objectives.

CHAPTER TWO

DESIGN AND OPERATIONAL FEATURES OF REGENERATIVE TURBOMACHINES

Many researchers are excited to study the regenerative turbomachines due to their unique design and operational features. The flow through these machines is helical superimposed on tangential flow through its flow channel. It combines radial and axial flow patterns; hence the design includes both axial and radial characteristics. A typical regenerative turbomachine is shown in Figures 2.1 and 2.2 [3].

The objective of this chapter is to present the essential components of regenerative turbomachine, to present the working principle and performance characteristics of RFC, to compare RFC with centrifugal compressors and to describe the application of RFCs in different sectors.

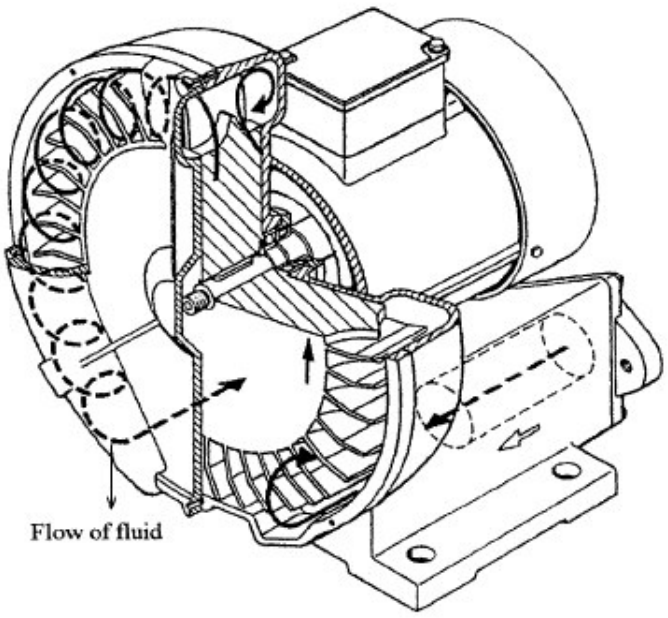

Figure 2.1: A Regenerative Turbomachine (Song [3])

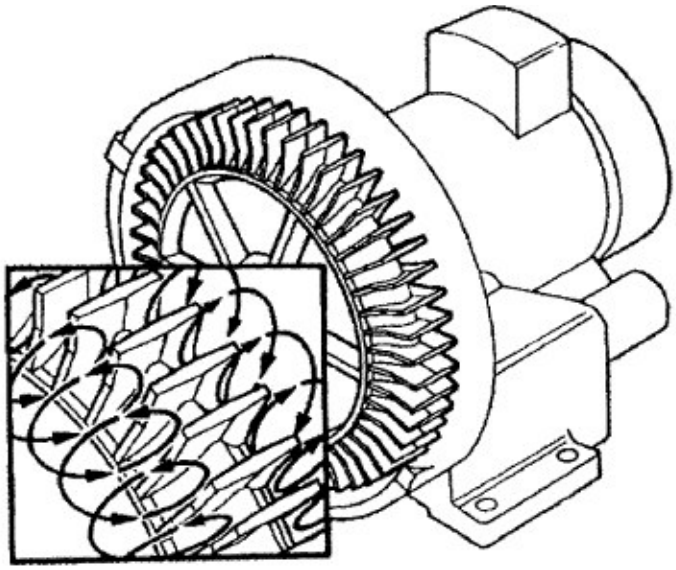

Figure 2.2: A Regenerative Turbomachine with magnified fluid flow between blades (Raheel [4])

2.1 Essential Components of Regenerative Turbomachine

The essential components of a regenerative turbomachine include impeller (rotor) with blades, inlet port, exit port, stripper, and flow channel (open channel) which are shown in Figure 2.3 below.

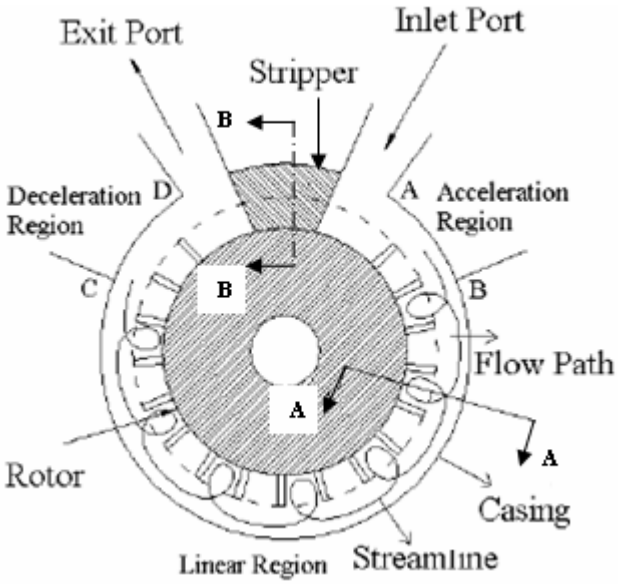

Figure 2.3: Schematic diagram of a Regenerative Turbomachine (Engda [2])

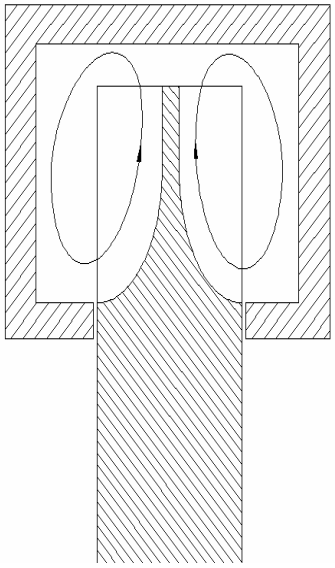

Figure 2.4: Section A-A enlarged

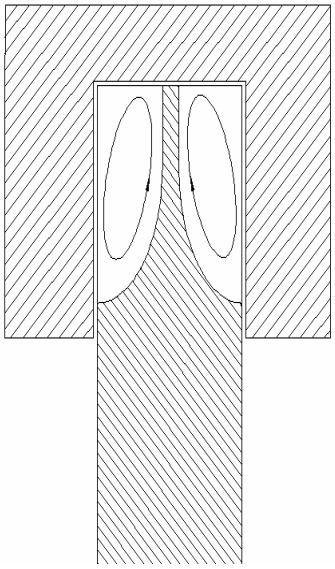

Figure 2.5: Section B-B enlarged

2.1.1 Impeller

In regenerative turbomachines the freely rotating impeller adds energy and hence pressure rise to the fluid passing through it. The impeller has blades which are cast or machined into each side of its periphery. For RFCs running at very high speeds a continuous toroidal flow pattern is less expected hence the energy addition to the fluid and the pressure rise is due to turbulent friction between the moving impeller and the fluid.

But at lower running speeds, where toroidal flow pattern is expected, the addition of energy to the fluid is imparted each time as it passes through the blades of the impeller, allowing substantially more motive force to be added which enables much higher pressures to be achieved. The fluid does not discharge freely from the tips of the blades rather the open channel forces it to circulates back to blades many times before leaving the impeller, hence enhancing helical flow pattern. This motion, which is composed of a peripheral motion induced in the peripheral open channel and circulatory motion between impeller blades, is

caused by the centrifugal pressure gradient. There is a gradual increase of pressure in peripheral direction.

The action of impeller blades, operating in series instead of in parallel to each other, makes them different from centrifugal turbomachines. Each passage through the blades may be regarded as a conventional stage of compression. It is due to the repeated flow through impeller blades that has made a regenerative compressor capable of replacing several stages of centrifugal compressors, producing the same head. Thus the equivalent of several stages of compression may be obtained from a single impeller in a relatively smaller compressor

The enclosing chambers conduct the fluid into twin vortices around the impeller blade as shown in Figure 2.4. A very small pressure rise occurs in the vicinity of each impeller blade.

Regenerative turbomachines can also be designed in multistage configurations to meet certain design requirements.

2.1.1.1 Impeller Blades

The impeller of regenerative turbomachines can have blades of different shapes. The commonly used blade types are radial blades, non-radial blades, semi-circular blades and aerofoil blades. Some examples of these blade shapes are given in Figures 2.6, 2.7 and 2.8 [4]. Regenerative turbomachines having aerofoil blades can be fitted with a core to guide the circulation through the blading and to minimize the loss due to formation of vortices at the tips of blades. The core can be fixed to the blades and rotate with them or be fixed to machine casing. The blades can be constructed as a single row, or as two rows side by side to provide parallel contra-rotating paths.

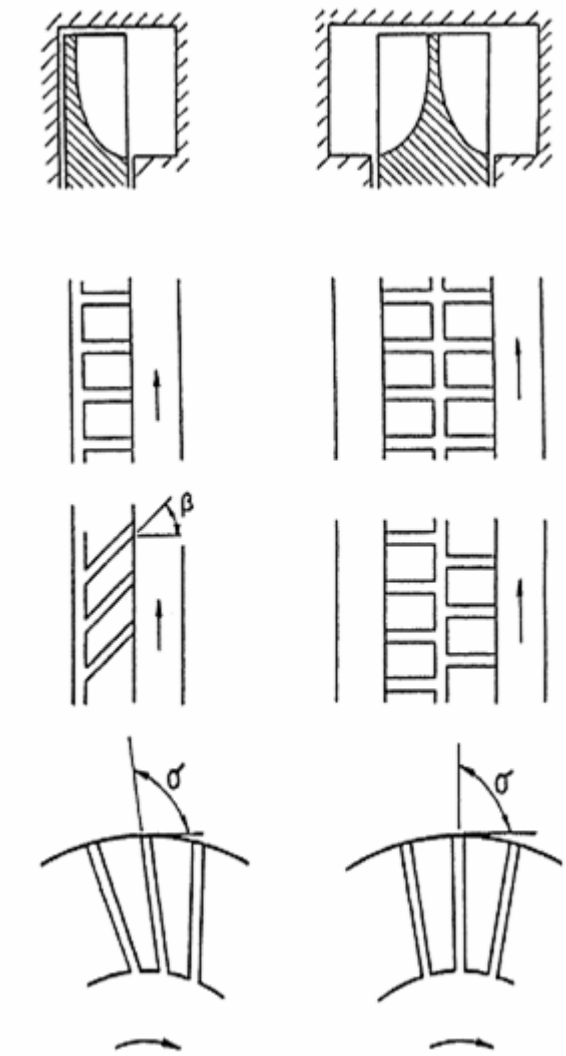

Figure 2.6: Regenerative Turbomachines blades with radial and non-radial profiles (Abdella [4])

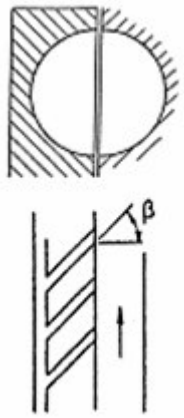

Figure 2.7: Regenerative Turbomachine blade with semi-circular profile (Abdella [4])

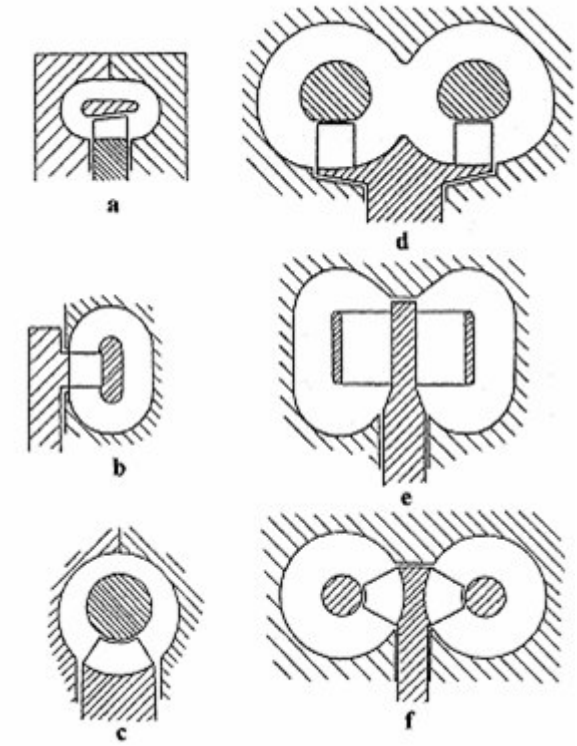

Figure 2.8: Regenerative Turbomachine blades with aerofoil profile and having a core (Abdella [4])

2.1.2 Inlet and Exit (Outlet) Ports

Inlet and exit ports are components which connects the external system piping to the flow channel. The fluid enters the flow channel via the inlet port, which is shaped to set up spiral flow around the annular channel. The fluid at high pressure is discharged to the external system through the exit port.

2.1.3 Stripper

Stripper, which is also known as septum, is used to block the high pressure fluid to be mixed with the fluid in the inlet region. As shown in Figure 2.5 the casing clearance is reduced so that the fluid is forced to exit the domain through the exit port. In this region, the open channel closes to within a very small tolerance of the sides and tip of the rotor and only the fluid between the blades allowed to pass through the suction.

Clearances between the impeller disk and the casing are kept to a minimum to prevent leakage from the high pressure side back to the low pressure side. The stripper also helps to establish and maintain the regenerative flow pattern.

2.1.4 Flow Channel

Flow channel forces the fluid to circulate back to the blades. The fluid between the blades is thrown out and across the flow channel which has cross sectional area greater that that of the impeller blades. After the fluid leaves the blades a violent mixing occurs in the flow channel and the angular momentum acquired by the fluid in its passage between the vanes is transferred to the fluid in this open channel. This mixing process results in high turbulence, and this implies inherent waste of power.

2.2 Working Principle

In regenerative turbomachine the predominant direction of flow is parallel to the velocity of the blades. Every time the fluid passes through the impeller blades, work is done on it and its stagnation pressure and tangential velocity are increased. The tangential velocity is removed, not by a row of stator blades as in a conventional turbomachine, but by the action of tangential pressure gradient around the periphery of the machine between the exit and inlet ports. Thus by the time the fluid re-enters the blade row, the magnitude of its tangential velocity will be reduced and its direction will be reversed. Hence during each loop of the spiral, the fluid is accelerated in the tangential direction as it passes through the blades and is decelerated by the tangential pressure gradient as it passes through the flow channel. Because the flow passes through the same blade row several times between the entry and exit, the work done on it and hence the pressure rise is considerably greater than that which can be obtained from a conventional turbomachine with the same tip speed. The specific speed is therefore low and the machines operate in the usual range of positive displacement machines [4]. Pressure variation of the fluid as it circulates through regenerative turbomachine is shown in Figure 2.9 [2]. These curves suggest five regions in the machines operation, which are also marked in Figure 2.3 [2].

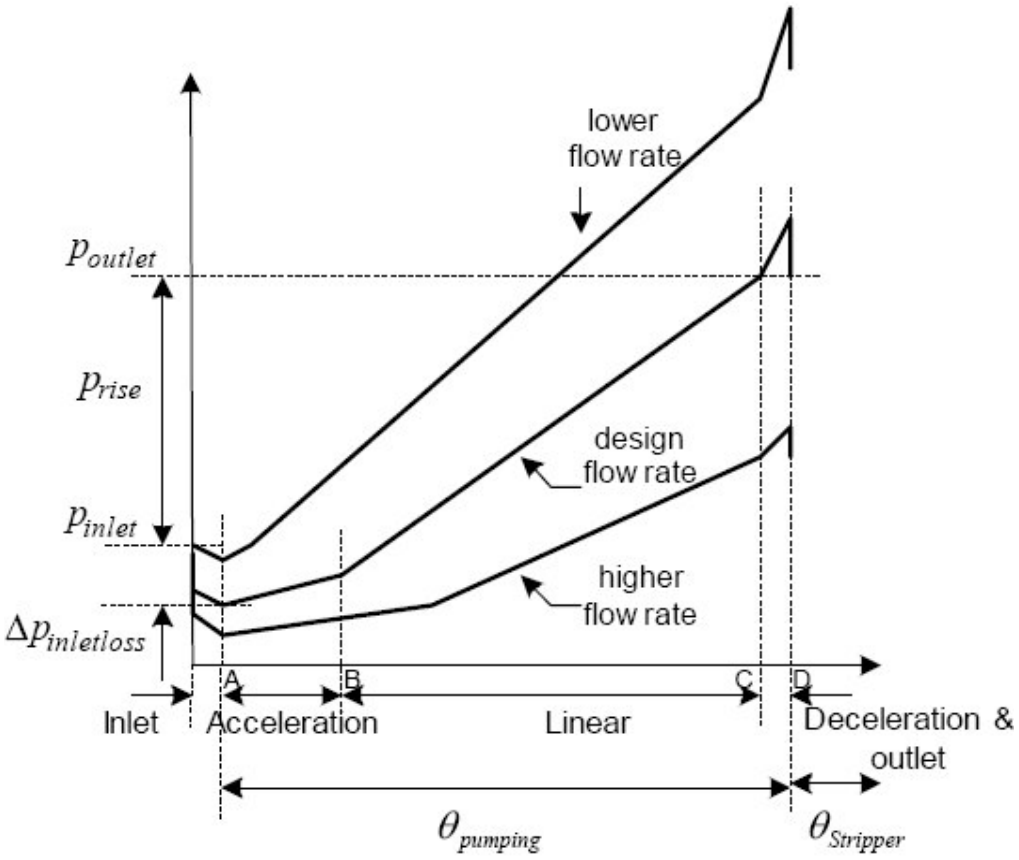

Figure 2.9: Tangential pressure variation in a Regenerative Turbomachine (Engda [2])

- Inlet region (A): The flow experiences some pressure loss through the inlet region.
- Acceleration region (A-B): The flow enters the working section of the compressor with a velocity and pressure dependent largely on the inlet region.
- Linear region (B-C): The pressure gradient is consistent as indicated in the diagram. This region is referred to as the working section of the compressor where the flow pattern is fully developed.

- Deceleration region (C-D): In this region, a deceleration occurs and the kinetic energy of the circulatory velocity is changed as a pressure rise. Therefore, there is a little pressure rise as shown in Figure 2.9 [2].
- Outlet region (D): A loss similar to that at the inlet region occurs at the outlet region.

2.3 Performance Characteristics of RFC

Most regenerative compressors have an isothermal efficiency less than 50 %, but still they have found many applications because they allow the use of fluid dynamic compressors in place of positive displacement compressors for duties requiring high head and low flow rates. Although regenerative turbomachines are widely used in the industry there is still a need to study and make design changes in their geometry to improve the performance.

The head, power, and efficiency relationships as a function of flow rate for a typical regenerative flow compressor are shown in Figure 2.10[4]. The maximum efficiency in this machine occurs at comparatively large flow rates. At low flow rates, high heads can be obtained at lower isothermal efficiency. This is due to the fact that circulatory velocity is higher at lower flow rate resulting in higher pressure rise. However, since the fluid enters the blades several times, the power requirement is also higher at low flow rates.

It should also be noted that in a very low specific speed ranges, regenerative flow compressors are more efficient than the centrifugal compressors.

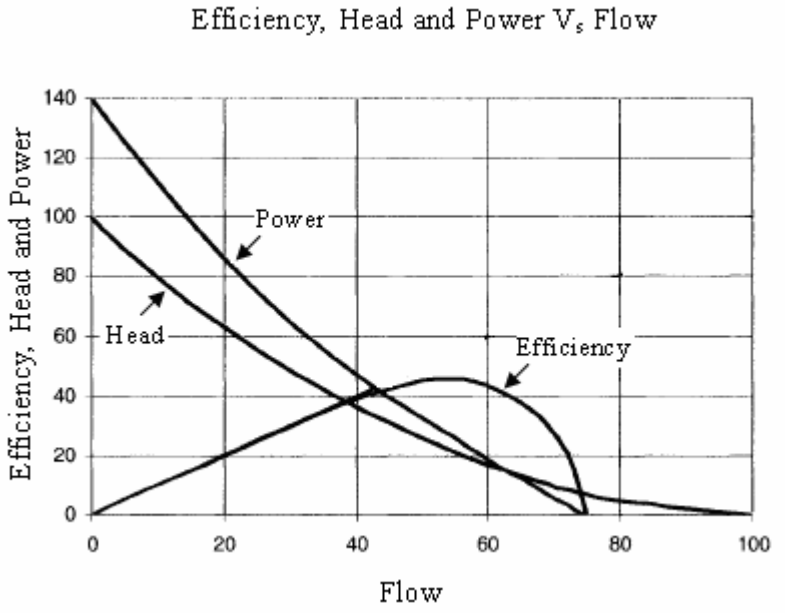

Figure 2.10: Performance characteristics of Regenerative Turbomachine (Raheel [4])

2.4 Comparison of Centrifugal and Regenerative Flow Compressors

These operationally different compressors are widely used in industries. For some special (*see application of RFCs*) duties regenerative compressors offers advantage over centrifugal compressors. Therefore, it is interesting to mention the relative merits of the two compressors. Some of the basic characteristics of both compressors are discussed below [4].

1. Centrifugal compressors take in the fluid at center of the impeller and push it radially outward with no axial component of velocity; however regenerative compressors impart both radial and an axial component to fluid flow.
2. In centrifugal compressors, fluid passes through the impeller only once while in regenerative compressors running at lower speeds, fluid is exposed to impeller many times, thus adding more energy to the fluid.

3. One of the most significant structural advantages of the regenerative type compressors is that no complex flow passages or vaning is required. They are simple and easy to machine and there is no need of diffusers. Regenerative compressors tend to have more internal components than the centrifugal compressors, and we can cast the centrifugal compressor impeller with the outside diameter machined, however regenerative compressor impeller is completely machined.
4. Centrifugal compressors have large axial length per stage and large overall diameter because of diffusers. On the other hand, in the regenerative compressors, the suction and discharge nozzles are at periphery, thus the axial and radial dimensions are small compared to centrifugal compressor. Regenerative compressors provide much more pressure rise in a more compact compressor design.
5. The power requirement of a regenerative compressor decreases with increasing flow rate, whereas the power requirement increases with increasing flow rate in case of a centrifugal compressor. Moreover, the head and flow rate characteristics of the two machines are also significantly different.
6. The centrifugal compressor surges at low flow rate, sometimes at flow rate as great as 50% of maximum flow rate. In a regenerative compressor, the flow can be shut off without surging; however, there will be a temperature rise. The regenerative compressors have advantages of stability, since they have a stable operation throughout the flow range (a regenerative compressor will not surge under any condition).

7. Higher rotational speeds and/or a large number of stages are usually required with centrifugal compressors. Regenerative compressors produce heads several times greater for a given impeller tip speed.
8. Another difference between a regenerative compressor and a centrifugal compressor is that in the centrifugal compressor, gain in pressure is proportional to the square of the peripheral velocity of the impeller, whereas in a regenerative compressor it is the relative velocity to the blades that depends on the pressure gradient.
9. The clearances for regenerative compressors are held to closer tolerances than for the centrifugal compressors.
10. The centrifugal compressors have no radial shaft loading except gravitational, but with usual design there can be high axial loading. However, in a regenerative compressor there are no axial shaft loadings with usual design, but there is a radial loading due to pressure difference around periphery.
11. Problems due to wear are minimal in regenerative compressors than in centrifugal compressors [5].
12. The compact size, high reliability and low noise of regenerative turbomachines make them attractive in certain applications. Better efficiency at low specific speeds makes them a tough competitor of centrifugal turbomachines in low specific speed applications [5].

2.5 Applications of Regenerative Flow Compressors

Regenerative compressors are being used in a number of applications that requires high pressure rise at low flow rates. The relative simplicity of construction and stable operating

characteristics of the regenerative flow compressors are making them more and more attractive to users in several areas, including chemical, power, food processing, petroleum, and nuclear industries.

RFCs have been proposed for use in hydrogen gas pipelines and as helium compressors for cryogenic applications in space vehicles [4].

RFCs can also be used as natural gas pipeline compressors; in fact, they can be designed to handle both natural gas or hydrogen or any mixture of the two. Further, it may be possible to accomplish this in a single design, which can be adjusted to handle a varying mixture by speed control or other means. Moreover, RFCs are advantageous for incorporation in small closed cycle helium refrigerators [4].

Because of the reliability, compact size and low maintenance, recently there is an increasing use of regenerative compressors in low pressure (1.38-103.5 kPa gauge) natural gas compression required by microturbine systems [2]. Other applications of RFC include boosting and recycling of hydrogen mixtures and hydrocarbon gases, gas phase reactor recycling, molecular sieve regeneration in gas drying processes, vent/purge gas recovery, fuel gas boosting for gas turbine feed and gas compression in many other industrial processes.

Regenerative blowers are used in scavenging of small S.I power plants [4]. The regenerative blower was found to be the most suitable option since it was able to match the engine air breath demand all over its utilization range. Regenerative blowers have found many industrial applications in solids conveying systems. Historically, the pressure and flow rates demanded by many solids conveying systems made roots or vaned-type blowers, almost automatic choice despite their limitations.

Many packaging and paper handling jobs were historically beyond the regenerative blowers capability, but now with increasing emphasis on working environment, the low noise regenerative blowers are welcomed in these areas. Regenerative blowers also find use in sewage treatment, which require considerable volume to be blown against a head of water. Regenerative blowers are also used for powder coating recovery applications, plating, cleaning and rinse tank agitation. Since regenerative blowers provide high airflow capacities at low pressure differentials, they become excellent for air moving applications, such as agitation of bath or aeration of a pond [4].

CHAPTER THREE

LITERATURE REVIEW

3.1 Introduction

Regenerative turbomachines have found many applications in different sectors. Despite this there was no much research conducted in the past and as compared to centrifugal and axial turbomachines the number of publications existing in literatures for regenerative turbomachine is very small. Both regenerative flow compressors and pumps have close operating principle; hence the literature review presented in this chapter is based on researches done on both machines. It is categorized in the following five areas of research:

1) Theoretical Models
2) Experimental Work
3) Loss in Regenerative Turbomachines
4) Impeller Blades Profile
5) CFD Work

3.2 Theoretical Models

Some theoretical models have been used in attempts to describe the flow in regenerative turbomachinery. Theories for the flow of compressible fluid in regenerative turbomachines are rarely found in literature.

Wilson [9] developed the momentum exchange theory for a radial blade impeller which was able to explain the helical flow pattern. He concluded that as the circulatory flow passes radially through the rotor its angular momentum in the direction of the rotor motion is

increased by virtue of the work of the impeller. To maintain the pressure gradient in the flow channel the angular momentum of the circulatory flow continually decreases after it leaves the rotor.

Andrew [1] used a simplified theoretical model to describe flow details in regenerative turbomachines. With the help of streamline passing through the impeller a cork screw flow pattern through regenerative turbomachine was shown.

Burton [3] made an effort and reported a simplified theory, which took account of area change and compressibility effects in regenerative flow compressors. He assumed that energy exchange is obtained through shear stress between the impeller and the fluid in casing. Any radial components of flow were ignored. The continuity, momentum and energy equations were applied to a linear control volume and differential equations were obtained. Burton's model was also based on shear stress theory which was experimentally proven as unable to explain the fluid motion inside regenerative turbomachines.

Sixsmith and Altmann [5] introduce the idea of aerofoil blades with addition of a core in the flow channel to direct the circulating flow and it resulted in significant improvements in performance. The flow channel had the core to assist in guiding the fluid such that it circulates through the blading with a minimum of loss. The core also acted as a shroud to reduce losses due to formation of vortices at the tips of the blades. The efficiency was considerably improved compared to the efficiency of regenerative compressor tested with radial blades.

3.3 Experimental Work

Most experimental work involved varying the geometry of regenerative turbomachines. This includes the proportions of blading to coverage of the flow channel, shape of the flow channel and impeller / blade profiles. There is limited data available on gases as the working fluids in regenerative turbomachines.

Raheel [4] presented the tested data's of several single and multi stage RFCs done by Capstone Turbine Corporation, CA. They are designed to compress natural gas for microturbine application. The single stage RFCs have rectangular flow channel with straight impeller blade profile and for the multi stage RFCs the flow channel is modified to semi-circular. The performance characteristics of these machine shows that the efficiency was improved by varying the basic geometries.

As described in Raheel [4], Cates also reported the test data of the regenerative compressor with a variety of gases having molecular weights of 4 to 400. He presented general characteristics in Mach numbers extending well into the compressible dominion of operation. The regenerative compressor operated satisfactorily without surging or unstable operation with the variety of gases. Compressibility effects had an important influence on performance because lower pressure ratios were measured at impeller tip mach numbers approaching 1. The other conclusion that was reached by the tests performed indicated that increasing impeller-to-casing clearances had little effect on performance.

Sixsmith and Altmann [6] tested two regenerative compressors MK1 and MK2 with aerofoil blading, a core and decompression ducts by blowing air through them. These regenerative compressors were designed to run up to 10,000 rpm and deliver 0.25m^3/sec at a pressure of

202.65 kPa. They differ in the number of blade, chord length of the blades and number of rows for the blades. MK2 has increased number of blades with reduced chord length and the row of blades is doubled (two rows) to increase the flow rate. The characteristics resembled to those of a positive displacement compressor and the efficiency was maintained over a wide range of operating conditions.

3.4 Loss in Regenerative Turbomachines

It is thought that more than 40 - 50% of the input power in a regenerative turbomachine is consumed in overcoming losses. The regenerative turbomachines operation is affected by different types of losses and they will be discussed in detail in chapter five. These include:

- ***Turbulent losses***: caused by turbulence, fluid friction and the blade drag occurring in the flow field.
- ***Shock loss***: is caused by difference between blade angle and flow angle when fluid enters the blades.
- ***Inlet and outlet loss***: are losses occurred at the inlet and exit ports respectively.
- ***Leakage loss***: is caused by leakage between clearances of the impeller face and the compressor casing.
- ***Carry over loss***: as the blades enter the stripper seal between the outlet and inlet ports, a high pressure compressed gas in the blade passages is carried through the stripper to the low pressure inlet region. The stream is mixed with the incoming gas and recompressed, and the work of recompression represents wasted energy.

Sixsmith and Altmann [5] concluded that the major source of loss of efficiency is due to turbulence, fluid friction and the blade drag. It is by far the greatest and efforts to raise the

efficiency should be directed towards its reduction. They replaced the usual straight radial blades by the aerodynamic blading and also redesigned the flow channel in order to reduce these losses. They proposed a circular cross section flow channel to promote vortex circulation and a minimum of turbulence. In addition to this loss, these authors pointed out leakage loss and carryover loss of compressed gas between the blades as they pass through the stripper. The flow rate delivered by the compressor was reduced by leakage through the clearances. A small fraction of the compressed gas was found to be carried through the stripper from the high pressure region and expanded down to the inlet pressure.

Sixsmith and Altmann [5] suggested that the blade angles should be designed to match fluid angles to ensure smooth entry to the blades to prevent shock losses.

Sixsmith and Altmann [6] adopted Burton idea that the carryover loss might be reduced by extracting some of the compressed gas passing through the stripper and feeding it back at an intermediate pressure to a less harmful flow channel region. The work of recompressing the gas expelled from the cells as they pass through the stripper seal is reduced so that the overall efficiency of the compressor is increased. Engda, Song and Raheel [3] further studied the effect of carry over losses on Sixsmith and Altmann RFC models. They concluded that this effect is more pronounced at lower flow rate.

3.5 Impeller Blade Profile

Many authors have studied regenerative turbomachines with radial blades. Blade shape is also responsible to turbulence and shock losses.

Sixsmith and Altmann [5] studied the regenerative compressor with aerofoil blades. They replaced the radial blades by blades with an aerofoil section. The blades were designed to

transfer momentum to the fluid with a minimum of turbulence and friction. There found an improved in efficiency as compared to radial blades. These authors reported a performance comparison to illustrate the advantages of aerofoil blade RFC over purely radial blade RFC design.

Engda and Raheel [2] conducted a design sensitivity analysis on regenerative flow compressors to propose guidelines and design criteria's. They concluded that, for best performance, the blade angle must be selected in the range between 135^{O} to 150^{O}.

3.6 CFD Work

There is little effort done in the past to apply CFD techniques to solve flow details inside regenerative turbomachines. The computational methods seem very attractive to be applied to regenerative turbomachines because they provide a possibility of analyzing the flow. It enables us to predict the effects of design modifications on performance and gaining a clearer insight into some of the losses.

An attempt to calculate the flow details in regenerative turbomachines was undertaken by Raheel [4] using commercial available CFD software - STAR CD. He used the results of CFD analysis as a comparison tool with the experimental output. He indicated that CFD analysis helps to validate the effect of proposed design changes on performance.

Generally these literatures give me a good insight to my objective. I have found that different geometries of the machine have to be considered to study their effect on the performance of the machine. As describe above the different losses are related to the basic geometries of the machine. The suggested geometry modifications will be considered when RFC models are developed. The flow channel and impeller / blade profile will be varied to alleviate or

minimize the losses in order to gain better performance. In this thesis different blade angles will be considered from the reference radial straight blades to aerofoil blade profiles and optimum performance will be expected in the suggested blade angle ranges.

CFD analysis on RFC will be performed using commercially available CFD software - FLUENT. An effort to calculate the flow in RFCs will be undertaken. The flow patterns inside RFC, as shown in the Figure 2.1 [3], will be examined and based on the results obtained design modifications will be suggested.

CHAPTER FOUR

ANALYSIS OF RFC USING FLUENT

4.1 Introduction

FLUENT is a CFD package for modeling fluid flow and heat transfer. FLUENT provides CAD/GUI based facility packages for generating unstructured meshes to solve flow problems in complex geometries.

The flow characteristics in the analysis of RFC, as described in chapter two are 3D, compressible, viscous, turbulent and rotating flow. It is also assumed to be steady where the flow variables become independent of time. The appropriate physical flow model, which is available in FLUENT, will then be specified based on these flow characteristics of the machine.

In this chapter the necessary governing equations that FLUENT uses to solve the flow in RFC along with the method of numerical computation of the flow variables will be discussed. It is based on the FLUENT documentation [8] which describes the numerical approach to solve the flow variables during CFD simulation.

4.2 Compressible Flow Theory

Compressibility effects are encountered in gas flows at high velocity and/or in which there are large pressure variations.

Compressible flows can be characterized by the value of the Mach number, M given as

$$M = \frac{v}{a} \tag{4.1}$$

Where v is the flow velocity and a is the speed of sound in the gas given as

$$a = \sqrt{\gamma RT} \tag{4.2}$$

If the Mach number is less than 1.0, the flow is termed subsonic. Generally at Mach numbers much less than 1.0 (M < 0.32), compressibility effects are negligible and the variation of the gas density with pressure can safely be ignored in flow modeling. As the Mach number approaches 1.0 (which is referred to as the transonic flow regime), compressibility effects become important. When the Mach number exceeds 1.0, the flow is termed supersonic, and may contain shocks which can impact the flow pattern significantly.

Cates, based on his test data's [4], suggested that the compressibility effects for RFC starts to appear when the value of Mach number is larger than 0.4. The operating machine Mach number for the models developed in this thesis ranges from 0.12 - 0.28, which is much smaller than 0.4. Hence the assumption of compressibility may results in mismatch with the experimental data's.

Physics of Compressible Flows: Compressible flows are typically characterized by the total pressure, p_o and total temperature, T_o of the flow. For an ideal gas, these quantities can be related to the static pressure and temperature by the following relations;

$$\frac{p_o}{p} = \exp\left(\frac{\int_{T}^{T_o} \frac{C_p}{T} dT}{R}\right) \tag{4.3}$$

For constant Cp, equation 4.3 reduces to

$$\frac{p_o}{p} = \left(1 + \frac{\gamma - 1}{2} M^2\right)^{\frac{\gamma}{\gamma - 1}}$$
$$\frac{T_o}{T} = 1 + \frac{\gamma - 1}{2} M^2 \qquad (4.4)$$

These relationships describe the variation of the static pressure and temperature in the flow as the velocity (Mach number) changes under isentropic conditions. For example, given a pressure ratio from inlet to exit (total to static), equation 4.4 can be used to estimate the exit Mach number which would exist in isentropic flow. But the efficiency of RFCs is very low so that we cannot directly apply those isentropic equations.

4.3 Flows in Rotating (Moving) Reference Frame

FLUENT solves the equations of fluid flow and heat transfer, by default, in a stationary (or inertial) reference frame. However, for problem which involves moving parts (such as rotating impellers blades in RFC) it is advantageous to solve the equations in a moving (or non-inertial) reference frame. In RFC since the impeller blades sweep the domain periodically the flow is unsteady in an inertial frame that is a domain fixed in the laboratory frame and the assumption of steady flow may result a mismatch. With a moving reference frame the flow around such moving part can be modeled as a steady-state problem with respect to the moving frame.

The moving cell zone capability in FLUENT provides a powerful set of features for solving problems in which the domain or parts of the domain are in motion like the fluid zones in RFC; one option is to model the flow in an accelerating reference frame. In this situation, the acceleration of the coordinate system is included in the equations of motion describing the

flow. Many such flows can be modeled in a coordinate system that is moving with the rotating equipment and thus experiences a constant acceleration in the radial direction. These classes of rotating flows are treated using the rotating reference frame capability in FLUENT.

4.4 Governing Equations

All the governing equations are based on the physical flow models defined above. These equations are written using inertial reference frame later they will be written in rotating reference frame and in integral form. For flows, FLUENT solves numerically the conservation equations for Mass and Momentum. In RFC since the flow involves compressibility an additional equation for energy conservation is solved. Moreover for turbulent flow an additional transport equations for a fluid in a given flow geometry is solved and the transport equations have different forms depending on the turbulence modeling used.

4.4.1 The Mass Conservation Equation

The equation for conservation of mass, or continuity equation, can be written as follows:

$$\frac{\partial \rho}{\partial t} + \nabla \cdot \left(\rho \vec{v}\right) = s_m \tag{4.5}$$

Equation 4.5 is the general form of the mass conservation equation and is valid for all flows. The source, S_m is the mass added to the continuous phase from the dispersed second phase (e.g., due to vaporization of liquid droplets) and any user-defined sources. This equation can be written to a reduced form for the flow in RFC as;

$$\nabla \cdot \left(\rho \vec{v}\right) = 0 \tag{4.6}$$

4.4.2 Momentum Conservation Equations

Conservation of momentum in an inertial (non-accelerating) reference frame is described by:

$$\frac{\partial}{\partial t}\left(\rho\vec{v}\right)+\nabla\cdot\left(\rho\vec{v}\vec{v}\right)=-\nabla p+\nabla\cdot\left(\bar{\bar{\tau}}\right)+\rho\vec{g}+\vec{F} \tag{4.7}$$

Where p is the static pressure, $\bar{\bar{\tau}}$ is the stress tensor given as;

$$\bar{\bar{\tau}}=\mu\left[\left(\nabla\vec{v}+\nabla\vec{v}^{T}\right)-\frac{2}{3}\nabla.\vec{v}I\right] \tag{4.8}$$

Where μ is the molecular viscosity, I is the unit tensor, and the second term on the right hand side is the effect of volume dilation.

And $\rho\bar{g}$ and $\vec{F}$ are the gravitational body force and external body forces (e.g., that arise from interaction with the dispersed phase), respectively. Also $\vec{F}$ contains other model-dependent source terms such as porous-media and user-defined sources. These terms can be ignored in the analysis of RFC hence the equation is reduced to;

$$\nabla\cdot\left(\rho\vec{v}\vec{v}\right)=-\nabla p+\nabla\cdot\left(\bar{\bar{\tau}}\right) \tag{4.9}$$

FLUENT also solves angular momentum equations for rotating flows. Power transferred to the impeller of RFC is determined from the product of torque and its angular velocity where the torque is the output result of FLUENT after solving the angular momentum equations. A simplified analysis applicable to RFC - Euler turbomachine equation is written as.

$$\frac{\partial}{\partial t}\left(\vec{r}\times\rho\vec{v}\right)+\nabla\cdot\left(\vec{r}\times\vec{v}\,\rho\vec{v}\right)=\vec{\mathrm{T}}_{shaft}+\vec{r}\times\rho\vec{g}+\vec{r}\times\vec{F} \tag{4.10}$$

In RFC analysis usually a large shaft torque is expected. Torques due to surface and body forces may be ignored. For steady flow, equation 4.10 reduces to

$$\vec{\mathrm{T}}_{shaft}=\nabla\cdot\left(\vec{r}\times\vec{v}\,\rho\vec{v}\right) \tag{4.11}$$

4.4.3 The Energy Equation

The energy equation solved by FLUENT correctly incorporates the coupling between the flow velocity and the static temperature, and should be activated whenever we are solving a compressible flow.

FLUENT solves the energy equation in the following form:

$$\frac{\partial}{\partial t}(\rho E)+\nabla\cdot\left(\vec{v}(\rho E+p)\right)=\nabla\cdot\left(k\nabla T-\sum h_j J_j+\left(\bar{\bar{\tau}}\cdot\vec{v}\right)\right)+s_h \tag{4.12}$$

Where k is the effective conductivity (which includes the turbulent thermal conductivity, defined according to the turbulence model being used), and J_i is the species diffusion flux. The first three terms on the right-hand side of equation 4.12 represent energy transfer due to conduction, species diffusion, and viscous dissipation, respectively. S_h includes heat of chemical reaction, and any other volumetric heat sources defined.

For the analysis of RFC the equation is reduced to;

$$\nabla\cdot\left(\vec{v}(\rho E+p)\right)=\nabla\cdot\left(k\,\nabla T+\bar{\bar{\tau}}\cdot\vec{v}\right) \tag{4.13}$$

In equation 4.13, E is the total energy given as

$$E=h-\frac{p}{\rho}+\frac{v^2}{2} \tag{4.14}$$

Where sensible enthalpy, h is defined for ideal gases as;

$$h=\int_{T_{ref}}^{T} C_p\,dT \tag{4.15}$$

Where T_{ref} is 298.15 K

- *Inclusion of Pressure Work and Kinetic Energy Terms*

Equation 4.13 includes pressure work and kinetic energy terms which are often negligible in incompressible flows. Pressure work and kinetic energy are always accounted for when compressible flow are modeled.

- *Inclusion of the Viscous Dissipation Terms*

Equation 4.13 includes viscous dissipation terms, which describe the thermal energy created by viscous shear in the flow. When the pressure based solver (defined later) is used, FLUENT's default form of the energy equation does not include them (because viscous heating is often negligible). When a problem requires inclusion of the viscous dissipation terms and using the segregated solver, the **Viscous Heating** option is activated using the **Viscous Model** panel. When one of the density based solvers (defined later) is used, the viscous dissipation terms are always included when the energy equation is solved.

4.5 Governing Equations in Rotating Reference Frame

When the equations of motion are solved in a rotating frame of reference, the acceleration of the fluid is augmented by additional terms that appear in the momentum equations.

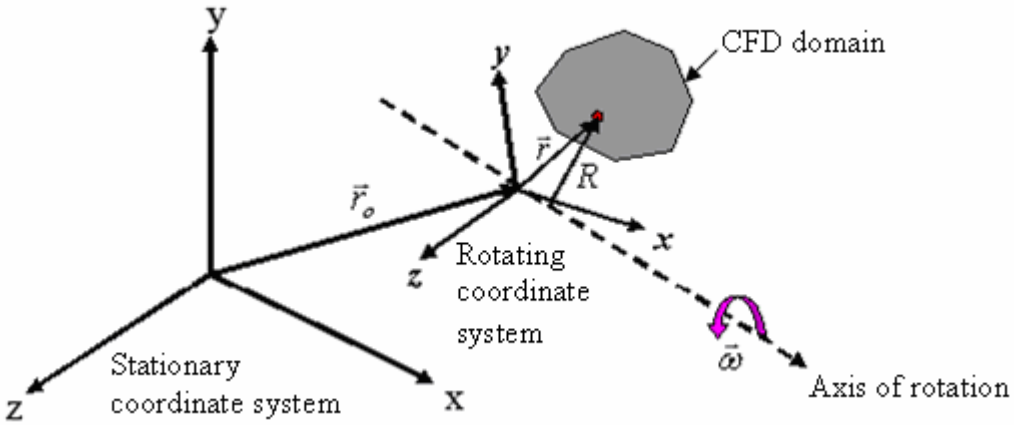

Figure 4.1: Stationary and Rotating Reference Frames ([8])

The computational domain for the CFD problem is defined with respect to the rotating frame such that an arbitrary point in the CFD domain is located by a position vector $\vec{r}$ from the origin of the rotating frame.

Rotating frame problems are solved using either the absolute velocity, $\vec{v}$ (the velocity viewed from the stationary frame), or the relative velocity, $\vec{v}_r$ (the velocity viewed from the rotating frame), as the dependent variable. The two velocities are related by the following equation:

$$\vec{v}_r = \vec{v} - \left(\vec{\omega} \times \vec{r}\right) \tag{4.16}$$

Where, $\vec{u}_r = (\vec{\omega} \times \vec{r})$ is the "whirl" velocity (the velocity due to the moving frame) and $\vec{\omega}$ is the angular velocity of the rotating frame.

Moreover, the governing equations can be formulated in two different ways:

- Expressing the momentum equations using the relative velocities as dependent variables (known as the relative velocity formulation).
- Expressing the momentum equations using the absolute velocities as dependent variables in the momentum equations (known as the absolute velocity formulation).

The selection of those velocity formulations depends on the model geometry. For the simulation of RFC considered in this thesis, since the non-rotating fluid domain in the flow channel is larger than in the impeller blades absolute velocity formulation is recommended for flow analysis.

Absolute Velocity Formulation and Integral form of Governing Equations

For the absolute velocity formulation, the governing equations of fluid flow and in integral form for a steadily rotating frame can be written as follows:

Conservation of mass:

$$\nabla.\left(\rho\vec{v}_r\right)=0 \tag{4.17}$$

The integral form of equation 4.17 can be written as:

$$\oint \rho\vec{v}_r \cdot d\vec{A} = 0 \tag{4.18}$$

Conservation of momentum:

$$\nabla.\left(\rho\vec{v}_r\,\vec{v}\right)+\rho\left(\vec{\omega}\times\vec{v}\right)=-\nabla p+\nabla\bar{\bar{\tau}} \tag{4.19}$$

The integral form of equation for the conservation of momentum can be written as:

$$\oint \rho\vec{v}\,\vec{v}\cdot d\vec{A} = -\oint p.d\vec{A}+\oint\bar{\bar{\tau}}.d\vec{A} \tag{4.20}$$

The integral form of angular momentum equations can be written as:

$$\vec{\mathrm{T}}_{shaft} = \oint\left(\vec{r}\times\vec{v}\,\rho\vec{v}\right).d\vec{A} \tag{4.21}$$

Conservation of energy:

$$\nabla.\left(\rho\vec{v}_r\,H+p\vec{u}_r\right)=-\nabla.\left(k\,\nabla T+\bar{\bar{\tau}}\,\vec{v}_r\right) \tag{4.22}$$

In this formulation, the coriolis, $(2\vec{\omega}\times\vec{v}_r)$ and centrifugal, $(\vec{\omega}\times\vec{\omega}\times\vec{r})$ accelerations can be collapsed into a single term $(\vec{\omega}\times\vec{v})$. In addition, the viscous stress $(\bar{\bar{\tau}})$ is identical to equation 4.8. The energy equation is written in terms of the total enthalpy, *H* also known as the rothalpy and is defined as:

$$H = E+\frac{p}{\rho} \tag{4.23}$$

Where total energy, E is given as:

$$E = h - \frac{p}{\rho} + \frac{1}{2}v^2 \tag{4.24}$$

The integral form of equation 4.22 can be written as:

$$\oint \left(\rho \vec{v}_r H + p\vec{u}_r\right).d\vec{A} = -\oint k\,T.d\vec{A} + \oint \bar{\bar{\tau}}\,\vec{v}_r.d\vec{A} \tag{4.25}$$

4.6 Turbulent Flow Models

Turbulent flows are characterized by fluctuating velocity fields. Since these fluctuations can be of small scale and high frequency, they are too computationally expensive to simulate directly in practical engineering calculations. Instead, the exact governing equations can be time-averaged, ensemble-averaged, or otherwise manipulated to remove the small scales, resulting in a modified set of equations that are computationally less expensive to solve. However, the modified equations contain additional unknown variables, and turbulence models are needed to determine these variables in terms of known quantities. The approach in solving the flow equations for a turbulent flow field is to solve the Reynolds Averaged Navier Stokes (RANS) equations. Reynolds Averaged approach transforms the momentum equations in such a way that the small-scale turbulent fluctuations do not have to be directly simulated. RANS equations represent transport equations for the mean flow quantities only. This greatly reduces the computational effort and all the scales of the turbulence are modeled.

There are various turbulence models available in FLUENT and the choice of those turbulence model depends on the flow model, the level of accuracy required, the available computational resources, and the amount of time available for the simulation. Amongst the realizable $k-\varepsilon$ is the widely accepted turbulence model for practical engineering flow

calculations and is found most appropriate for the CFD analysis of flow inside a RFC. This turbulence model provides better performance for flows involving rotation under adverse pressure gradients, separation, and recirculation.

The realizable $k-\varepsilon$ model is a semi-empirical model based on model transport equations for the turbulence kinetic energy (k) and its dissipation rate (ε). These quantities can be evaluated based on the turbulence specification method used. When the intensity and hydraulic diameter (defined later in next chapter) method is used values for k and ε are evaluated as;

$$k = \frac{3}{2}\left(v_{avg} I\right)^2 \tag{4.26}$$

$$\varepsilon = C_{\mu}^{3/4} \frac{k^{3/2}}{l} \tag{4.27}$$

Where v_{avg} is the mean flow velocity, I is the turbulent intensity given as a ratio of the velocity fluctuations, v' to the mean flow velocity, v_{avg}. $C_{\mu} = 0.09$ is an empirical constant specified for a turbulence model. l is the turbulence length scale and is a physical quantity related to the size of the large eddies that contain the energy in turbulent flows. An approximate relationship for turbulence length is $l = 0.07D_H$ where D_H is the hydraulic diameter of the flow.

4.6.1 Transport Equations for the Realizable k- ϵ Model

The transport equations are the modelling basis for all engineering processes involving momentum, mass or heat transfer. They express the conservation relationship for intensive properties in terms of accumulation, advection, diffusion, generation and destruction.

The modeled transport equations for k and ε in the realizable $k-\varepsilon$ model are,

$$\frac{\partial}{\partial t}(\rho k)+\frac{\partial}{\partial x}(\rho k v)=\frac{\partial}{\partial x}\left[\left(\mu+\frac{\mu_t}{\sigma_k}\right)\frac{\partial k}{\partial y}\right]+G_k+G_b-\rho\varepsilon-Y_M \tag{4.28}$$

and

$$\frac{\partial}{\partial t}(\rho\varepsilon)+\frac{\partial}{\partial y}(\rho\varepsilon v)=\frac{\partial}{\partial x}\left[\left(\mu+\frac{\mu_t}{\sigma_\varepsilon}\right)\frac{\partial \varepsilon}{\partial y}\right]-\rho C_2\frac{\varepsilon^2}{k+\sqrt{v\varepsilon}}+C_{1\varepsilon}\frac{\varepsilon}{k}C_{3\varepsilon}G_b \tag{4.29}$$

In these equations; G_k represents the generation of turbulence kinetic energy due to the mean velocity gradients. From the exact equation for the transport of *k*, the term, G_k may be defined as,

$$G_k=-\rho\overline{u'v'}\frac{\partial v}{\partial x} \tag{4.30}$$

To evaluate G_k in a manner consistent with the Boussinesq hypothesis,

$$G_k=\mu_t S^2 \tag{4.31}$$

Where S is the modulus of the mean rate-of-strain tensor and defined as,

$$S\equiv\sqrt{2S_{ij}S_{ij}} \tag{4.32}$$

G_b is the generation of turbulence kinetic energy due to buoyancy.

Y_M represents the contribution of the fluctuating dilatation in compressible turbulence to the overall dissipation rate.

$$Y_M=2\rho\varepsilon M_t^2 \tag{4.33}$$

Where M_t is the turbulent Mach number, defined as

$$M_t=\sqrt{\frac{k}{a^2}} \tag{4.34}$$

Where $a=\sqrt{\gamma RT}$ is the speed of sound. This compressibility modification always takes effect when the compressible form of the ideal gas law is used.

$C_2 = 1.9$ and $C_{1\varepsilon} = 1.44$ are constants. $\sigma_k = 1.0$ and $\sigma_\varepsilon = 1.2$ are the turbulent Prandtl numbers for k and ε, respectively.

For flow in RFC equations (4.28) and (4.29) can be reduced to,

$$\frac{\partial}{\partial x}(\rho k v) = \frac{\partial}{\partial x}\left[\left(\mu + \frac{\mu_t}{\sigma_k}\right)\frac{\partial k}{\partial y}\right] + G_k - \rho\varepsilon \; - Y_M \tag{4.35}$$

and

$$\frac{\partial}{\partial y}(\rho \varepsilon v) = \frac{\partial}{\partial y}\left[\left(\mu + \frac{\mu_t}{\sigma_\varepsilon}\right)\frac{\partial \varepsilon}{\partial y}\right] - \rho C_2 \frac{\varepsilon^2}{k + \sqrt{\nu\varepsilon}} \tag{4.36}$$

4.7 Numerical Computation

There are two numerical methods used in FLUENT. Either pressure based or density based solver can be used to solve the governing integral equations for the conservation of mass, momentum, energy and other scalars such as turbulence. In both cases a control volume based technique is used which consists of:

- Division of the domain into discrete control volumes using a computational grid.
- Integration of the governing equations on the individual control volumes to construct algebraic equations for the discrete dependent variables ("unknowns") such as velocities, pressure, temperature, and conserved scalars.
- Linearization of the discretized equations and
- Solution of the resultant linear equation system to yield updated values of the dependent variables.

The two numerical methods employ a similar discretization process (finite-volume), but the approach used to linearize and solve the discretized equations is different. For the CFD

analysis of flow through the RFC pressure-based solver, which is a memory-efficient, is used.

4.7. 1 Pressure-Based Segregated Algorithm

The pressure-based solver uses a solution algorithm where the governing equations are solved sequentially (i.e., segregated from one another). Because the governing equations are non-linear and coupled, the solution loop must be carried out iteratively in order to obtain a converged numerical solution.

In the segregated algorithm, the individual governing equations for the solution variables (e.g., u, v, w, p, T, k, ε etc) are solved one after another. Each governing equation, while being solved, is decoupled / segregated from other equations.

The segregated algorithm is memory-efficient, since the discretized equations need only be stored in the memory one at a time. However, the solution convergence is relatively slow, in as much as the equations are solved in a decoupled manner. With the segregated algorithm, each iteration consists of the steps illustrated in the figure and outlined below:

1. Update fluid properties (e.g., density, viscosity, specific heat) on the current solution.
2. Solve the momentum equations (u, v, and w) one after another, using the recently updated values of pressure and face mass fluxes.
3. Solve the pressure correction equation using the recently obtained velocity field and the mass-flux.
4. Correct face mass fluxes, pressure, and the velocity field using the pressure correction obtained from Step 3.

5. Solve the equations for additional scalars, if any, such as turbulent quantities and energy using the current values of the solution variables.
6. Check for the convergence of the equations.

These steps are continued until the convergence criteria are met.

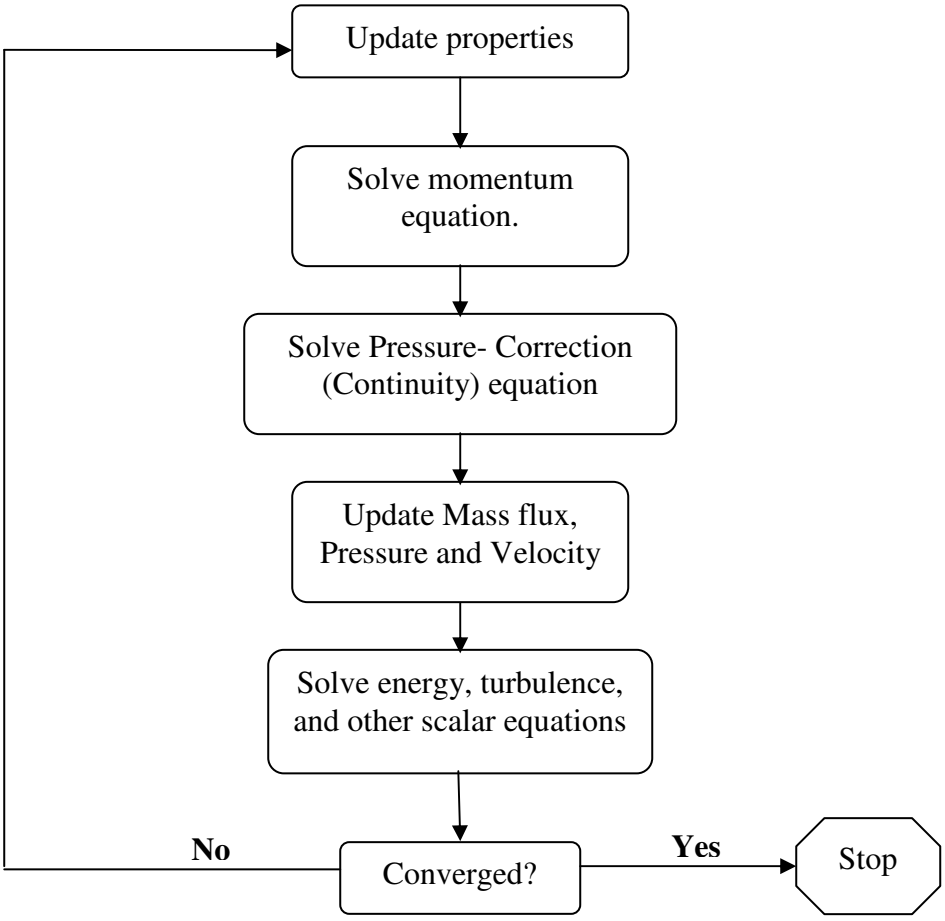

Figure 4.2: Overview of the Pressure-Based Solution Methods [8]

4.7. 2 Discretization Technique in FLUENT

FLUENT uses a control volume based technique to convert a general scalar transport equation to an algebraic equation that can be solved numerically. This control volume

technique consists of integrating the transport equation about each control volume, yielding a discrete equation that expresses the conservation law on a control volume basis.

Considering the integral form of conservation equation of the flow in RFC, for transport of a scalar quantity ϕ for an arbitrary control volume *V*, the discretization of the governing equations is given by:

$$\oint \rho\phi \vec{v}_r \cdot d\vec{A} = \oint \Gamma_\phi \nabla\phi \cdot d\vec{A} \tag{4.37}$$

Where;

ρ = density

$\vec{v}$ = relative velocity vector

$\vec{A}$ = surface area vector

Γ_ϕ = diffusion coefficient for ϕ

$\nabla\phi$ = gradient of ϕ $\left(= \frac{\partial \phi}{\partial x} i + \frac{\partial \phi}{\partial y} j + \frac{\partial \phi}{\partial z} k \right)$

The scalar quantity, ϕ can be 1, v or H when solving the mass, momentum and energy conservation equation respectively. Equation 4.37 is applied to each control volume, or cell, in the computational domain. The two dimensional, triangular cell shown in Figure 4.3 is an example of such a control volume. Discretization of equation 4.37 on a given cell yields,

$$\sum_f^{N_{faces}} \rho_f \vec{v}_{rf} \phi_f \cdot \vec{A}_f = \sum_f^{N_{faces}} \Gamma_\phi (\nabla\phi)_n \cdot \vec{A}_f \tag{4.38}$$

Where;

N_{faces} = number of faces enclosing the cell

ϕ_f = value of ϕ convected through face f

$\rho_f \vec{v}_{rf} \cdot \vec{A}_f$ = mass flux through the face

$\vec{A}_f$ = area of face f, $|A|$ $(= |A_x i + A_y j + A_z|)$

$\nabla \phi_f$ = gradient of ϕ $(= \frac{\partial \phi}{\partial x} i + \frac{\partial \phi}{\partial y} j + \frac{\partial \phi}{\partial z} k)$ normal to face f

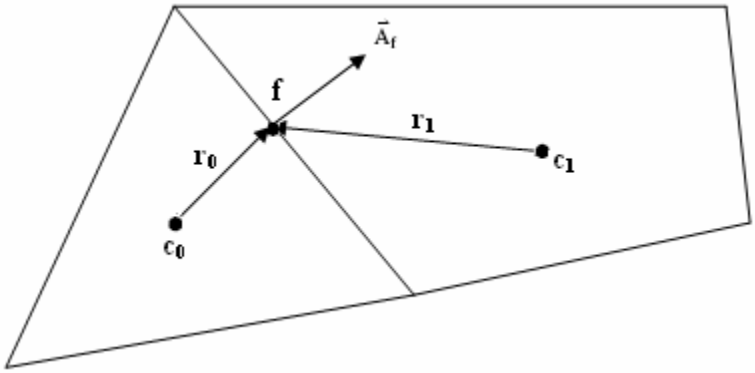

Figure 4.3: Control Volume used to illustrate discretization of a scalar transport equation [8]

4.7.2.1 Solving the Linear System

The discrete, non-linear governing equations are linearized to produce a system of equations for the dependent variables in every computational cell. The resultant linear system is then solved to yield an updated flow-field solution. The discretized scalar transport equation (equation 4.38) contains the unknown scalar variable ϕ at the cell center as well as the unknown values in surrounding neighbor cells.

This equation will, in general, be non-linear with respect to these variables. A linearized form of equation 4.38 can be written as;

$$a_P \phi = \sum_{nb} a_{nb} \phi_{nb} + b \tag{4.39}$$

Where the subscript *nb* refers to neighbor cells, and a_P & a_{nb} are the linearized coefficients for ϕ and ϕ_{nb}.

The number of neighbors for each cell depends on the grid topology, but will typically equal to the number of faces enclosing the cell except the boundary cells.

Similar equations can be written for each cell in the grid. This results in a set of algebraic equations with a sparse coefficient matrix. For scalar equations, FLUENT solves this linear system using a point implicit linear equation solver (Gauss-Seidel scheme) in conjunction with an algebraic multigrid (AMG) method, which will be described later.

4.7.2.2 Spatial Discretization

By default, FLUENT stores discrete values of the scalar ϕ at the cell centers (c_0 and c_1 in Figure 4.3). However, face values ϕ_f are required for the convection terms in equation 4.38 and must be interpolated from the cell center values. This is accomplished using an upwind scheme.

Upwinding means that the face value ϕ_f is derived from quantities in the cell upstream, or "upwind", relative to the direction of the normal velocity v_n in equation 4.38. First-order upwind and second-order upwind schemes have been utilized in the CFD analysis of RFC. They are described as follows;

- ***First-Order Upwind Scheme (FOU)***

When first-order accuracy is desired, quantities at cell faces are determined by assuming that the cell-center values of any field variable represent a cell-average value and hold throughout the entire cell; the face quantities are identical to the cell quantities. Thus when first-order

upwind scheme is selected, the face value ϕ_f is set equal to the cell-center value of ϕ in the upstream cell.

- ***Second-Order Upwind Scheme (SOU)***

When second-order accuracy is desired, quantities at cell faces are computed using a multidimensional linear reconstruction approach. In this approach, higher-order accuracy is achieved at cell faces through a Taylor series expansion of the cell-centered solution about the cell centroid. Thus when second-order upwinding is selected, the face value ϕ_f is computed using the following expression:

$$\phi_f = \phi + \nabla\phi \cdot \vec{r} \tag{4.40}$$

Where ϕ and $\nabla\phi$ are the cell-centered value and its gradient in the upstream cell, and $\vec{r}$ is the displacement vector from the upstream cell centroid to the face centroid.

4.7.2.3 Evaluation of Gradients and Derivatives

Gradients are needed not only for constructing values of a scalar at the cell faces, but also for computing secondary diffusion terms and velocity derivatives. The gradient ϕ of a given variable ϕ is used to discretize the convection and diffusion terms in the flow conservation equations. There are three methods by which gradients are computed in FLUENT these are green-Gauss cell-based, green-Gauss node-based and Least Squares cell-based. All the methods are based on Green-Gauss Theorem which is written as;

$$(\nabla\phi)_{c_0} = \frac{1}{V}\sum_f \bar{\phi}_f \vec{A}_f \tag{4.41}$$

Where ϕ_f is, the value of ϕ at the cell face centroid, computed by the three methods available in FLUENT and V is the cell volume. The summation is over all the faces enclosing the cell.

- ***Green-Gauss Node-Based Gradient Evaluation***

The node-based averaging scheme is known to be more accurate for unstructured meshes (defined later), most notably for triangular and tetrahedral meshes. For green-gauss node-based gradient evaluation ϕ_f can be computed by the arithmetic average of the nodal values on the face.

$$\bar{\phi}_f = \frac{1}{N_f}\sum_{n}^{N_f}\bar{\phi}_n \tag{4.42}$$

Where N_f is the number of nodes on the face.

The nodal values, ϕ_n in equation 4.42, are constructed from the weighted average of the cell values surrounding the nodes. This scheme reconstructs exact values of a linear function at a node from surrounding cell-centered values on arbitrary unstructured meshes by solving a constrained minimization problem, preserving a second-order spatial accuracy.

4.7.2.4 Implicit Linearization

The manner in which the governing equations are linearized may take an "implicit" or "explicit" form with respect to a set of variables of interest. In the pressure based solution method each discrete governing equation is linearized implicitly with respect to that equation's dependent variable. This will result in a system of linear equations with one equation for each cell in the domain. Because there is only one equation per cell, this is sometimes called a "scalar" system of equations. A point implicit linear equation solver is

used in conjunction with an algebraic multigrid (AMG) method to solve the resultant scalar system of equations for the dependent variable in each cell. For example, the x -momentum equation is linearized to produce a system of equations in which u velocity is the unknown. Simultaneous solution of this equation system (using the scalar AMG solver) yields an updated u velocity field. The pressure based approach solves for a single variable field by considering all cells at the same time. It then solves for the next variable field by again considering all cells at the same time, and so on. There is no explicit option for the pressure based solver.

4.7.2.5 Pressure Interpolation and Pressure - Velocity Coupling

The momentum and continuity equations are solved sequentially. In this sequential procedure, the continuity equation is used as an equation for pressure.

The discrete form of the x-momentum equation can be derived from equation 4.39 as;

$$a_{\mathrm{P}}u = \sum_{nb} a_{nb}u_{nb} + \sum p_f A \cdot \hat{i} + S \tag{4.43}$$

If the pressure field and face mass fluxes were known, equation 4.43 could be solved and a velocity field obtained. However, the pressure field and face mass fluxes are not known a priori and must be obtained as a part of the solution. The important issues with respect to the storage of pressure and the discretization of the pressure gradient term are discussed next. FLUENT uses a co-located scheme, whereby pressure and velocity are both stored at cell centers. However, equation 4.43 requires the value of the pressure at the face between cells c_0 and c_1. The second-order scheme for pressure interpolation reconstructs the face pressure in the manner used for second-order accurate convection terms. This scheme may provide

some improvement over the standard and linear schemes for compressible flow. But it may have some trouble if it is used at the start of a calculation and/or with a bad mesh, hence it is recommended to start with standard scheme for few iterations.

The discrete form of the continuity equation can also be given as;

$$\sum_{f}^{N_{faces}} J_f A_f = 0 \tag{4.44}$$

Where J_f is the mass flux through face, f given as, ρv_n.

In order to proceed further, it is necessary to relate the face values of velocity, $\vec{v}_n$ to the stored values of velocity at the cell centers. Linear interpolation of cell-centered velocities to the face results in unphysical value of pressure. To prevent this the face value of velocity is not averaged linearly instead momentum weighted averaging, using weighting factors based on the a_P coefficient from equation 4.39, is performed. Using this procedure, the face flux J_f may be written as;

$$J_f = \hat{J}_f + d_f (p_{\varepsilon 0} - p_{\varepsilon 1}) \tag{4.45}$$

Where $p_{\varepsilon 0}$ and $p_{\varepsilon 1}$ are the pressures within the two cells on either side of the face, and $\hat{J}_f$ contains the influence of velocities in these cells. The term d_f is a function of $\bar{a}_P$.

The SIMPLE (Semi-Implicit Method for Pressure-Linked Equations) algorithms is used for introducing pressure into the continuity equation. Pressure-velocity coupling is achieved by using equation 4.45 to derive an equation for pressure from the discrete continuity equation.

The SIMPLE algorithm uses a relationship between velocity and pressure corrections to enforce mass conservation and to obtain the pressure field.

If the momentum equation is solved with a guessed pressure field p^*, the resulting face flux, J_f^* computed from equation 4.45 does not satisfy the continuity equation.

$$J_f^* = \hat{J}_f^* + d_f(p_{\varepsilon 0}^* - p_{\varepsilon 1}^*) \tag{4.46}$$

Consequently, a correction $J_f^{'}$ is added to the face flux J_f^* so that the corrected face flux J_f satisfies the continuity equation.

$$J_f = J_f^* + J_f^{'} \tag{4.47}$$

The SIMPLE algorithm postulates that $J_f^{'}$ be written as;

$$J_f^{'} = d_f\left(p_{c0}^{'} - p_{c1}^{'}\right) \tag{4.48}$$

Where $p^{'}$ is the cell pressure correction

The SIMPLE algorithm substitutes the flux correction equations (equations 4.47 and 4.48) into the discrete continuity equation (equation 4.44) to obtain a discrete equation for the pressure correction $p^{'}$ in the cell;

$$a_P p^{'} = \sum_{nb} a_{nb} p_{nb}^{'} + b \tag{4.49}$$

Where the source term b is the net flow rate into the cell;

$$b = \sum_{f}^{N_{faces}} J_f^* A_f \tag{4.50}$$

The pressure-correction equation (equation 4.49) may be solved using the algebraic multigrid (AMG) method (described later). Once a solution is obtained, the cell pressure and the face flux are corrected using;

$$p = p^* + \alpha_p p^{'} \tag{4.51}$$

$$J_f = J_f^* + d_f(p'_{\varepsilon 0} - p'_{\varepsilon 1}) \tag{4.52}$$

Here α_P is the under-relaxation factor for pressure. The corrected face flux, J_f satisfies the discrete continuity equation identically during each iteration.

4.7.2.6 Density Interpolation Schemes

For compressible flow calculations (i.e., calculations that use the ideal gas law for density), FLUENT applies upwind interpolation of density at cell faces. Several interpolation schemes are available for the density up-winding at cell faces. The first-order upwind scheme (the default) provides stability for the discretization of the pressure-correction equation, and gives good results for most classes of flows.

4.7.2.7 Under-Relaxation

Because of the nonlinearity of the equation set being solved by FLUENT, it is necessary to control the change of ϕ during iteration. This is typically achieved by under-relaxation, which reduces the change of ϕ produced during each iteration. It is the main technique by which the solver is stabilised. In a simple form, the new value of the variable ϕ within a cell depends upon the old value (ϕ_{old}) the computed change in ϕ ($\Delta\phi$) and the under-relaxation factor (α) as follows;

$$\phi = \phi_{old} + \alpha\Delta\phi \tag{4.53}$$

Reducing the under-relaxation factor α will stabilise the solver at the expense of slowing the rate of convergence.

4.8 Multigrid Method

FLUENT uses a multigrid scheme to accelerate the convergence of the solver by computing corrections on a series of coarse grid levels. The use of this multigrid scheme can greatly reduce the number of iterations and the computer processing time required to obtain a converged solution, particularly when the model contains a large number of control volumes.

4.8.1 The Need for Multigrid

Implicit solution of the linearized equations on unstructured meshes is complicated by the fact that there is no equivalent of the line-iterative methods that are commonly used on structured grids. Point implicit solvers like Gauss-Seidel method are the best choices for solving realistic problems on unstructured meshes. Although the Gauss-Seidel scheme rapidly removes high-frequency errors in the solution, low-frequency errors are reduced at a rate inversely related to the grid size. Thus, for a large number of nodes, the solver stalls and the residual reduction rate becomes prohibitively low.

Multigrid techniques allow global error to be addressed by using a sequence of successively coarser meshes. This method is based upon the principle that low-frequency error existing on a fine mesh can be represented on a coarse mesh where it again becomes accessible as high-frequency error, because there are fewer coarse cells overall, the global corrections can be communicated more quickly between adjacent cells. Since computations can be performed at exponentially decaying expense in both CPU time and memory storage on coarser meshes, there is the potential for very efficient elimination of global error. The fine-grid relaxation scheme or smoother, in this case the point-implicit Gauss-Seidel, is not required to be

particularly effective at reducing global error and can be tuned for efficient reduction of local error.

4.8.2 Algebraic Multigrid (AMG)

This algorithm is referred to as an algebraic multigrid scheme because the coarse level equations are generated without the use of any geometry or re-discretization on the coarse levels a feature that makes AMG particularly attractive for use on unstructured meshes. The advantage being that no coarse grids have to be constructed or stored, and no fluxes or source terms need be evaluated on the coarse levels. However, once the system is linearized, non-linearities are not felt by the solver until the fine level operator is next updated, which is a demerit for non-linear problems, since non-linearities in the system are carried down to the coarse levels through the re-discretization.

Consider the set of discretized linear (or linearized) equations given by,

$$A\phi_e + b = 0 \tag{4.54}$$

Where ϕ_e is the exact solution.

Before the solution has converged there will be a defect, d associated with the approximate solution ϕ;

$$A\phi + b = d \tag{4.55}$$

We seek a correction ψ to ϕ such that the exact solution is given by,

$$\phi_e = \phi + \psi \tag{4.56}$$

Substituting equation 4.56 into equation 4.54 gives,

$$A(\phi + \psi) + b = 0 \tag{4.57}$$

$$A\psi + (A\phi + b) = 0 \tag{4.58}$$

Now using equations 4.55 and 4.58 we obtain,

$$A\psi + d = 0 \tag{4.59}$$

Which is an equation for the correction in terms of the original fine level operator A and the defect, d. Assuming the high-frequency errors have been sufficiently damped by the relaxation scheme on the fine level, the correction ψ will be smooth and therefore more effectively solved on the next coarser level.

4.9 Standard Wall Functions

Wall functions are a collection of semi-empirical formulas and functions that in effect link the solution variables at the near-wall cells and the corresponding quantities on the wall. They are used to bridge the viscosity affected region between the wall and the fully turbulent region. The basis of standard wall functions in FLUENT is most widely used for industrial flows.

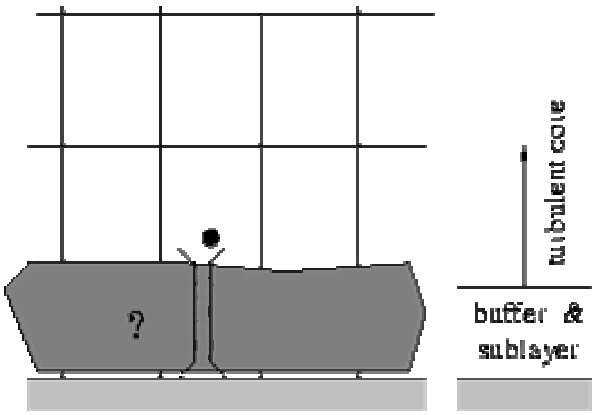

Figure 4.4: Near-Wall Treatments in FLUENT [8]

Momentum

The law-of-the-wall for mean velocity, U^* yields:

$$U^* = \frac{1}{\kappa}\ln(E\, y^*) \tag{4.60}$$

Where,

$$U^* \equiv \frac{U_P C_\mu^{1/4} k_P^{1/2}}{\tau_\omega / \rho}$$

$$y^* = \frac{\rho C_\mu^{1/4} k_P^{1/2} y_P}{\mu}$$

and κ = von Kármán constant (= 0.42)

E = empirical constant (= 9.793)

C_μ = empirical constant (= 0.09)

U_P = mean velocity of the fluid at point P

k_P = turbulence kinetic energy at point P

y_P = distance from point P to the wall

μ = dynamic viscosity of the fluid

The logarithmic law for mean velocity is known to be valid for $y^* >$ about 30 to 60. In FLUENT, the log-law is employed when $y^* > 11.225$.

When the mesh is such that $y^* < 11.225$ at the wall-adjacent cells, FLUENT applies the laminar stress-strain relationship that can be written as,

$$U^* = y^* \tag{4.61}$$

It should be noted that, in FLUENT, the laws-of-the-wall for mean velocity and temperature are based on the wall unit, y^* rather than $(y^+ \equiv \rho u_\tau y / \mu)$. These quantities are approximately equal in equilibrium turbulent boundary layers.

Energy

The law-of-the-wall implemented in **FLUENT** has the following composite form,

$$T^* = \frac{\left(T_w - T_p\right)\rho C_p C_\mu^{1/4} k_p^{1/2}}{q''}$$

$$= \begin{cases} pr\, y^* + \frac{1}{2}\rho\, pr \frac{C_\mu^{1/4} k_p^{1/2}}{q''} U_p^2 & (y^* < y_T^*) \\ pr_t\left[\frac{1}{k}\ln(E_y^*) + P\right] + \frac{1}{2}\rho \frac{C_\mu^{1/4} k_p^{1/2}}{q''}\left\{pr_t U_p^2 + (pr - pr_t)U_c^2\right\} & (y^* > y_T^*) \end{cases}$$

(4.62)

Where P is computed by using the formula,

$$P = \frac{\pi/4}{\sin(\pi/4)}\left(\frac{A}{k}\right)^{1/2}\left(\frac{pr}{pr_t} - 1\right)\left(\frac{pr_t}{pr}\right)^{1/4} \tag{4.63}$$

and

k_f = thermal conductivity of fluid

ρ = density of fluid

c_p = specific heat of fluid

q'' = wall heat flux

T_P = temperature at the cell adjacent to wall

T_w = temperature at the wall

Pr = molecular Prandtl number

Pr_t = turbulent Prandtl number (0.85 at the wall)

A = Van Driest constant (= 26)

k = 0.42 (von Karman's constant)

E = 9.793 (wall function constant)

U_c = mean velocity magnitude at $y^* = y_T^*$

Note that, for the segregated solver, the terms

$$\frac{1}{2}\rho\, pr \frac{C_\mu^{1/4} k_p^{1/2}}{q''} U_p^2$$

and

$$\frac{1}{2}\rho \frac{C_\mu^{1/4} k_p^{1/2}}{q''} \left\{ pr_t U_p^2 + (pr - pr_t) U_c^2 \right\}$$

will be included in equation 4.62 only for compressible flow calculations.

The non-dimensional thermal sub-layer thickness, y^*_T, in equation 4.62 is computed as the y^* value at which the linear law and the logarithmic law intersect, given the molecular Prandtl number of the fluid being modeled. The procedure of applying the law-of-the-wall for temperature is as follows. Once the physical properties of the fluid being modeled are specified, its molecular Prandtl number is computed. Then, given the molecular Prandtl number, the thermal sub-layer thickness, y^*_T, is computed from the intersection of the linear and logarithmic profiles, and stored.

During the iteration, depending on the y^* value at the near-wall cell, either the linear or the logarithmic profile in equation 4.62 is applied to compute the wall temperature T_w or heat flux q'' (depending on the type of the thermal boundary conditions).

Turbulence

In the $k-\varepsilon$ models, the k equation is solved in the whole domain including the wall-adjacent cells. The boundary condition for k imposed at the wall is,

$$\frac{\partial k}{\partial n} = 0 \tag{4.64}$$

Where n is the local coordinate normal to the wall.

The production of kinetic energy, G_k and its dissipation rate, ε at the wall-adjacent cells are computed on the basis of the local equilibrium hypothesis. Under this assumption, the production of k and its dissipation rate are assumed to be equal in the wall-adjacent control volume.

Thus, the production of k is computed from,

$$G_k \approx \tau_\omega \frac{\partial U}{\partial y} = \tau_\omega \frac{\tau_\omega}{\kappa \rho C_\mu^{1/4} k_P^{1/2} y_P} \tag{4.65}$$

and ε is computed from:

$$\varepsilon_P = \frac{C_\mu^{3/4} k_P^{3/2}}{\kappa y_P} \tag{4.66}$$

The ε equation is not solved at the wall-adjacent cells, but instead is computed using equation 4.66.

As shown here, the wall boundary conditions for the solution variables, including mean velocity, k and ε are all taken care of by the wall functions; therefore, no need to be concerned about the boundary conditions at the walls.

The standard wall functions work reasonably well for a broad range of wall-bounded flows. However, they tend to become less reliable when the flow situations depart too much from the ideal conditions that are assumed in their derivation. Among others, the constant-shear

and local equilibrium hypotheses are the ones that most restrict the universality of the standard wall functions. Accordingly, when the near-wall flows are subjected to severe pressure gradients, and when the flows are in strong non-equilibrium, the quality of the predictions is likely to be compromised.

CHAPTER FIVE

RFC MODIFICATION AND SIMULATION PROCEDURES

5.1 Introduction

Capstone Turbine Corporation, CA [4] has tested single stage RFCs with air as working fluids. The base machine for the CFD study in this thesis is taken from the non-dimensionalized geometric and performance data's for single stage RFCs that are available from CA. This base machine is a commercially available RFC for the compression of natural gas in a microgasturbine application. It will be analyzed using FLUENT and the output results are compared with the existing tested data's of the machine. Various modifications will be done on the basic geometries with the intent of reducing the different losses and each will be compared with the base machine.

The objective of this chapter is to:

- introduce non-dimensional design parameters which are used in the design and performance investigation of a regenerative flow compressor,
- introduce the geometry and performance characteristic of the base machine,
- describe the major losses that are responsible for a low efficiency in RFC,
- present the various modification proposed on the base machine together with the reason of the proposal and
- present the major steps involved in the simulation analysis of the machines using FLUENT. This includes building of the geometry, meshing, processing

in FLUENT, displaying and reporting of simulation results. Where these results of the analysis will then be discussed in detail in chapter six.

This chapter starts by introducing the non-dimensional parameters used in the design and performance investigation of a RFC.

5.2 Non-dimensional Design Parameters

The parameters such as the flow rate, speed and power can be made dimensionless and be used for the performance comparison. Dimensional analysis of turbomachines is employed to normalize these performance parameters by using geometric variable, controlled variable and fluid properties. These three variables includes impeller tip diameter which determines the shape and size of the machine; inlet density, ratio of specific heat and the inlet sonic velocity of the gas which characterizes the flow; and shaft speed which is an externally observed variable controlled by the motor.

The following six non-dimensional parameters are used in the design and performance analysis of a regenerative flow compressor. These are; pressure ratio, impeller tip (machine) Mach number, isothermal efficiency, power coefficient, flow coefficient and specific mass flow rate; and are discussed below.

a. ***Pressure Ratio***, π***:*** the job of RFC is to increase the pressure of the fluid. This increase in pressure is measured by the compressor pressure ratio (CPR) given as a ratio of outlet to inlet total pressure.

$$\text{CPR, } \pi = \frac{p_{out}}{p_{in}} \tag{5.1}$$

b. ***Impeller Tip (Machine) Mach Number***, M_{OT}*:* it is a non-dimensional parameter defined as the ratio of the impeller tip speed to the inlet sonic velocity of the gas.

$$M_{OT} = \frac{u_2}{a_{in}}$$

$$\Rightarrow M_{OT} = \frac{r_2 \omega}{\sqrt{\gamma R_{gas} T_{in}}} \tag{5.2}$$

c. ***Isothermal Efficiency***, η_{iso}***:*** RFC usually operates under isothermal condition. During compression the compressor work / power can be reduced by maintaining the temperature of the gas as low as possible, i.e. $T_{in} = T$ = Constant. Isothermal efficiency is then used to qualify the mass flow and power performance characteristics of RFC.

At constant temperature the equation of state becomes,

$$pV = mR_{gas}T_{in} = \text{constant}$$

$$\Rightarrow p_1V_1 = p_2V_2 = pV = \text{constant}$$

$$\Rightarrow p = \frac{p_1V_1}{V} = \frac{mR_{gas}T_{in}}{V} \tag{5.3}$$

The work, W_S which is theoretically required to compress a gas under constant temperature from a given inlet pressure to discharge pressure can be determined from;

$$W_S = \oint pdV$$

$$\Rightarrow W_S = mR_{gas}T_{in} \ln\left(\frac{p_{out}}{p_{in}}\right) \tag{5.4}$$

And the theoretical power is given as;

$$\dot{W}_S = \dot{m} R_{gas}T_{in} \ln\left(\frac{p_{out}}{p_{in}}\right) = \dot{m} R_{gas}T_{in} \ln(\pi) \tag{5.5}$$

The actual power delivered, $\dot{W}_a$ can be determined from the product of torque and angular speed, ω of the shaft;

$$Power\ Drawn = \dot{W}_a = \mathrm{T}_{shaft} \times \omega \tag{5.6}$$

Hence isothermal efficiency is defined as the ratio of isothermal power to actual power.

$$\eta_{iso} = \frac{\dot{W}_S}{\dot{W}_a}$$

$$\Rightarrow \eta_{iso} = \frac{\dot{m} R_{gas} T_{in} \ln(\pi)}{\mathrm{T}_{shaft} \times \omega} \tag{5.7}$$

d. ***Flow Coefficient***, λ***:*** the flow coefficient is a dimensionless parameter used in RFC design and performance analysis where the suction (inlet) volume flow rate, Q_S is normalized by the impeller tip diameter, *D* and angular speed of the machine.

$$\lambda = \frac{Q_S}{\omega D^3}$$

$$\Rightarrow \lambda = \frac{\dot{m}}{8 \rho_{in} \omega r_2^{\ 3}} \tag{5.8}$$

e. ***Power Coefficient***, Υ***:*** the power coefficient is also a non-dimensional parameter where the power drawn is normalized by the impeller tip diameter, inlet density and angular speed of the machine.

$$\Upsilon = \frac{Power\ Draw}{\rho_{in} \omega^3 D^5}$$

$$\Rightarrow \Upsilon = \frac{Power\ Draw}{32\rho_{in}\omega^3 r_2^{\ 5}} \tag{5.9}$$

f. ***Specific Mass Flow Rate***, ϕ***:*** Specific Mass Flow Rate is another non-dimensional parameter defined by normalizing mass flow rate through the machine using the impeller tip diameter, inlet density and inlet sonic velocity of the gas. It is given as;

$$\phi = \frac{\dot{m}}{\rho_{in}\ a_{in}\ D^2}$$

Substituting ideal gas relation for density;

$$\phi = \frac{\dot{m}}{(p_{in}/RT_{in})(\sqrt{\gamma R_{gas}T_{in}})\ D^2}$$

$$\Rightarrow \phi = \frac{\dot{m}}{4r_2^2\ p_{in}}\sqrt{\frac{R_{gas}T_{in}}{\gamma}} \tag{5.10}$$

Where $r_2\ (=\frac{D}{2})$ is impeller tip radius in m, ω is the angular speed in rad/s, u_2 is impeller tip speed in m/s, T_{in} is inlet temperature of gas in K, γ is ratio of specific heat, p is the total pressure in Pa, Q_S is volume flow rate at inlet in m^3/s, R_{gas} is gas constant in J/ kg K, ρ_{in} is the density of the gas at inlet in kg/m^3, T_{shaft} is the shaft power (power transferred to the impeller) in N-m, a_{in} is the inlet sonic velocity in m/s and $\dot{m}$ is the mass flow rate in kg/s.

5.3 Base Regenerative Flow Compressor

Microgasturbines are employed for small scale power generation. They offer a number of advantage compared to other technologies of the same. This advantage includes a small

number of moving parts, compact size, light weight, greater efficiency, lower emission and opportunity to use waste fuels [4]. They can burn various types of fuels but usually natural gas because it provides the advantage of less cost, no storage problems, cleaner burning, less NO emissions and more power output at higher efficiency. As compared to a high cost centrifugal compressors, RFC is highly accepted for raising a low pressure natural gas supply to that required for injection into the combustion system at low flow rate. And RFC operates with better performance.

For this purpose four different geometric configuration of a single stage RFCs were tested by Capstone Turbine Corporation, CA. All has the same impeller tip diameter and they consist of a straight and radial blade with rectangular flow channel. The differences between these configurations are the impeller hub diameter and the width of the flow channel. Among the different configuration, configuration 3 (***S3***) has higher pressure ratio and better efficiency. But the flow channel geometry, where its cross sectional area varies linearly from inlet to exit port, lacks data to develop the model hence configuration 4 (***S4***) is considered as a base machine. Configuration 4 (***S4***) has a constant flow channel cross sectional area. It has nearly the same pressure ratio and close efficiency with configuration 3 (***S3***).

5.3.1 Dimensions of the Base Machine

Non-dimensionalized geometric data of configuration 4(***S4***) is presented in Table 5.1. Stations A and B refer to peripheral locations near inlet and outlet respectively. Below a schematic diagram of impeller and flow channel shape is shown for the base machine.

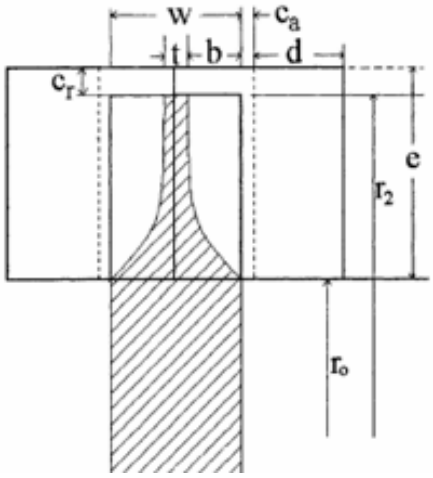

Figure 5.1: Schematic of impeller and flow channel geometry for single stage RFC (Raheel [4]).

The impeller tip radius is, $r_2 = 41.91mm$

Table 5.1: Non-dimensionalized geometric data's for configuration 4 (***S4***) in reference to Figure 5.1

Non-Dimensional				
radius ratio $\frac{r_2}{r_0}$	blade depth $\frac{b}{r_2}$	blade height $\frac{e}{r_2}$	radial clearance $\frac{c_r}{r_2}$	blade thickness $\frac{t}{r_2}$
0.757	0.0606	0.298	0.0566	0.018
Non-Dimensional				
axial clearance $\frac{c_a}{r_2}$	depth at inlet $\frac{d_A}{r_2}$	depth at exit $\frac{d_B}{r_2}$	channel area ratio $\frac{A_{in}}{A_{out}}$	pitch to cord length ratio PC
0.00302	0.0908	0.0908	1	0.287

Chord length: flow path length in the impeller blades,

$$cl = r_2 - r_0 \tag{5.11}$$

Pitch length: the peripheral spacing between blades,

$$pl = \frac{2\pi\ r_2}{Z_b} \tag{5.12}$$

Where Z_b is the number of blade

Table 5.2: Geometric data's calculated for ***S4***

Geometry	Dimensions in *mm*
r_2	41.91
r_0	31.726
e	12.489
b	2.539
t	0.754
d	3.8054
cl	10.184

And number of blades,

Z_b	90

5.3.2 Operation Points of the Base Machine

The operation points of the base machine is obtained from the experimental data's for a single stage RFCs tested by Capstone Turbine Corporation. It is designed to operate at:

Impeller tip Mach number, $M_{OT} = 0.36$

Rotational speed, ω= 28,910 rpm

Pressure ratio, Π = 1.3

Inlet temperature, T_{in} = 70^0F (294.26K)

Inlet pressure, p_{in} = 100000 Pa

During the test, air is used as a working fluid but here it is also simulated using natural gas. The properties of both gases are:

For air;

Molecular weight, M = 28.97 kg/K mol

C_{pa} = 1005.244 J/ kg K C_{va} = 718 J/kg K

R_a = 287 J/kg K

Ratio of specific heat, γ = 1.4

For natural gas;

Molecular weight, M = 16 kg/K mol

C_{pNG} = 2253.7 J/ kg K C_{vNG} = 1735.4 J/kg K

R_{NG} = 518.3 J/kg K

Ratio of specific heat, γ = 1.31

5.3.3 Performance characteristic of the Base Machine

Below the performance characteristics for the base machine is shown for comparison and discussion purpose. From the performance characteristics a peak isothermal efficiency of 8.1% can be obtained at Mach number 0.325 and specific flow rate of $9.73x10^{-4}$. The corresponding pressure ratio at these operating points is 1.19. Performance at operation points is calculated by correlating the test data's and it is found that an efficiency of 8.13%

can be achieved for configurations 4. Hence, this can be used as the start for the improvement of performance.

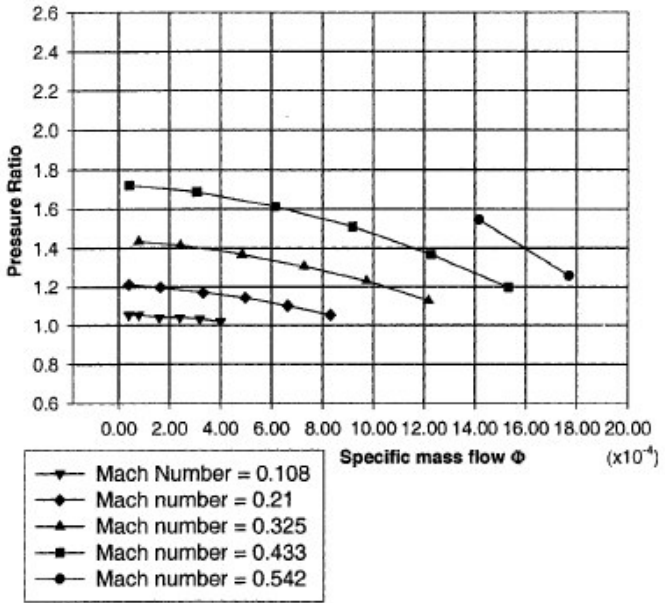

Figure 5.2: Pressure ratio vs Specific mass flow rate at various tip Mach number (Raheel [4])

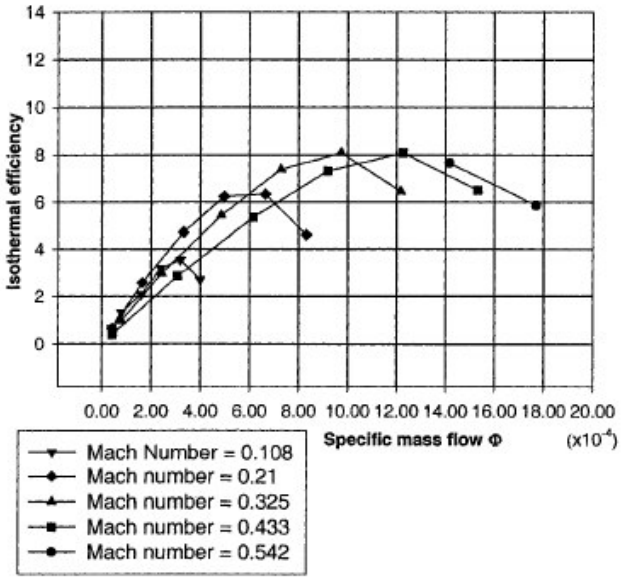

Figure5.3: Isothermal efficiency vs Specific mass flow rate at various tip Mach number (Raheel [4])

5.4 Modification of the Base RFC

Many literatures state that the different losses in RFC are highly related to the geometry of the machine. Some modifications are then made on the base machine to improve the performance by reducing these losses. Before discussing the modification done it is imperative to see in detail the major losses in RFC.

5.4.1 Major Losses in RFC

The major losses in RFC are turbulent loss, shock loss, inlet and outlet losses, carry-over loss and leakage loss. They are described as follows:

- ***Turbulent Loss***

In a regenerative compressor a major source of loss of efficiency is due to turbulence, fluid friction and the blade drag. Turbulence is caused by 180° turn of the fluid through the flow channel without guide vanes. Mixing of a fluid after passing through blade with incoming stream of flow from the flow channel and a sudden expansion due to an increase in flow area when fluid flows from blades to flow channel region are also causes for turbulence. Blade drag is caused by pressure difference between any two adjacent blades of an impeller; it causes a secondary circulation about each blade such that the fluid leaving the impeller deviates from the path prescribed by the blade surface, backwards with respect to the positive direction of impeller rotation. The result is that the fluid tangential velocity at exit is less than that which would be expected from the velocity triangle based on the outlet blade angle.

Hence to promote circulation with minimum turbulence, friction and blade drag a careful design of the flow channel and impeller / blade profile is necessary for the reduction of this loss.

- ***Shock loss***

Shock or incidence losses are caused by difference between blade angle and flow angle when fluid enters the blades. Flow channels should be designed properly to avoid a huge mismatch between the blade angle and fluid angle. The blade angles also are designed to match fluid angles to ensure smooth entry to the blades.

- ***Inlet and outlet losses***

Some losses are also introduced at the inlet and outlet ports. To reduce these losses the inlet port should be designed to project the fluid towards the inlet edge of the blade with the velocity and direction needed to ensure smooth entry. The outlet port should be followed by a conical diffuser to reduce the fluid velocity there by converting some of the kinetic energy to a further gain in pressure.

- ***The Carry - Over loss***

When the blades enter the stripper seal between the outlet and inlet ports, compressed gas in the blade passages is carried through the stripper seal from the high pressure delivery region to the low pressure inlet region. Gas is carried through at the delivery pressure and expanded down to the inlet pressure as the pockets between the blades open into the flow channel at the inlet end. The stream which escapes from the blade pockets is mixed with the incoming gas and recompressed, and the work of recompression represents wasted energy. The flow rate and the high pressure of the expelled stream cause the inlet flow rate to reduce, this represent unavoidable loss of efficiency.

- ***Leakage losses***

This is also other source of loss where the flow rate is reduced due to leakage through the clearance spaces.

During the simulation of RFC the last two losses are not optimized. In the actual machine to reduce carry-over loss decompression ducts (pipes) may be employed to extract the compressed gases from the blade pockets and return it to the flow field with relatively higher pressure magnitude than the inlet and leakages are also considered. Therefore this will results in mismatch with the experimental data's.

5.4.2 Modification on the Basic Geometries

Referring the previous discussion, the lower efficiency of the base machine is due to these losses caused by its geometry. To improve the performance of the machine the following modifications are made on the basic geometries.

a. Rectangular flow channel area and straight impeller do not guide the flow properly and there can be huge mismatch between the blade and flow angle (*see figure 5.5*). Therefore first the flow channel is modified to be semi-circular in cross section and the impeller is made semi-elliptic. By doing this the flow is guided properly and circulation is promoted with minimum losses.

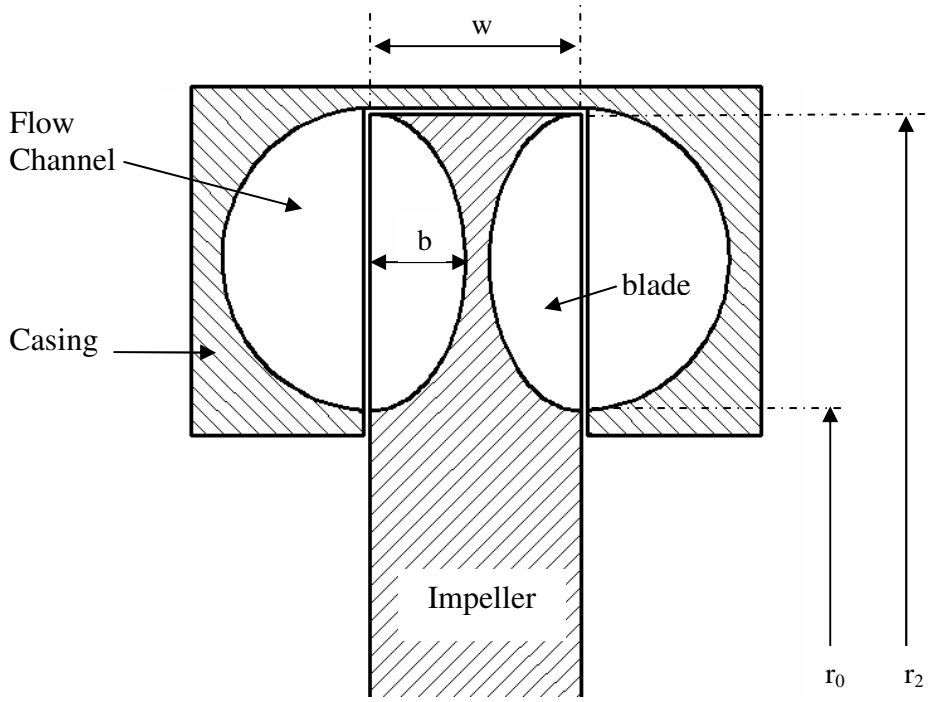

Figure 5.4: Modified schematic of flow channel and impeller geometry.

b. To ensure smooth entry to the blades, the blades angle should be modified to match with the fluid angle. Many authors suggest that turbulence, fluid friction and shock losses are minimized by changing the blades angle / chevroning, also increases the pressure ratio. The flow is guided and circulation is well promoted so that better performance can be obtained. The modified geometry above (Figure 5.4) is then used as a base for developing the blade variations considered. The flow channel and impeller profile are the same for all blades angle variations.

The blade geometries considered and velocity triangles in the flow field are shown below;

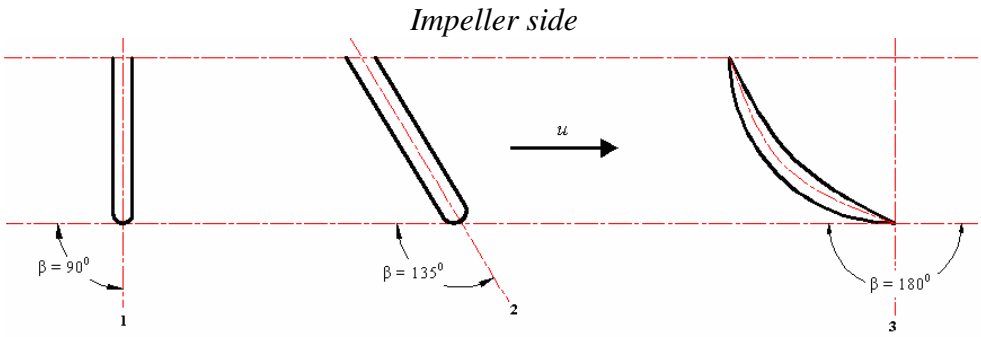

** Developed cylindrical view at mean radius and β is measured in the direction perpendicular to the peripheral velocity.*

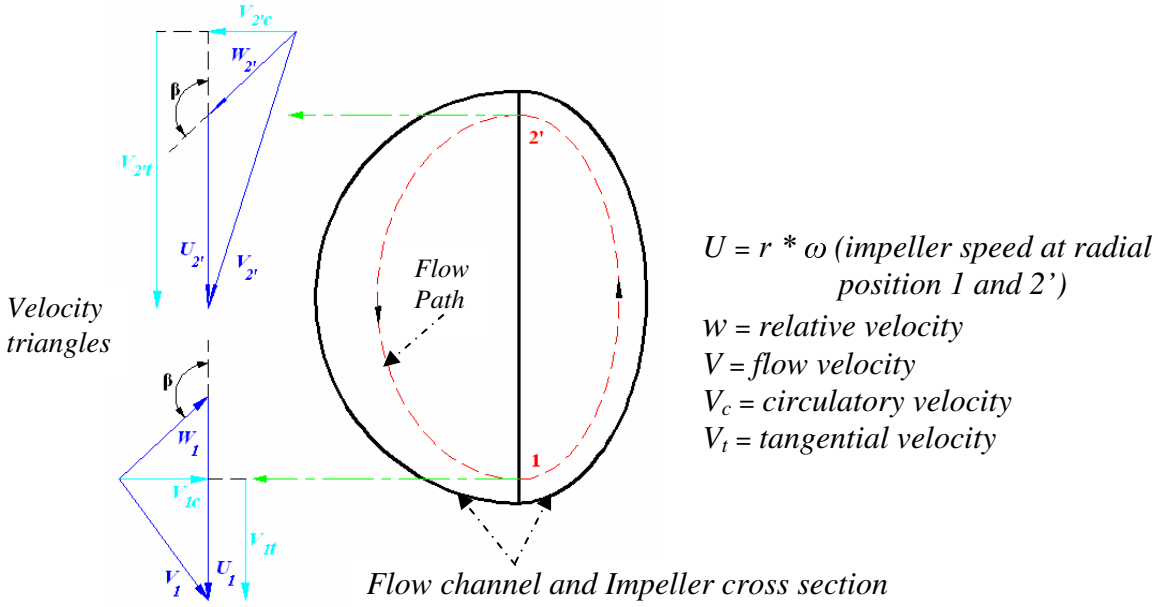

Figure 5.5: Blade variations with blade angle - β and velocity triangles on the cross section of the flow field.

In figure 5.5 the first blade angle is for the base machine and the others are for the modified geometry in **a**. The aerofoil blade sections be drawn using a circle on the outer and an arc on the inner side by maintaining the blade thickness at the mid-point. In figure 5.6-3 the blade profile is for $\beta = 180^0$ we have also a similar profile for $\beta = 135^0, 145^0, 150^0$ and 160^0.

c. To see the effect of flow channel area on friction and turbulent losses only the flow channel is modified to semi-elliptic by maintaining the optimum blade angle ($\beta = 145^0$ where better performance is obtained among the other six blade angles) and the other geometries.

d. A circular core, for guiding the circulatory flow and to minimize losses, is added for an optimum blade angle ($\beta = 145^0$). The core also avoids local vortices in the blade and flow channel region. Both the impeller / blade profile and flow channel area in this case is changed to semi-circular.

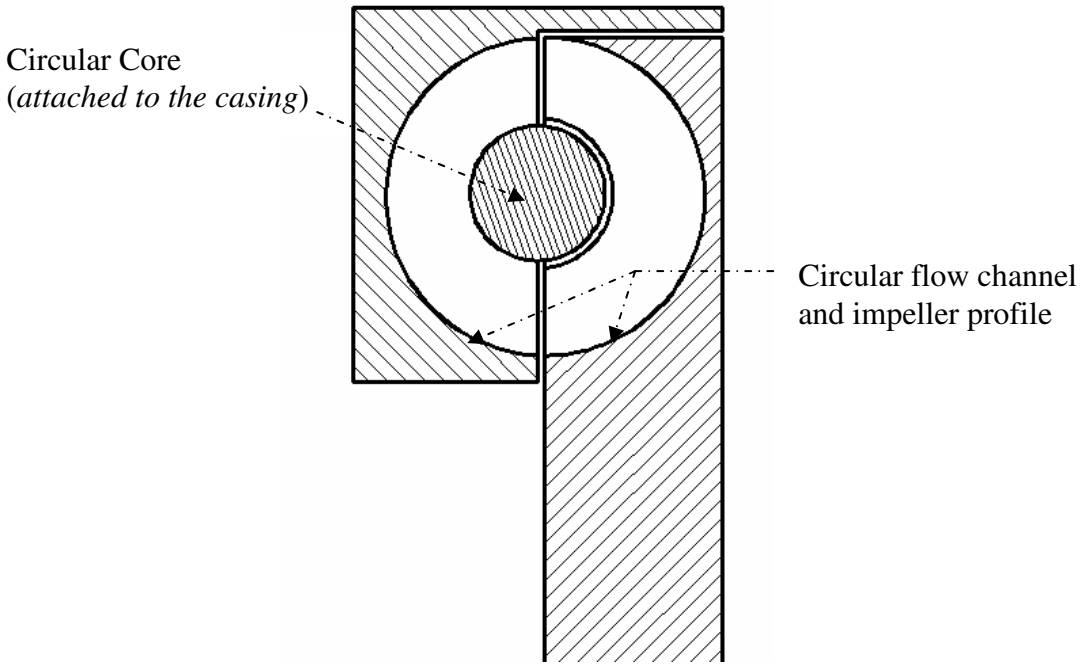

Figure 5.6: Modified schematic geometry with core (only one side)

Along with the above geometric modifications inlet & outlet ports are designed for best output. The inlet port is responsible to set up circulatory flow pattern in RFC thus as shown in Figure 5.8 it is designed to direct the flow in such away that the fluid and blade angles will

much. The outlet port is aligned in the tangential direction to have smooth flow and shaped as a diffuser to further exploit the kinetic energy of the flow for pressure rise. The inlet and exit ports are separated by stripper angle which is about 30^O of the periphery. To save computation time only one-side of the blade and flow channel section is considered for CFD analysis. Clearances are neglected for the simulation analysis due to the difficulty in mesh generation. To investigate the effect of the working fluid the model, for optimum blade angle in **b** ($\beta = 145^O$), will also be simulated for natural gas where natural gas is the actual working fluid. The working conditions (i.e. speed, inlet and discharge pressure) are also kept the same for each simulation.

The following are the different RFC models developed.

1. The base machine (***S4***) with straight and radial blade profile for $\beta = 90^0$: **RFCR-90**
2. Semi-elliptic impeller and semi-circular flow channel with radial blade profile and $\beta = 135^0$: **RFCS-135**
3. Airfoil blade profile with semi-elliptic impeller, semi-circular flow channel and $\beta = 135^0$: **RFCA-135**
4. Airfoil blade profile with semi-elliptic impeller, semi-circular flow channel and $\beta = 145^0$: **RFCA-145**
5. Airfoil blade profile with semi-elliptic impeller, semi-circular flow channel and $\beta = 150^0$: **RFCA-150**
6. Airfoil blade profile with semi-elliptic impeller, semi-circular flow channel and $\beta = 160^0$: **RFCA-160**

7. Airfoil blade profile with semi-elliptic impeller, semi-circular flow channel and $\beta = 180^0$: **RFCA-180**

For the remaining models the blade angle, $\beta = 145^0$, where better performance is obtained among the other six blade angles, is used.

8. Airfoil blade profile with semi-elliptic flow channel and semi-elliptic impeller for $\beta = 145^0$: **RFCSEA-145**
9. Airfoil blade profile with semi-elliptic impeller and semi-circular flow channel with natural gas as a working fluid and for $\beta = 145^0$:**RFCNGA-145**
10. Airfoil blade profile with semi-circular flow channel and impeller having a core for $\beta = 145^0$: **RFCCA-145**

5.5 Basic Steps for CFD Analysis

Before CFD analysis begins using FLUENT, careful consideration of the issues here will contribute significantly to the success of modeling effort. This section provides details about the simulation procedure in FLUENT. It is extracted from FLUENT 6.3.26 documentations [8]. Topics presented in these subsequent sections are:

- the three major steps involved for the CFD analysis using FLUENT, namely Preprocessing, Processing and Post processing,
- steps for building RFC geometries using GAMBIT,
- meshing and specifying boundary condition of the flow domain in GAMBIT,
- importing of mesh and further steps of CFD analysis in FLUENT and
- the necessary output results of FLUENT that are used to analyze and compare the performance of the base machine and other models with the tested data's.

FLUENT software package constitutes FLUENT, the solver and GAMBIT, the preprocessor for geometry modeling and mesh generation. After the important features of the problem are determined the basic procedural steps in Figure 5.7 will be followed.

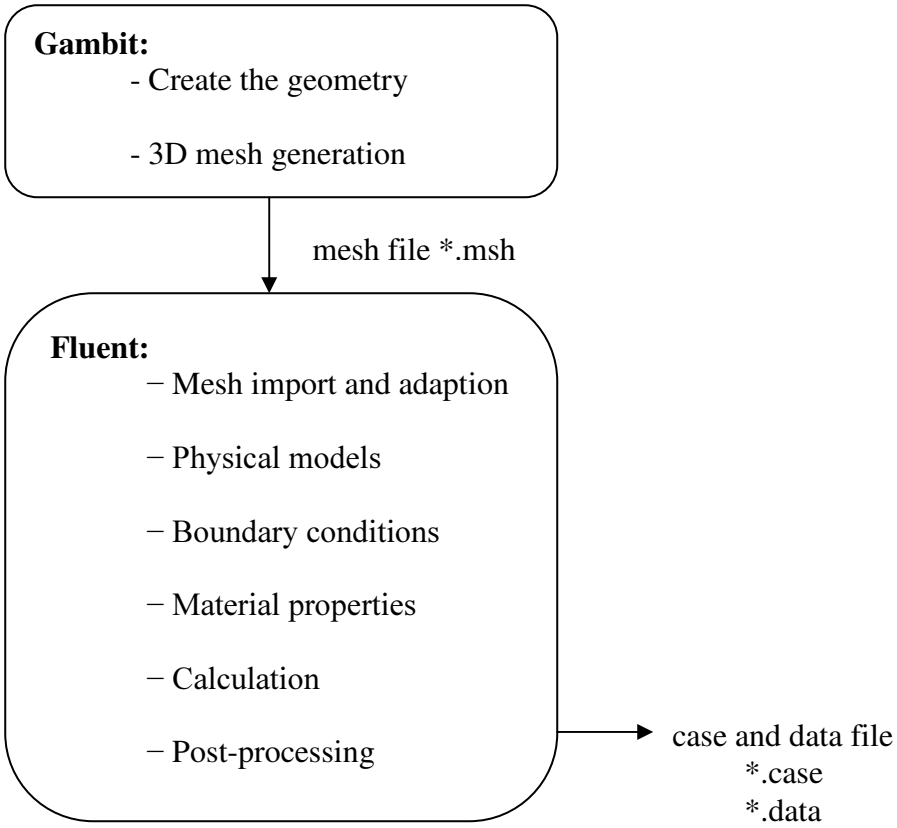

Figure 5.7: Basic Program Structure [8]

The principal steps involved for the CFD analysis could be categorized into three major stages, namely *Preprocessing, Processing and Post processing*. Details of the activities in each of these categories are presented next.

Preprocessing is the first step, which includes preparing of the geometrical model for the computation. It consists of creating geometry, mesh generation and set up of boundary zones

in GAMBIT and reading mesh file, checking grid, scaling grid, smooth/swap the grid, specifying physical flow models, fluid properties, boundary conditions, etc in FLUENT.

Processing is the second step where the solution control and monitoring are carried on along with the actual computation process in FLUENT.

Postprocessing is the activity of displaying of graphical results, reporting control variables and plotting of solution files for areas of interest in the flow field.

5.5.1 Preprocessing of Simulation

The preprocessing procedures of the CFD simulation are classified in to two categories. These are preprocessing in GAMBIT and preprocessing in FLUENT.

5.5.1.1 Preprocessing in GAMBIT

The GAMBIT package is used to build the geometry, to generate meshes and set up boundary zones of the RFC model for the CFD simulation analysis. The mesh file contains the coordinates of all the nodes, connectivity information that tells how the nodes are connected to one another to form faces and cells, and the zone types and numbers of all the faces. The grid file does not contain any boundary conditions, flow parameters, or solution parameters. It is an intermediate steps in the overall process of creating a usable model which is exported, as a mesh file, to be read in FLUENT.

- **Building the Geometry of RFC**

GAMBIT uses vertices, edges, faces and volumes to draw geometry of the flow domain of the RFC and by generating complex 3D volumes through unite & split operations.

Steps to create the flow geometry of RFC in GAMBIT

1. The side view of the flow channel and the impeller are drawn by locating the respective vertices for the edges.
2. Faces are created from the bounding edges of those components independently. These faces are then used for developing volume entities through 3D CAD operations i.e. by revolving and sweeping of faces.
3. The blade geometry is drawn independently through the steps above and they are copied 89 number of times, i.e. $Z_b - 1$ with 4^0 between them, i.e. $\frac{360}{Z_b}$ which are then united to the impeller. The fluid zone between the blades is created by subtracting this resulting geometry from a solid cylinder having similar overall dimension of the impeller.
4. The face representing cross section of the flow channel is used to create stripper volume by revolving through 30^0, i.e. θ_s. Then subtract it from the channel geometry.
5. To draw the outlet and the inlet ports, Coordinate axes are declared at their respective locations in such a way that the 3D operations can be used easily. Vertices, Edges, Faces and Volumes of those components are created in the same way above.
6. The fluid zone in casing is defined by uniting the flow channel (step-4) volume, the outlet port volume and the inlet port volume.
7. The volume enclosed by the two fluid zones constitutes the flow field in RFC which is now to be meshed and exported for the CFD analysis.

Meshing the Flow domain

Solutions by numerical methods require physical discretization/meshing of the domain. A good solution is obtained if good meshes for the models are generated. The accuracy of the solutions depends on the sizes of the meshes. Finer cells are more accurate but are usually less stable and they require large computing capacity and time. Mesh types are selected based on the problem at our hand. The following general points are considered when models are meshed in GAMBIT.

***Setup Time*:** many flow problems solved in engineering practice involve complex geometries like RFC. The creation of structured or block structured grids for such flow problems can be extremely time consuming. Therefore unstructured grids are generated for each RFC models to minimize setup time.

Computational Expense: when the range of length scales of the flow is large, a tetrahedral mesh can often be created with far fewer cells than the equivalent mesh consisting of quadrilateral/hexahedral elements. This is because a tetrahedral mesh allows cells to be clustered in selected regions of the flow domain. However, a large aspect ratio in a tetrahedral cell will invariably affect its skewness which is undesirable as it may impede accuracy and convergence.

Numerical Diffusion: a dominant source of error in multidimensional situations is numerical diffusion. All practical numerical schemes for solving fluid flow contain a finite amount of numerical diffusion. This is because numerical diffusion arises from truncation errors that are a consequence of representing the fluid flow equations in discrete form. The second-order

discretization scheme is made use of to help reduce the effects of numerical diffusion on the solution of the CFD simulation analysis of the RFC.

In Figure 5.8 the numerical RFC model with its inlet port, outlet port, stripper, impeller blades and the fluid zones is shown. The flow field is divided into two zones. The first zone contains the fluid volumes in between the impeller blades with cells of an interval size 1mm and the second zone is the fluid inside the flow channel and the ports with cells of an interval size 1.5mm. Even though setting the interval size of the cells needs some experience, these values are set after checking for various combinations.

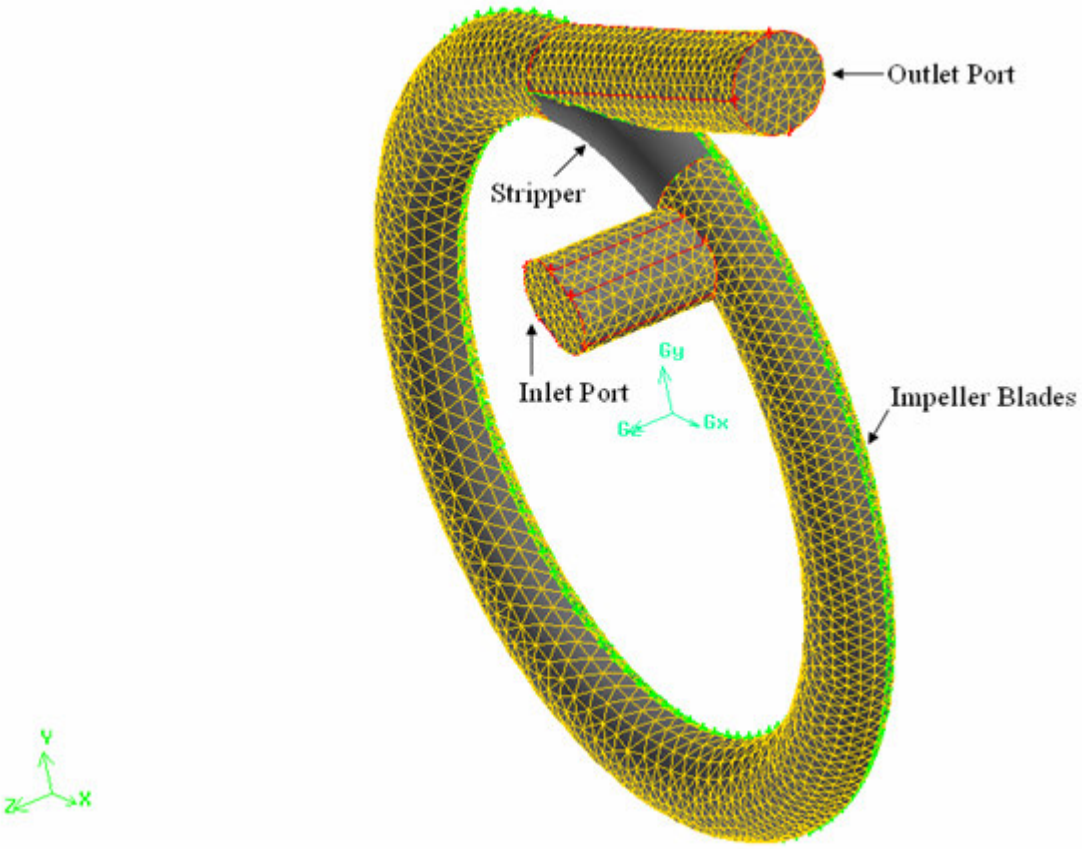

Figure 5.8: Numerical model of Regenerative Flow Compressor

- **Specifying Zone Types**

Zone-type specifications define the physical and operational characteristics of the model at its boundaries and within specific regions of its domain. There are two classes of zone-type specification: Boundary types and Continuum types

Boundary type specifications: when the model is developed in GAMBIT the solver type FLUENT has been set initially so that boundary conditions relevant to the RFC simulation are made available. Boundary-type specifications, such as pressure inlet, pressure outlet, walls and the fluid zones, described in the previous section for defining rotating reference frame, are set in GAMBIT.

Continuum type specifications: defines the characteristics of the model, such as fluid or solid, within specified regions of its domain. In most turbomachinery problems, only the fluid region is prepared for numerical computation and the solid regions are walls which bounds the flow. Hence, only fluid type of continuum is specified for both zones of the numerical RFC model and walls that corresponds to the fluid zones are set by default.

After specifying the boundary zones and the continuum types, the mesh and geometry developed in GAMBIT is saved in a database file *.dbs. This model is exported to a mesh file *.msh so that FLUENT can read the grid information and use it for further preprocessing and computation analysis.

5.5.1.2 Preprocessing in FLUENT

Preprocessing in FLUENT starts with reading the mesh file which was exported from GAMBIT. The mesh file does not contain any information on boundary conditions, fluid properties, flow models and solution parameters. Case files contain the grid, boundary types,

and solution parameters for a problem, as well as information about the user interface and graphics environment. Therefore, the main purpose of this section is to upgrade the mesh file into a case file equipped with the proper information for the CFD analysis of the flow through a RFC. The mesh first read by FLUENT and on the console window the following information's are printed.

> Reading "D:\Thesis\Gambit Geometry (RFC)\Semi-Elliptic\airfoil-55\mesh.msh"...

12887 nodes.

19266 mixed wall faces, zone 4.

72 mixed mass-flow-inlet faces, zone 5.

88 mixed pressure-outlet faces, zone 6.

80857 mixed interior faces, zone 8.

20631 tetrahedral cells, zone 2.

24654 tetrahedral cells, zone 3.

Building...

grid,

Note: Separating wall zone 4 into zones 4 and 1.

wall -> wall (4) and wall:001 (1)

Note: Separating interior zone 8 into zones 8 and 7.

default-interior -> default-interior (8) and default-interior:007 (7)

Note: Separating interior zone 8 into zones 8 and 9.

default-interior -> default-interior (8) and default-interior:009 (9)

materials,

interface,

domains,

zones,

default-interior:009

default-interior:007

wall:001

default-interior

outlet

inlet

wall

rotor_fluid

flow channel_fluid

shell conduction zones,

Done.

Grid Manipulation

This is the opening stage on the imported mesh file before the start of the computation process. These include scaling, smoothing/swapping, checking and displaying the grid.

Scaling the Grid: when the computational grid is read by FLUENT, all the dimensions are considered in meters, m and internally FLUENT stores the data's in meters. But grid of the RFC geometry was created in units of mm in the GAMBIT application and scaling of the grid to units of meters must be performed so that each node coordinate will be multiplied by the corresponding scale factor.

Smoothing/Swapping the Grid: the mesh quality can be further improved for better accuracy and stability of the numerical computation. FLUENT provides the capability to improve the smoothness by refining the mesh based on the change in cell volume. Smoothing and face

swapping are used as grid adaption, they increase the quality of the final numerical mesh by modifying the cell connectivity through repositioning of interior nodes to decrease the skewness of cells to a specified minimum value (default value = 0.8) and until the number of swapped faces comes to 0. Skewness can be defined as the difference between the cell's shape and the shape of an equilateral cell of equivalent volume. Rapid changes in cell volume between adjacent cells translate into larger truncation errors. Highly skewed cells can also decrease accuracy and destabilize the solution.

Checking Mesh: here the domain extents, volume statistics, grid topology and verification of simplex counters are checked. It is generally a good idea to check the grid in order to detect any grid trouble before getting started with the problem setup. The domain extents list the minimum and maximum x, y, and z coordinates in meters. The volume statistics include minimum, maximum, and total cell volume in m^3. A negative value for the minimum volume indicates that one or more cells have improper connectivity. This must be eliminated before continuing the flow solution process for flow.

Displaying Grids: grids can be visually inspected to check grid problems and to take action if necessary. Later grids can also be used when examining solution results to include surfaces, the outline of all or part the domain, the grid lines, the nodes on the domain surfaces and the solid surfaces.

- **Defining Analysis Bases**

Analysis bases such as the solver type, physical models for the flow nature, fluid properties, boundary conditions and solution parameters are set after the grid manipulations were performed in the preprocessing step of FLUENT.

Setting Models: the flow in RFC is 3D, steady-state, compressible, turbulent, viscous and rotating flow (rotating reference frame). These flow models are set for the simulation process to determine the governing equations of the CFD analysis discussed in chapter four.

Setting Materials: the material types with their physical properties will be set in the material panel. The RFC is intended to operate in a microturbine for the compression of natural gas but since it is tested with air we take properties of air first. The solid material used for the casing and impeller blades is the default, aluminum. For isothermal condition we can set a constant magnitude for properties of air except for density which is defined by an equation. FLUENT provides several options for definition of the fluid density for compressible flow, and are either temperature and/or composition-dependent. For compressible flows, the ideal gas law is the appropriate density relationship. The gas law has the following form;

$$\rho = \frac{p_{op} + p}{RT} \tag{5.13}$$

Where p is the local relative pressure predicted by FLUENT and p_{op} is the operating pressure defined in the operating conditions panel and the recommended value is zero.

Table 5.3: Material Properties

Material	ρ [kg/m^3]	**Cp** [J/kg-K]	**k** [w/m-K]	**μ** [kg/m-s]
Air	-	1005.244	0.02575561	1.7924e-05
Natural Gas	-	2222	0.0332	1.087e-05
Aluminum	2719	871	202.4	-

Defining Boundary Conditions: boundary conditions specify the flow and thermal variables on the boundaries of the physical model. They are a critical component of FLUENT simulation and it should be specified appropriately. The boundary conditions are applied first

in GAMBIT as discussed above and here also they are re-applied for the flow condition of RFC.

a. Pressure Inlet boundary condition: It can be used in compressible flow inlets to set the inlet total pressure. This is in contrast to the mass flow inlet boundary condition where the total pressure is fixed while the mass flux varies to design point. Hence; $p_{in} = 100000\text{pa}$ .The other properties of the flow at inlet, the hydraulic diameter (8.6902mm), turbulence intensity (4.579%), total temperature (294.26K) and flow direction (normal to boundary) are also specified.

b. Pressure Outlet boundary condition: This is used to define the static pressure of the flow at outlets for initial back flow calculations and a constant pressure of 130000Pa is set. The other properties of the flow at outlet, the hydraulic diameter (10.18mm), turbulence intensity (4.79%), total temperature (294.26K) and flow direction (normal to boundary) are also specified.

c. Rotating Reference Frame: the rotating boundaries become stationary relative to the rotating frame. That is, on imposing the boundary conditions for RRF, the impeller blades are made stationary while the surrounding fluid appears to move with a specified rotational speed in opposite direction relative to the actual impeller motion. An angular speed of 28,910 rpm is set for the RFC in the direction of positive Z-axis.

d. Wall boundary conditions: are used to bound fluid regions of the flow domain. The casing boundaries as well as the impeller blades are represented as walls in the flow simulation of the RFC. In viscous flows, the no-slip boundary condition is

enforced at walls by default and a tangential velocity component is incorporated in terms of the rotational motion of the wall boundary. Fixed temperature condition is selected at the walls

5.5.2 Processing in FLUENT

When the discretized equations are solved iteratively there should be some convergence criteria specified. A number of iterations are usually required to reach a converged solution. In FLUENT convergence is reached when:

- Changes in solution variables from one iteration to the next reach to prescribed values known as residuals that provide a mechanism to help monitor this trend or,
- Overall property conservation is achieved.

Convergence is not mean accuracy. The solution is accurate if it matches with experimental data. The accuracy of a converged solution depends upon appropriateness and accuracy of physical models, grid resolution and problem setup.

The other problem is the high degree of coupling between the momentum equations when the rotational term is large. A high degree of rotation introduces a large radial pressure gradient which drives the flow in the axial and radial directions, thereby setting up a distribution of the rotation in the field. This coupling may lead to instabilities in the solution process, and hence require special solution techniques to obtain a converged solution. One of the most effective controls exerted on the solution is to start with a low rotational speed and then slowly increase the rotation up to the desired level. The procedure used to accomplish this is as follows:

1. Set up the problem using a low rotational speed in the inputs for boundary conditions and for the angular velocity of the reference frame. The rotational speed in this first attempt might be selected as 10% (2891 rpm) of the actual operating condition.
2. Solve the problem at these conditions.
3. Save this initial solution data.
4. Modify your inputs (i.e., boundary conditions and angular velocity of the reference frame). Increase the speed of rotation, perhaps doubling it.
5. Continue the calculation using the solution data saved in Step 3 as the initial guess for the new calculation. Save the new data.
6. Continue to increment the rotational speed, following Steps 4 and 5, until you reach the desired operating condition.

5.5.2.1 Setting of Solution Controls

Solution controls in FLUENT are under-relaxation factors and discretization schemes. The pressure based solver uses under-relaxation factors to control the update of computed variables at each iteration. The default settings 0.3 for pressure, 1 for density, 1 body force, 0.7 for momentum, 0.8 for turbulence kinetic energy and dissipation rate, 1 for turbulence viscosity and 1 for energy can be used safely in the simulation of flow in the RFC. The SIMPLE pressure-velocity is used for the pressure correction. Second Order for pressure interpolation is selected. The default discretization scheme is chosen initially for solving each scalar equation, i.e. momentum, turbulence kinetic energy, turbulence dissipation rate and energy. Then using the converged solution as an initial data, the other can be applied to

reduce the effects of numerical diffusion on the solution arising from truncation errors and, hence, increase the accuracy of the converged solution.

5.5.2.2 Selecting Solution Monitors

Graphical monitoring of residuals and representative flow variables or reports of overall balances can be used to check the convergence of the solution.

Monitoring the Residuals: residual plots can be used to monitor the solution until the residual values have reached the specified tolerance. After simulation, the residuals have decreased by at least 3 orders of magnitude to at least 10^{-3}. For the pressure-based solver, the scaled energy residual must decrease to 10^{-6}.

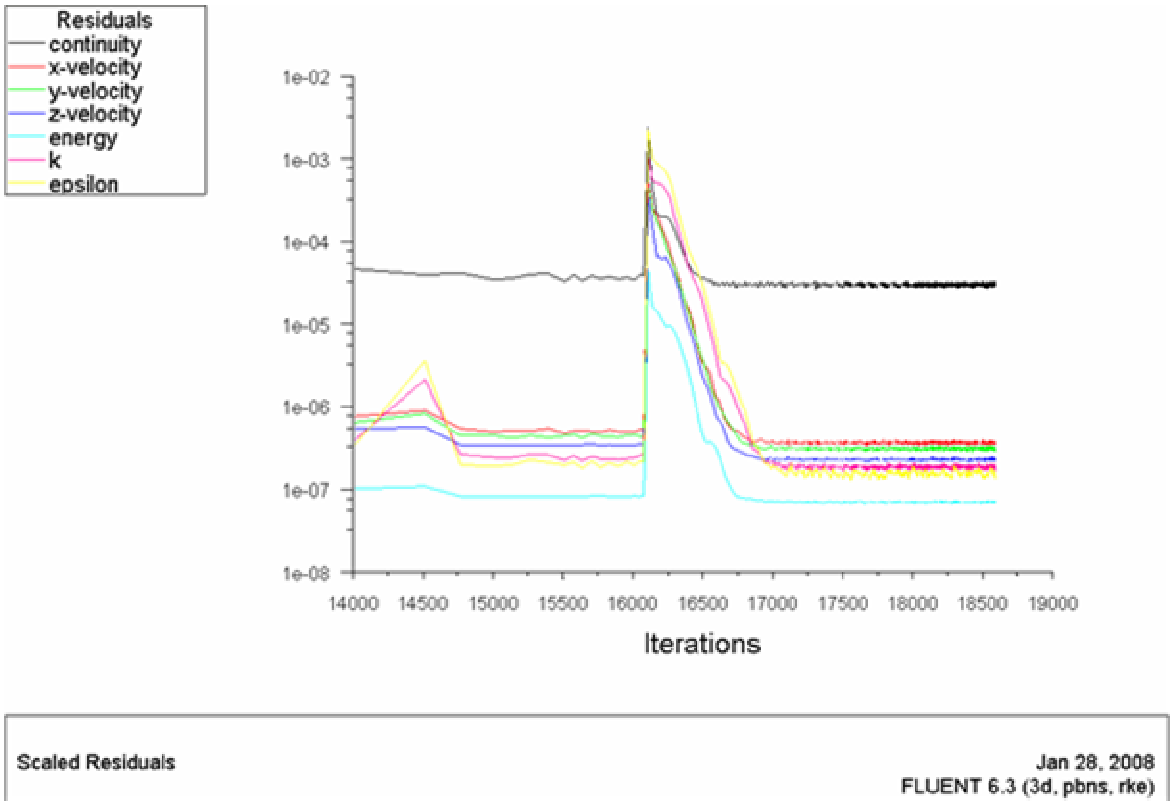

Figure 5.9: Scaled residuals at the final iterations for Model **RFCA-145**

Surface Monitoring: if the convergence criteria's are too large the residuals may not fall below the set values. In such cases, check for convergence could be done by monitoring representative flow variables after several iterations. Here total pressure and mass flow rate on the surface at the exit port are monitored.

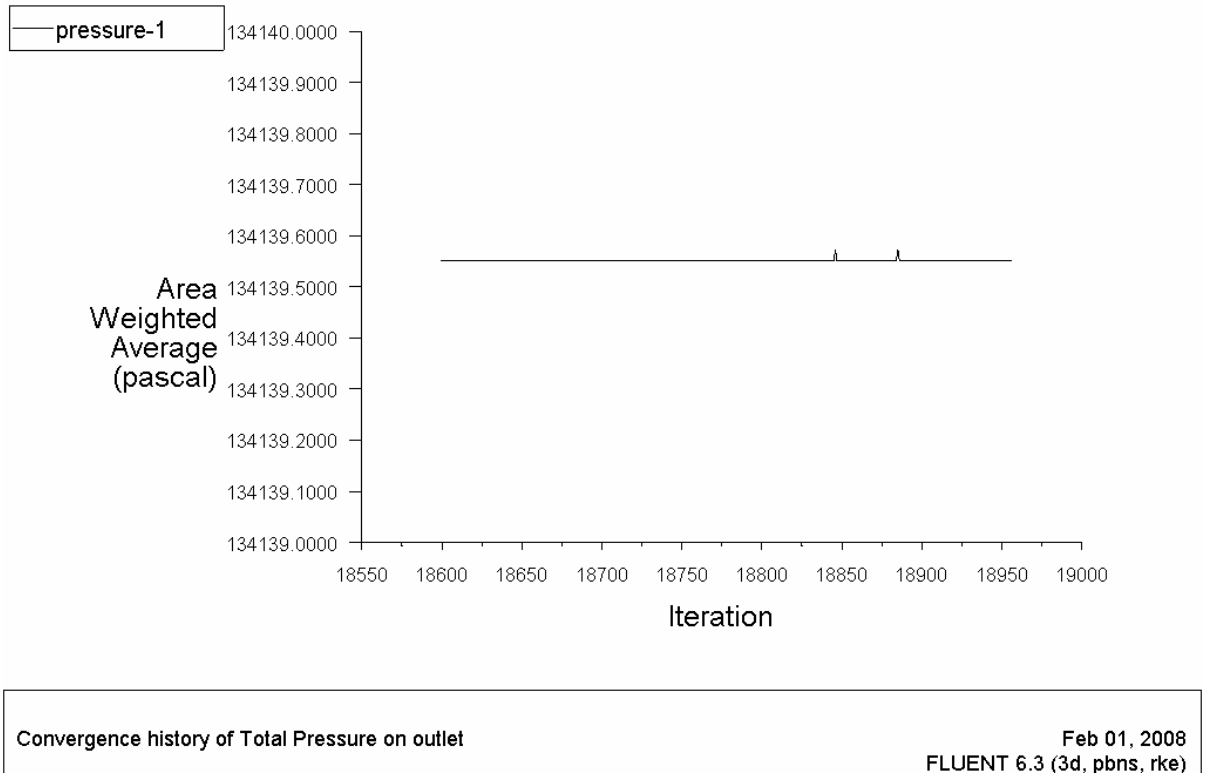

Figure 5.10: Convergence history of total pressure at exit port for Model **RFCA-145**

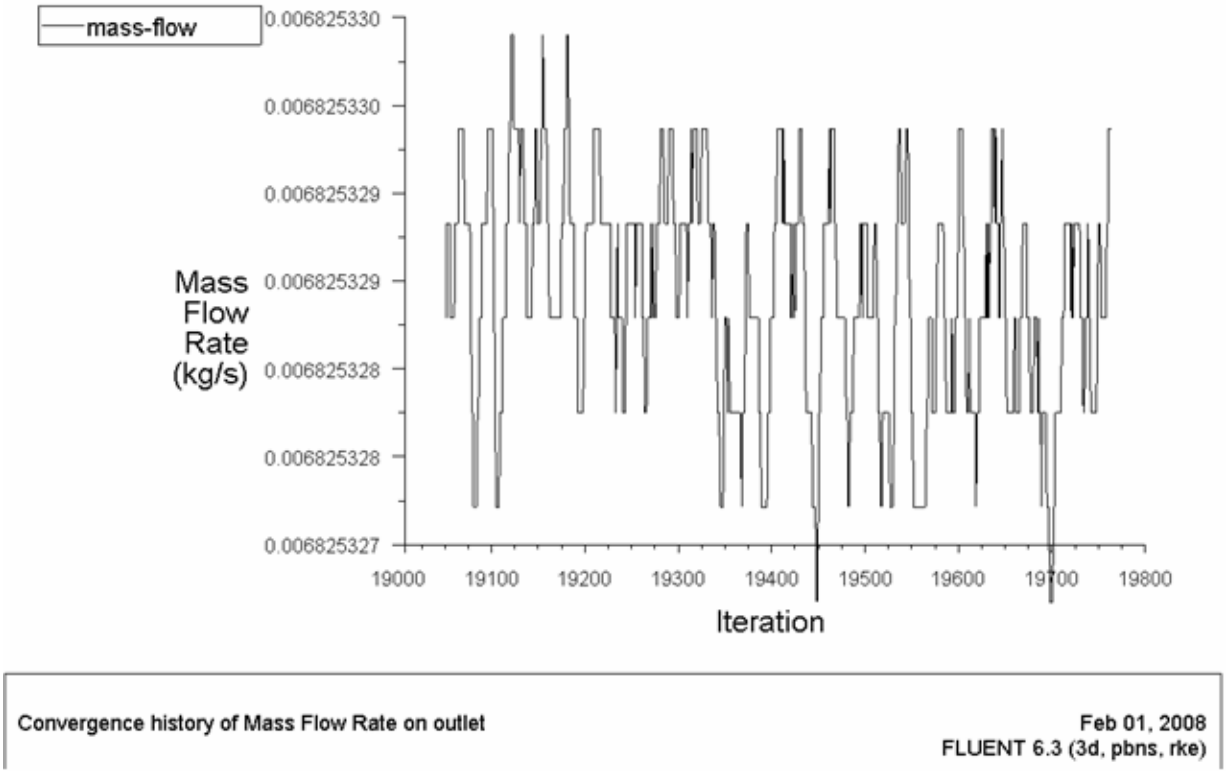

Figure 5.11: Convergence history of mass flow rate at exit port for Model **RFCA-145**

Report of Overall balances: overall balance of mass flow rate can also be used as another means to monitor convergence of solution after simulation.

Mass Flow Rate	(kg/s)
Inlet	0.006825326
Outlet	0.0068253237
Net	2.3283064e-09

The overall imbalance can be calculated as percentage of the net mass flow out of the mass flow at outlet and is compared to the minimum tolerable value of 0.2%.

5.5.2.3 Solution Computing

This is the last step in the CFD analysis of the flow in RFC. Calculation of solutions needs initialization of the flow field with specified initial values of the flow variables for the entire domain or a zone in the domain to start the iterating process.

Initializing the Solution: FLUENT needs an initial guess for starting the solution flow field. Initialization of the flow field in the RFC simulation begins by setting the inlet values in the starting 2891rpm. The converged solution at previous iteration of rpm is provided as an initialization for the next increment of rpm until the final design point speed (28910rpm) is reached.

Performing Calculations*:* for the first 100 iterations the flow is considered to be compressible to stabilize the solution then the incompressible flow condition is activated to proceed by adding more iteration until the solution is satisfactorily converged to any of the specified solution monitoring methods. Plots of residuals and other solution monitors are displayed in separate graphics windows while the iterations going on.

As shown in Figure 5.7 FLUENT stores the inputs that define the problem and the results computed in two separate files; the case file and the data file. When starting the calculations from current solution data, FLUENT begins at the last iteration performed, using the current solution data as its starting point.

5.5.3 Post processing in FLUENT

In post processing, the results are examined to review the solution and to extract useful data's. It can be through graphical display or numerical report. In graphical display the overall flow pattern and determination of key flow features can be examined while in

numerical reporting necessary integral quantities can be computed at boundaries of the flow domain. Amongst; the mass flow rate on boundaries, the moments about a specified center for selected wall zones and area-weighted average field variables on a surface in the domain are reported.

In the next chapter details of these output results will be presented.

CHAPTER SIX

RESULTS AND DISCUSION

6.1 Introduction

Different modifications on the basic geometries were investigated to optimize the performance of the machine. First a model for the base machine was developed by taking its geometric data's from literature [4] and the performance data's serve as a reference for comparing the performance of the modified. As shown in Figure 5.1 and 5.3-1 the base machine (RFCR-90) has rectangular flow channel and a straight impeller / blade profile. Then different models were developed by varying both, the flow channel and impeller / blade profile with the intent of minimizing losses and improving the performance of the machine. An attempt was made to solve the flow details using FLUENT. Each model undergoes through all simulation procedures; and evaluation is performed by using the output results and computed values from these output results.

The objective of this chapter is:

- to present and discuss the output results i.e. plots and numerical outputs which shows the flow characteristics in the base machine and the modified ones,
- to compute the design parameters for the comparison purpose with the performance data's of the base machine,
- to analyze the performance of the base RFC simulated and to compare the output results with the available performance data's.

- to analyze the performance of the modified geometries and to check if improvements are obtained

6.2 Results of CFD Analysis

As discussed in the previous chapter the results of the analysis in FLUENT can be shown by using graphical displays and numerical outputs. They are used to investigate the flow characteristics in RFC. The outputs here are to illustrate such graphical displays and numerical outputs for the base machine (RFCR-90) and for model RFCA-145. Similar output results of the other modified geometries are also shown in table 6.1 and in the appendix.

6.2.1 Graphical Displays

Graphical displays allow us to easily view the overall flow pattern and change of flow variables in RFC. The necessary graphical displays for in RFC are shown below.

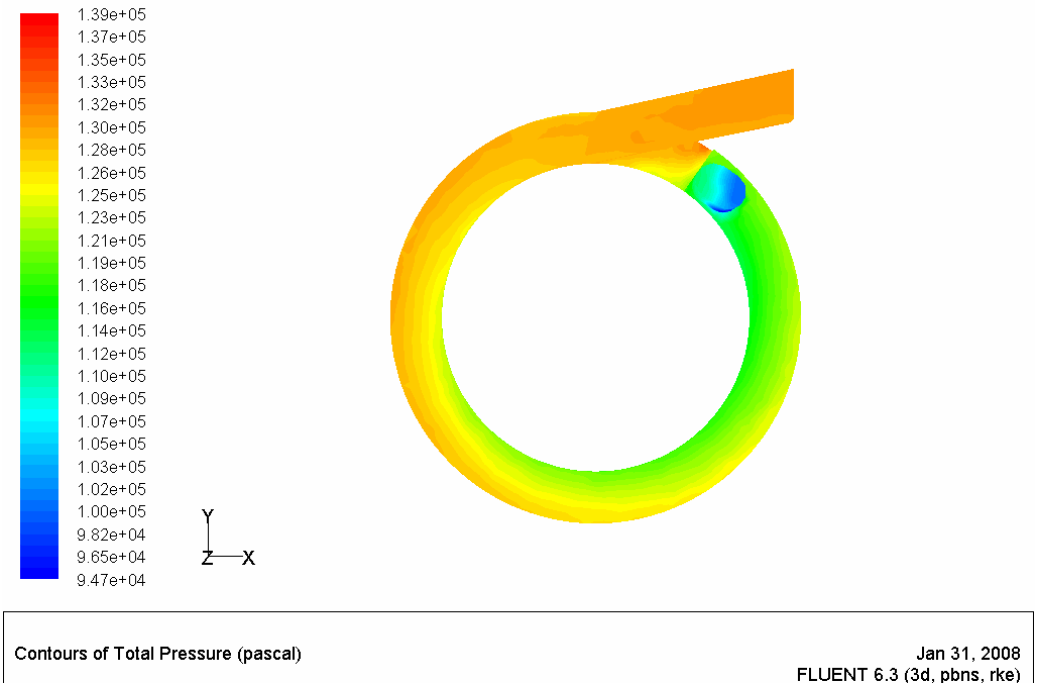

Figure 6.1: Plot of total pressure contours over the entire flow field for Model **RFCR-90** (*at design point running speed, 28910 rpm*)

Figure 6.1 shows the contour of total pressure for model RFCR-90 over the entire flow field. As can be shown in the figure the pressure of the fluid increases gradually from inlet to the exit port and an averaged total pressure of 129996.31 pa is obtained at the outlet. The flow channel was then modified to be semi-circular in cross section and the impeller made semi-elliptic with the intent of maximizing the pressure ratio (performance) of the machine. This modified geometry then used as a base for developing subsequent blade variations. By doing this an increase in total pressure is observed for the modified models and for model RFCA-145 an averaged total pressure of 134139.55 pa is obtained at design point running speed.

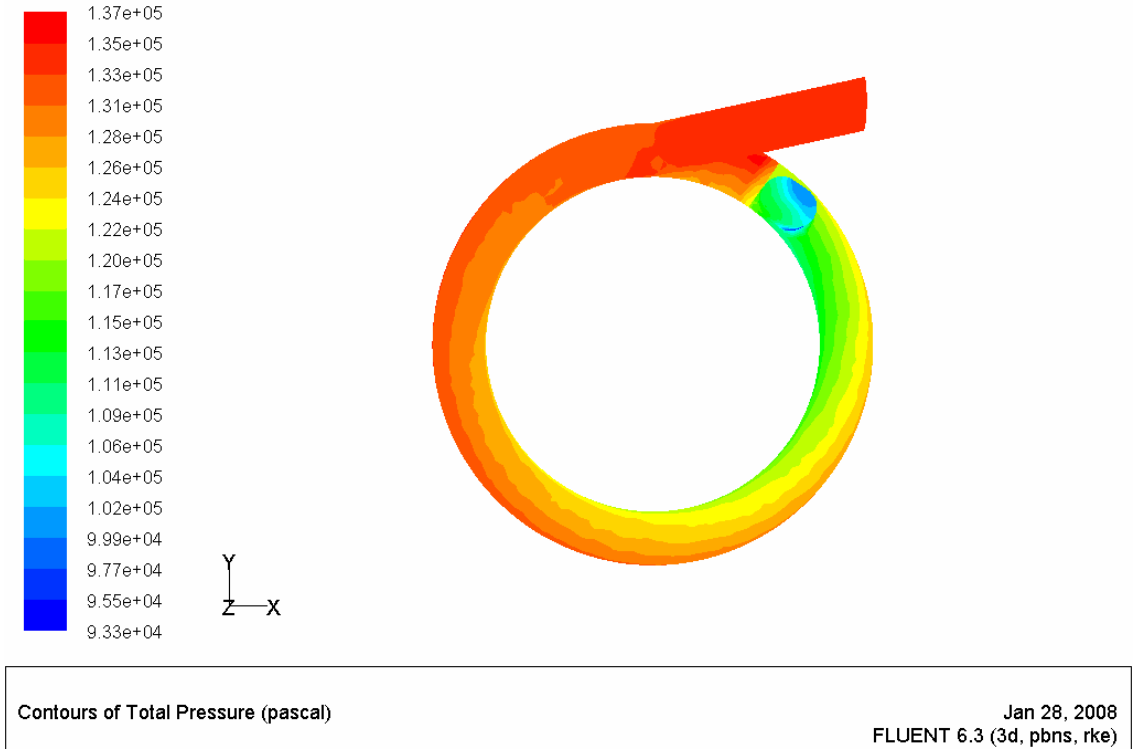

Figure 6.2: Plot of total pressure contours over the entire flow field for Model **RFCA-145** (*at design point running speed, 28910 rpm*)

Figure 6.3 shows the contour of density for model RFCA-145 over the entire flow field. As can be shown in the figure the density of the fluid also increases gradually from inlet to the exit port which confirms the compressible flow characteristic in regenerative flow compressors where we have gradual increase in density. This characteristic is observed for all of the models considered (*see the appendix*).

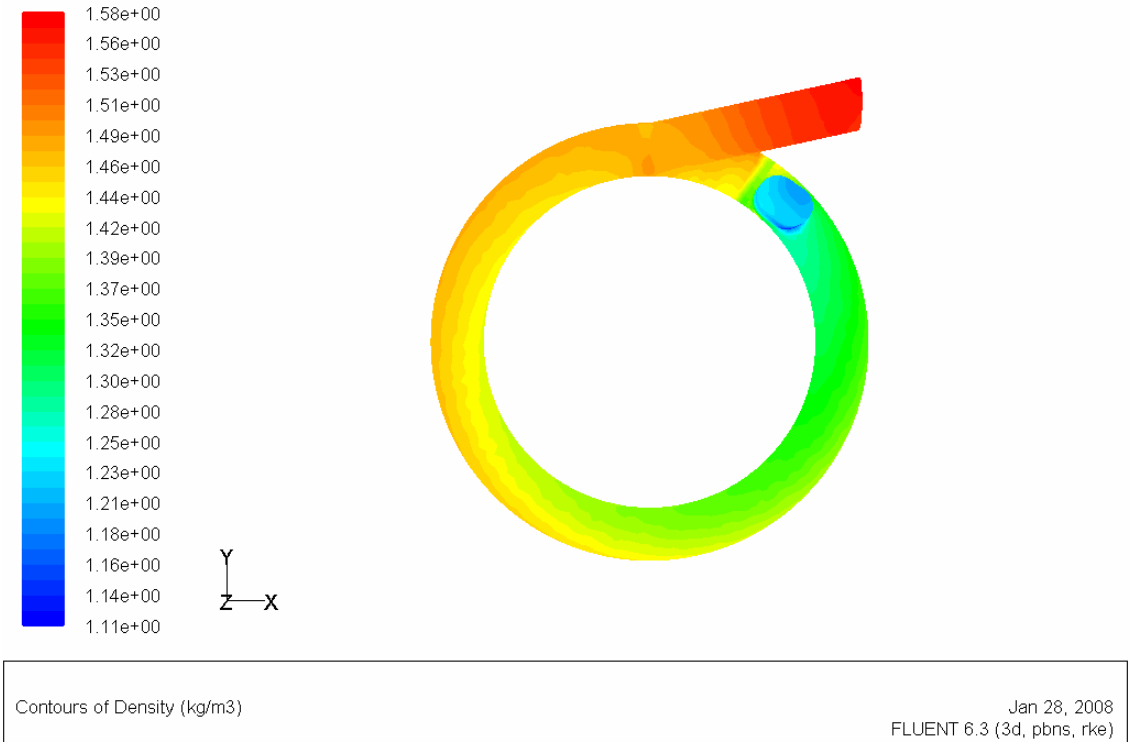

Figure 6.3: Plot of density contours over the entire flow field for Model **RFCA-145** (*at design point running speed, 28910 rpm*)

Figure 6.4 and 6.5 below show the path followed by a fluid particle from inlet to the exit port for model RFCA-145 running at the starting speed, 2891 rpm. As shown on the figure, the flow circulates through the blades and flow channel a number of times. This repetitive action of the impeller blades on the fluid accounts for a pressure rise at lower running speed. The

impeller hits the fluid and adds energy to it, which is recovered as pressure rise. The figures also confirm the cork screw flow pattern inside RFC as described in many literatures [4] [5] [6] and [7]. But this flow pattern diminishes as the speed of the machine increases and not obtained at the design speed, 28910 rpm. The reason is, the tendency of the fluid particle to re-enter the blade a number of times decreases for higher running speed and a continuous cork screw flow pattern is less expected. This same phenomenon is confirmed by investigating plots of the isothermal power gained by the fluid particle along its path (see Figure 6.7). Therefore, in RFC running at higher speed, the energy gain and hence the pressure rise of the fluid particle must be due to the turbulence effect as it enters the blade and flow channel in its passage.

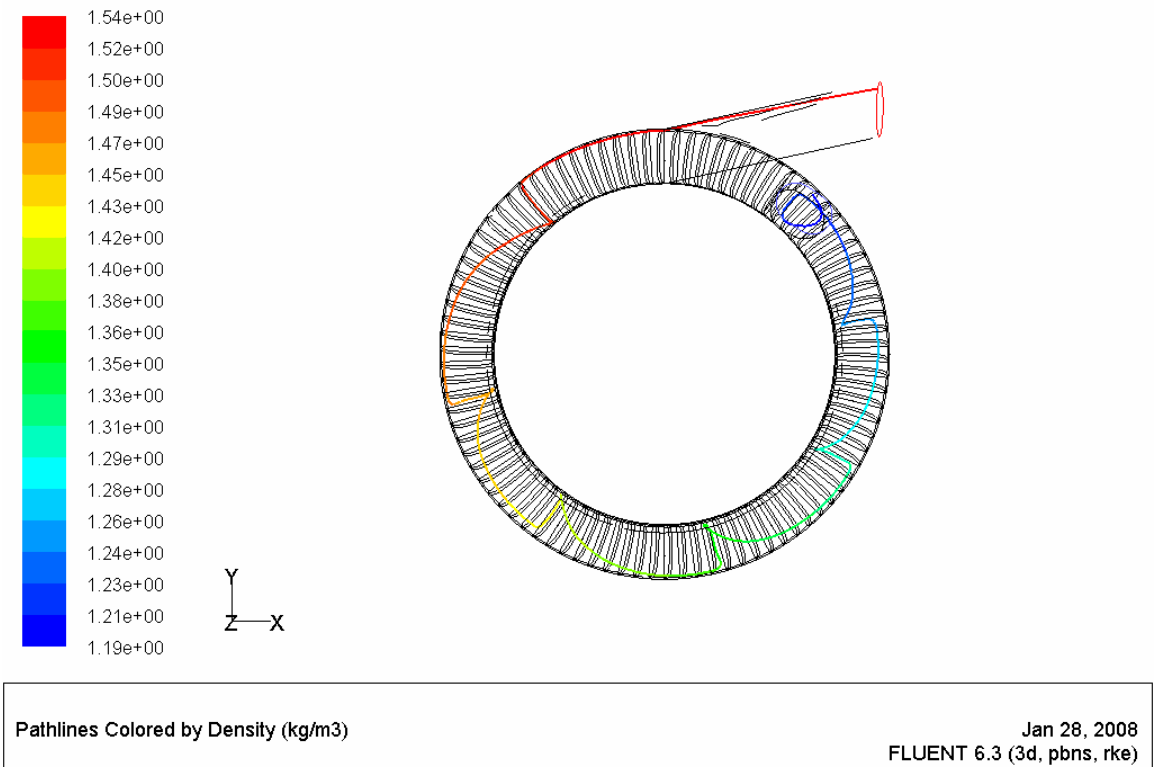

Figure 6.4: Plot of a particle path line from inlet to exit port for Model **RFCA-145** (*at starting running speed, 2891 rpm*)

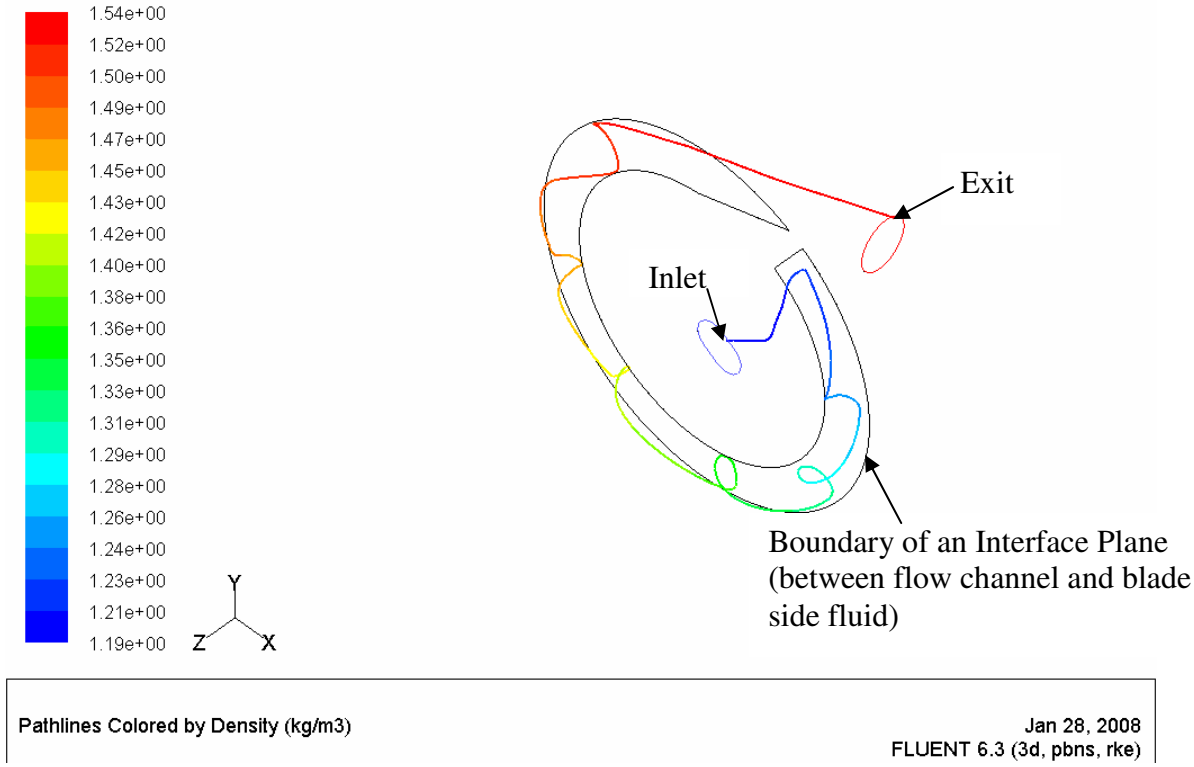

Figure 6.5: Detail view of plot of a particle path line from inlet to exit port for Model **RFCA-145** (*at starting running speed, 2891 rpm*)

For the base machine its geometries i.e. rectangular flow channel area and a straight impeller / blade profile make it difficult to obtain continuous particle path line from inlet to exit port, even at the starting running speed (2891 rpm), where at this speed a fully developed cork screw flow pattern is observed for the other modified models as shown above and in the appendix.

The isothermal power gained by the fluid particle, which are recorded on the path line as it goes from inlet to the exit port, are shown in Figure 6.6 to 6.11. These XY files are with isothermal power gained by the fluid particle vs. its path length. For the base machine, in all speed range, the isothermal power gained by the fluid particle increases with out regenerative

effect; hence confirms the difficulty of obtaining cork screw flow pattern at lower speed as shown below.

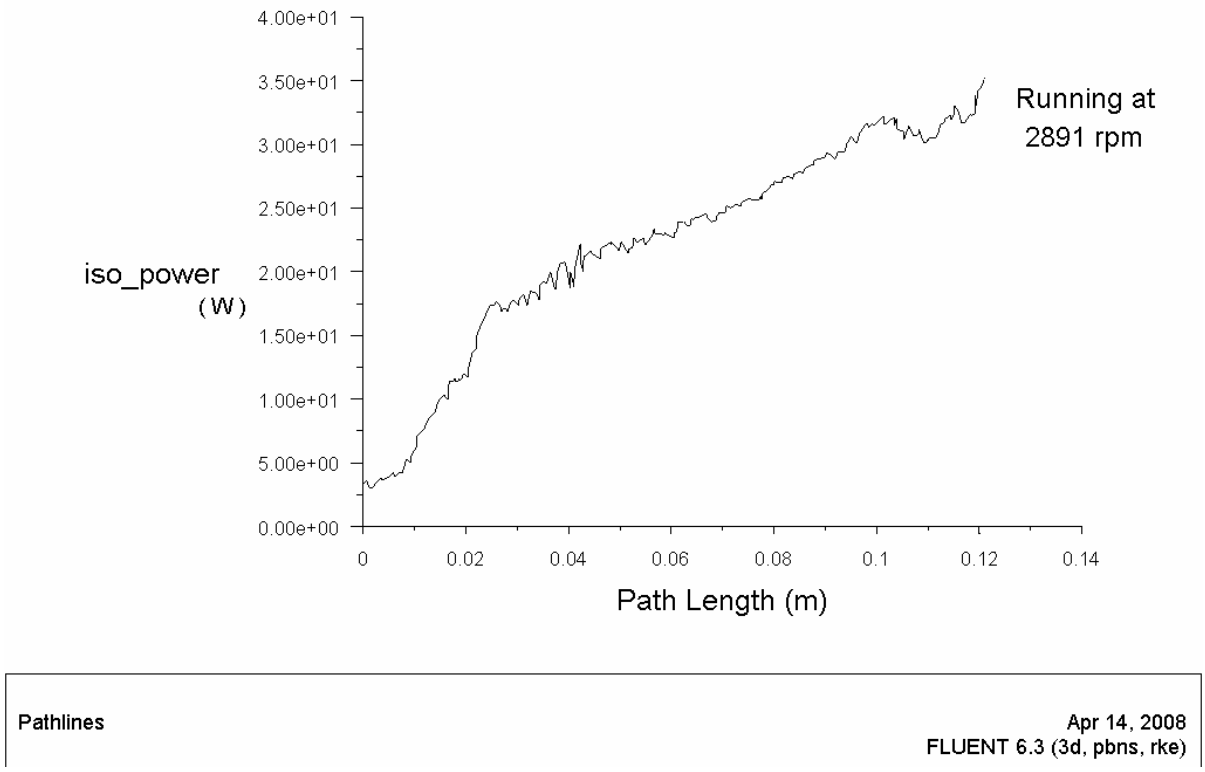

Figure 6.6: Plot of Isothermal power gained by a particle along its path line from inlet to exit port for Model **RFCR-90** (*at starting running speed, 2891 rpm*)

Figure 6.7, 6.8, 6.9 and 6.10 are plot of isothermal power gained by a particle for Model RFCA-145 at a running speed of 2891, 5782, 8673 and 11564 rpm respectively. These figures illustrate the regenerative energy gain pattern of the flow at lower running speeds as it moves from inlet to outlet; hence confirming the typical regenerative characteristics of the machine at lower speeds. It can be seen that the energy of the fluid increases as it moves through the impeller blades, becomes stable as it moves through the side channel to maintain the circulatory flow. And as shown in the figures the regenerative effect decreases as the speed increases.

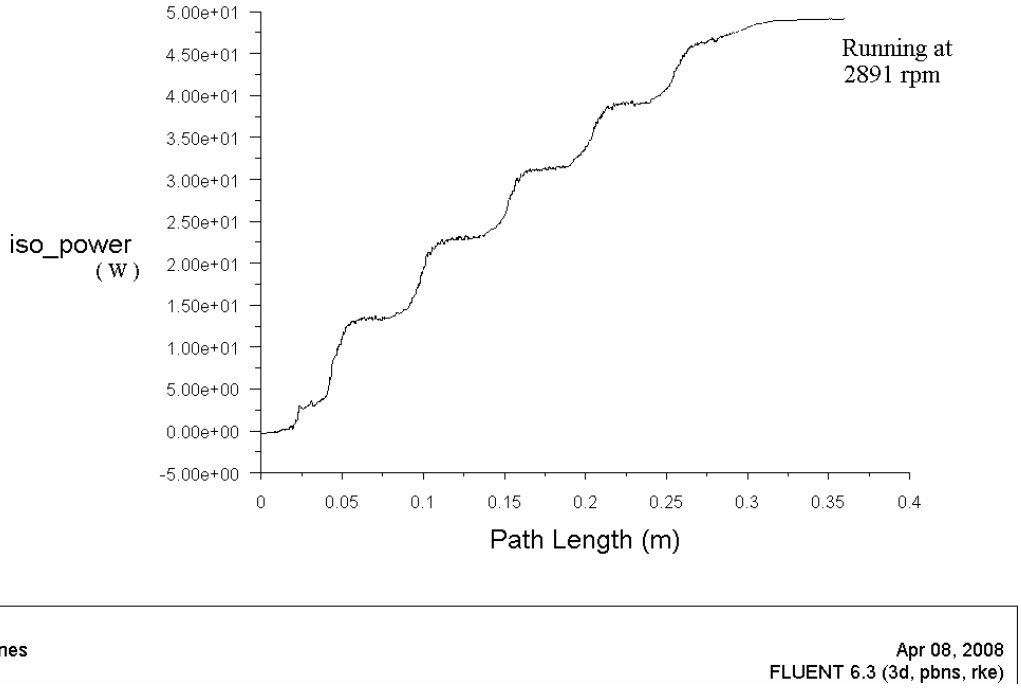

Figure 6.7: Plot of Isothermal power gained by a particle along its path line from inlet to exit port for Model **RFCA-145** (*at starting running speed, 2891 rpm*)

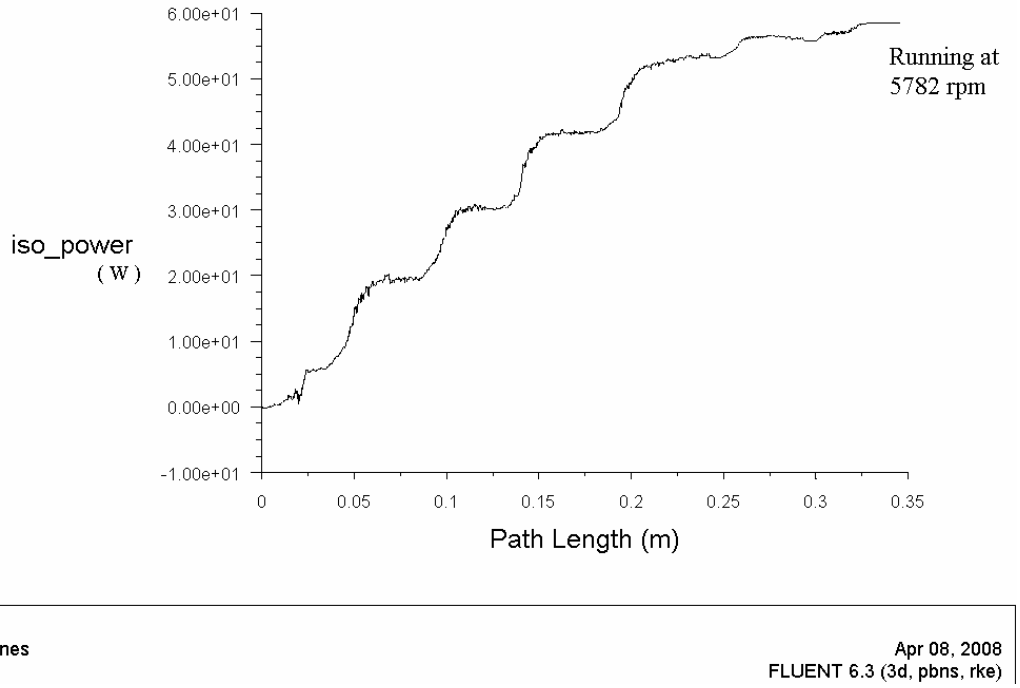

Figure 6.8: Plot of Isothermal power gained by a particle along its path line from inlet to exit port for Model **RFCA-145** (*at the second running speed, 5782 rpm*)

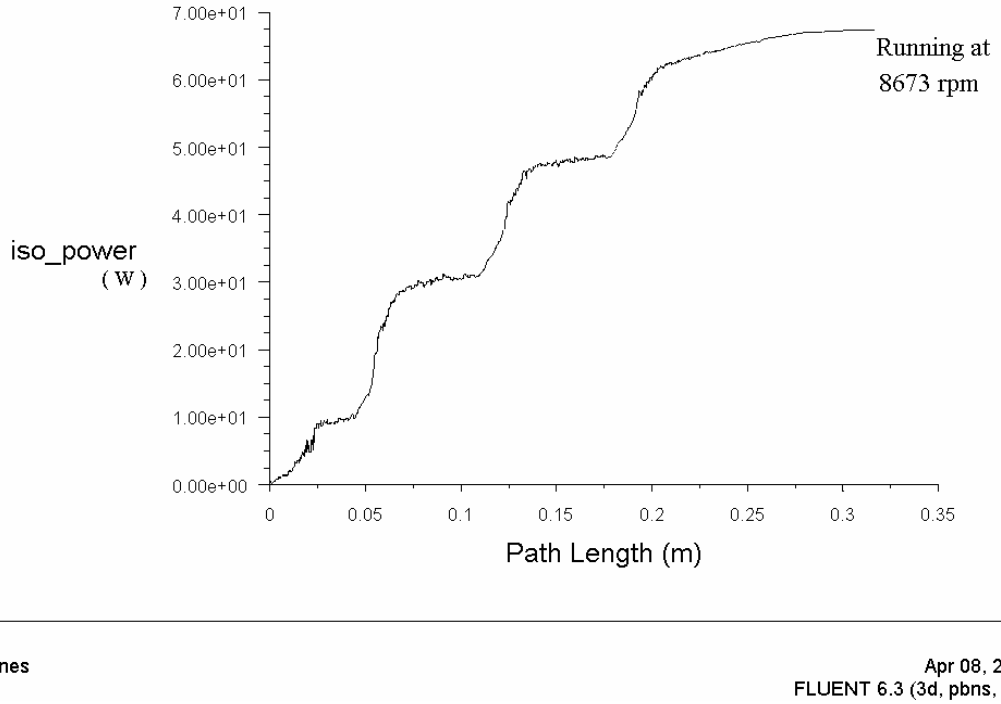

Figure 6.9: Plot of Isothermal power gained by a particle along its path line from inlet to exit port for Model **RFCA-145** (*at the third running speed, 8673 rpm*)

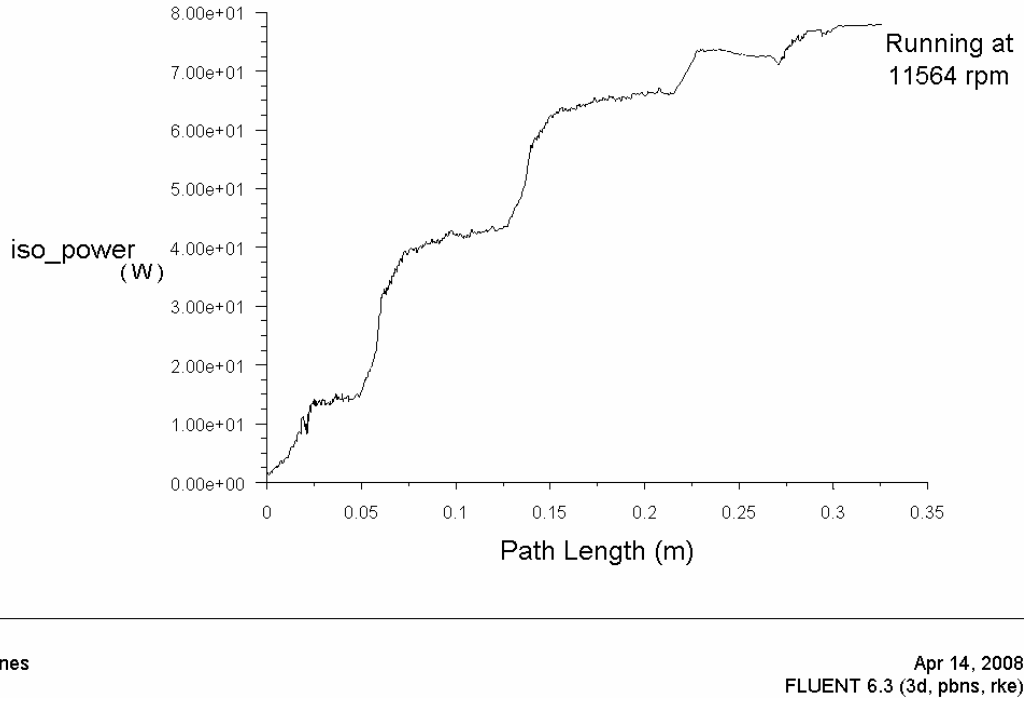

Figure 6.10: Plot of Isothermal power gained by a particle along its path line from inlet to exit port for Model **RFCA-145** (*at the fourth running speed, 11564 rpm*)

As the speed increases further and at the design point running speed, 28910 rpm the regenerative energy gain pattern diminishes. As stated before, since a continuous cork screw flow pattern can not be obtained at higher speeds it makes difficult to have regenerative energy gain pattern of the flow, but the fluid particle still gains energy, as shown in Figure 6.11 and 6.12 below. Therefore, for RFC running at higher speed the energy gain of the fluid particle in its passage from inlet to the outlet port is due to the turbulence effect.

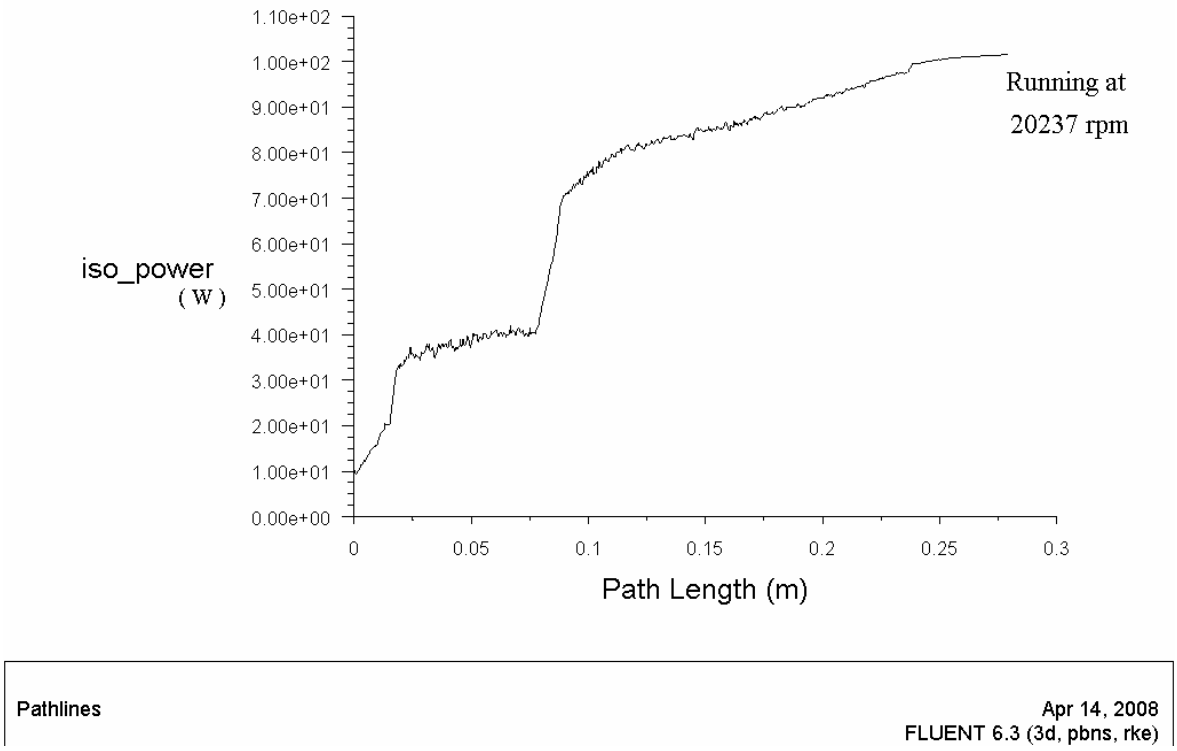

Figure 6.11: Plot of Isothermal power gained by a particle along its path line from inlet to exit port for Model **RFCA-145** (*at running speed, 20237 rpm*)

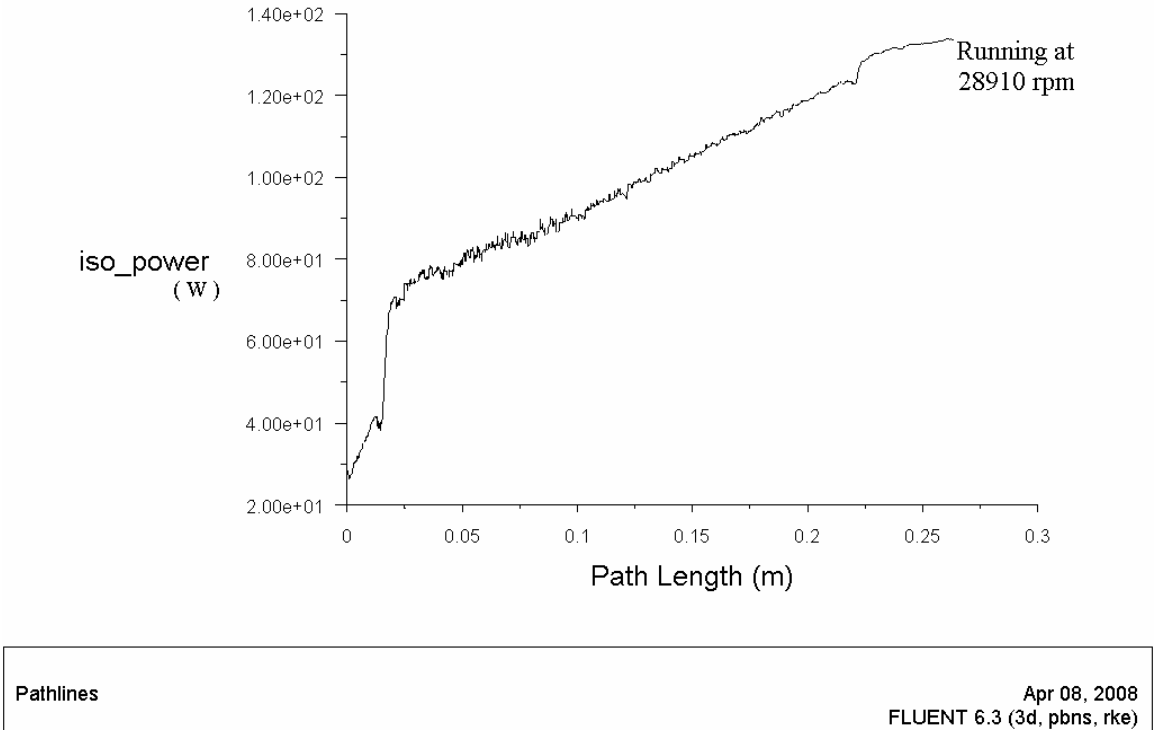

Figure 6.12: Plot of Isothermal power gained by a particle along its path line from inlet to exit port for Model **RFCA-145** (*at the design point running speed, 28910 rpm*)

Figure 6.13 and 6.14 below show the flow pattern on the cross-sectional surface of the blade and flow channel region by using relative velocity vectors. This flow pattern shows how the flow enters the blade and re-circulates back to the flow channel. As shown in the figures below the geometry of the flow channel and impeller / blade profile is responsible to this flow pattern and better performance is achieved if circulatory flow pattern is well promoted. The geometry of the base machine makes difficult to obtain a fully developed circulatory flow pattern, even at low speeds and is well promoted for the modified ones as illustrated below.

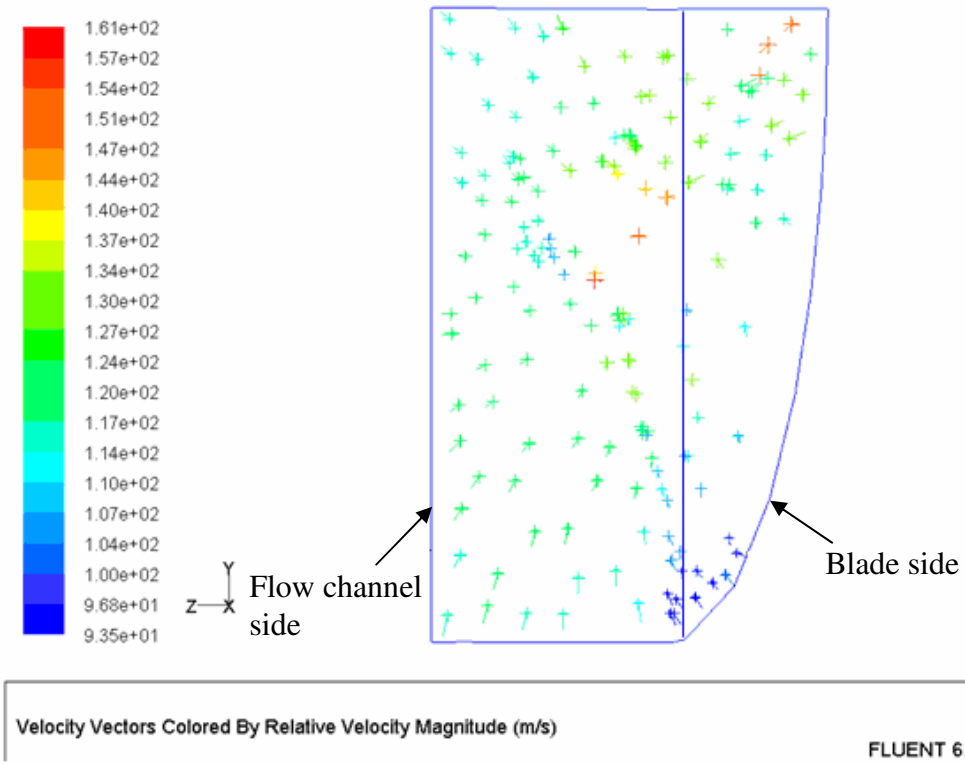

Figure 6.13: Plot of relative velocity vectors on a cross-sectional surface in the flow field for Model **RFCR-90** (*at the design point running speed, 28910 rpm*)

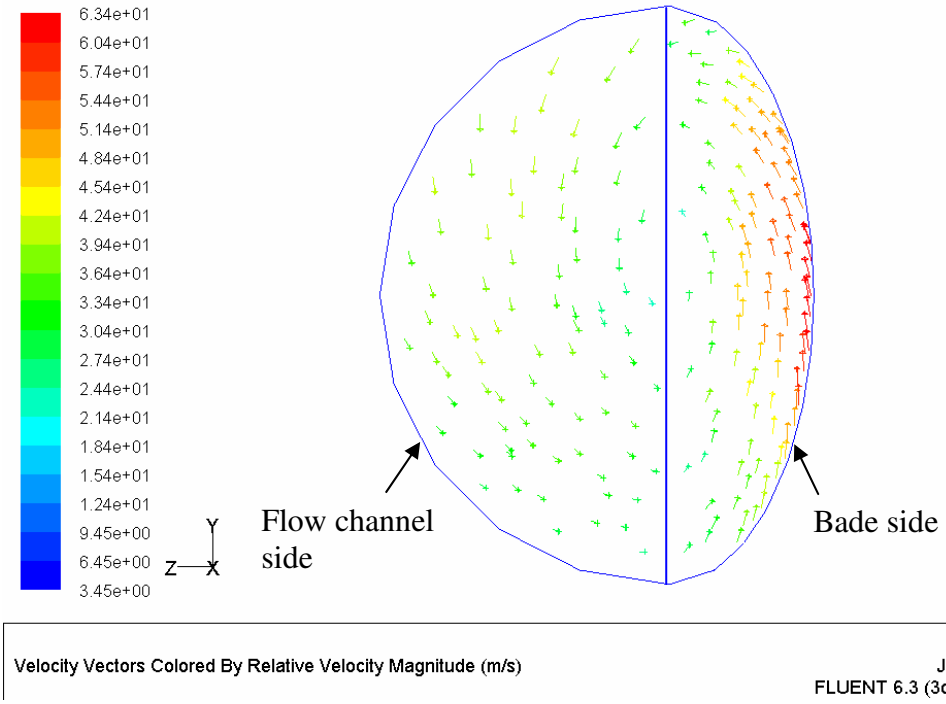

Figure 6.14: Plot of relative velocity vectors on a cross-sectional surface in the flow field for Model **RFCA-145** (*at the design point running speed, 28910 rpm*)

6.2.2 Numerical Results

After convergence is reached printed quantitative results like flux balances, moments and surface integrated quantities are taken for the evaluation of design parameters. Reports of area-weighted average field variables on inlet and outlet surfaces, mass flow rate on inlet and outlet surfaces and moment about center (0, 0, 0) are illustrated below for model RFCA-145.

Area-weighted average field variables are the average value of field variables on inlet and outlet surfaces. They are computed by dividing the summation of the product of the selected field variable and facet area by the total area of the surface.

Area-Weighted Average

Total Pressure	(Pascal)
Inlet	106464.97
Outlet	134139.55

Area-Weighted Average

Density	(kg/m^3)
Inlet	1.2178888
Outlet	1.5376899

As shown in the results the inlet values slightly deviates from the prescribed inlet values. It is caused by the carry over loss and becomes more noticeable at higher speed. This can be considered as the draw back of CFD analysis of RFCs where the required pressure ratio may not be obtained [4].

The total moment vector about center (0, 0, 0) is computed by summing the pressure and viscous moment vectors on the rotor wall. The z-component of total moment is then taken for the evaluation of shaft power.

Moment Center: (0, 0, 0)

Zone name	total moment, M (x, y, z: in N-m)		
Rotor-wall	(-0.12781679	-3.2379046	0.12876165)

The mass flow rate through the inlet and outlet boundaries is also computed by FLUENT. As described in chapter five there should be a mass flow rate balance at the inlet and out let boundaries.

Mass Flow Rate	(kg/s)
Inlet	0.006825326
Outlet	0.0068253237

Table 6.1 below shows a summary of numerical inputs, output results obtained and computed design parameters for different RFC models. The design parameters evaluated from the numerical output results are then used for comparison purpose and for suggesting new design geometries of a regenerative flow compressor.

6.3 Evaluation of Design Parameters

The design parameters i.e. pressure ratio, isothermal efficiency, power coefficient, flow coefficient and specific mass flow rate are evaluated from the numerical output results of FLUENT. These parameters are used to compare the performance characteristics of RFC models. They were defined in Chapter five, section 5.2 and here they will be evaluated for each model.

$$\text{Isothermal efficiency, } \eta_{iso} = \frac{P_{out}}{P_{in}} = \frac{\dot{W}_S}{\dot{W}_a} \tag{6.1}$$

$$\text{Pressure ratio, } \pi = \frac{p_{out}}{p_{in}} \tag{6.2}$$

$$\text{Flow coefficient, } \lambda = \frac{\dot{m}}{8\,\rho_{in}\,\omega\,r_2^{\,3}} \tag{6.3}$$

$$\text{Power Coefficient, } \Upsilon = \frac{Power\ Draw}{32\,\rho_{in}\,\omega^3\,r_2^5} \tag{6.4}$$

$$\text{Specific mass flow rate, } \phi = \frac{\dot{m}}{4r_2^2\,p_{in}}\sqrt{\frac{R_{gas}\,T_{in}}{\gamma}} \tag{6.5}$$

Where;

P_{in} is the actual power transferred to impeller and evaluated as,

$$P_{in} = Power\ Drawn = \dot{W}_a = \mathrm{T}_{shaft} \times \omega \tag{6.6}$$

P_{out} is a power used to compress the fluid under isothermal condition (isothermal power gained by the fluid) and evaluated as,

$$P_{out} = \dot{W}_S = \dot{m}\,R_{gas}\,T_{in}\ \ln\left(\frac{p_{out}}{p_{in}}\right) \tag{6.7}$$

Output result of FLUENT are,

$\dot{m}$ = mass flow rate [kg/s]

p_{in} = total pressure at inlet [Pa]

p_{out} = total pressure at exit port [Pa]

T_{shaft} = shaft torque (the moment on rotor-wall about the z-axis, $\mathrm{M_z}$ [N-m])

ρ_{in} = density at inlet [kg / $\mathrm{m^3}$]

Input variable are,

n = rotational speed [rpm]

ω = angular speed of impeller [rad/s] $= \dfrac{2\,\pi\,n}{60}$ (6.8)

T_{in} = total temperature at inlet [K]

R_{gas} is the gas constant

Table 6.1: Numerical inputs and results of CFD analysis for RFC Models developed

		RFCR-90	RFCS-135	RFCA-135	RFCA-145	RFCA-150	RFCA-160
Geometric data's	Impeller tip dia, mm	82.82 (It is the same for all)					
	Impeller hub dia, mm	63.46 (It is the same for all)					
	Blade depth, mm	2.54	2.54	2.54	2.54	2.54	2.54
	Flow channel depth, mm	3.805	5.09	5.09	5.09	5.09	5.09
	Mesh size, mm	1.5, 1	1.5, 1	1.5, 1	1.5, 1	1.5, 1	1.5, 1
Input Variables	Inlet pressure, p_{in} [pa]	100000	100000	100000	100000	100000	100000
	Outlet pressure, p_{out} [pa]	130000	130000	130000	130000	130000	130000
	Inlet temperature, T_{in} [K]	294.26	294.26	294.26	294.26	294.26	294.26
	Angular velocity, rpm	28910	28910	28910	28910	28910	28910
Fluid Property	Gas constant, R [J/kg K]	287	287	287	287	287	287
FLUENT Output Values	Density at inlet, kg/s	1.1825112	1.2144295	1.2103574	1.2178888	1.2094109	1.2042608
	Density at outlet, kg/s	1.5210673	1.5189388	1.5193921	1.5676898	1.5202744	1.5204897
	Mass flow rate, kg/s	0.0061007	0.00665797	0.006584102	0.006825324	0.006557565	0.006502501
	Torque, M_z [N-m]	0.32542422	0.14210897	0.1186897	0.12876165	0.11520059	0.11967433
	Inlet pressure, p_{in} [pa]	105869.22	106373.05	106139.9	106464.97	106030.04	105984.47
	Outlet pressure, p_{out} [pa]	129996.31	129984.43	129982.46	134139.55	130042.62	130032.91
Computed Values	Pressure ratio, $\pi = \frac{p_{out}}{p_{in}}$	1.227895228	1.221967688	1.224633338	1.259940711	1.226469593	1.226905319
	Output power P_{out} [w]	105.7754625	112.7166072	112.6777154	133.1894783	113.0533357	112.2990869
	Input power, P_{in} [w]	985.2049432	430.2275341	359.3269092	389.8192153	348.7638097	362.3078254
	Isothermal efficiency, η_{iso} [%]	10.73639178	26.19930112	31.35799533	34.16698641	32.41544351	30.99549031
	Flow Coefficient, λ	0.002999798	0.003187771	0.00316301	0.003258616	0.003152727	0.003139623
	Power Coefficient, Υ	0.007705753	0.003276571	0.002745806	0.002960393	0.002667174	0.002782601
	Specific Mass Flow Rate, ϕ	0.002063393	0.002241209	0.002221212	0.00229556	0.002214551	0.0021969

Table 6.1 continued …

		RFCA-180	RFCSEA-145	RFCNGA-145	RFCCA-145
Geometric data's	Impeller tip dia, mm	82.82 (It is the same for all)			
	Impeller hub dia, mm	63.46 (It is the same for all)			
	Blade depth, mm	2.54	2.54	2.54	5.09
	Flow channel depth, mm	5.09	3.5	5.09	5.09
	Mesh size, mm	1.5, 1	1.5, 1	1.5, 1	1.5, 1
Input Variables	Inlet pressure, p_{in} [pa]	100000	100000	100000	100000
	Outlet pressure, p_{out} [pa]	130000	130000	130000	130000
	Inlet temperature, T_{in} [K]	294.26	294.26	294.26	294.26
	Angular velocity, rpm	28910	28910	28910	28910
Fluid Property	Gas constant, R [J/kg K]	287	287	518.3	287
FLUENT Output Values	Density at inlet, kg/s	1.2120155	1.2052342	0.67401302	1.2390414
	Density at outlet, kg/s	1.5193557	1.519486	0.85708404	1.8343834
	Mass flow rate, kg/s	0.006608611	0.004491471	0.004114687	0.006834687
	Torque, M_z [N-m]	0.1321011	0.075259293	0.12511495	0.17364538
	Inlet pressure, p_{in} [pa]	106186.64	103597.59	104136.99	106455.79
	Outlet pressure, p_{out} [pa]	129989.84	129981.82	131930.06	156406.52
Computed Values	Pressure ratio, $\pi = \frac{p_{out}}{p_{in}}$	1.224163793	1.254679959	1.266889508	1.469215719
	Output power P_{out} [w]	112.8831128	86.05953	148.4564641	222.0681946
	Input power, P_{in} [w]	399.9292269	227.8436051	378.7790202	525.7023793
	Isothermal efficiency, η_{iso} [%]	28.22577227	37.77131684	39.19342312	42.24218937
	Flow Coefficient, λ	0.00317044	0.00216688	0.003549654	0.00320738
	Power Coefficient, Υ	0.003051889	0.001748474	0.005197702	0.00392417
	Specific Mass Flow Rate, ϕ	0.002228499	0.001552427	0.00196554	0.002298907

6.4 Validation

Performance of the model of the base machine is compared with its tested data's for validation purpose. The base machine was tested at operation points and an isothermal efficiency of 8.13% was achieved. The simulation result gives an isothermal efficiency of 10.74%, which is close to the tested value, and a pressure ratio of 1.228 is obtained for the base machine. As discussed in chapter five the mismatch may arise from the unidentified losses which are not considered during the simulation process.

The geometry of the base machine i.e. rectangular flow channel area and a straight impeller / blade profile is a major cause for this very low efficiency value. As discussed before cork screw and circulatory flow patterns can not be obtained for this machine. It results in high turbulence and mismatches between flow and blade angles, so that the losses become dominant.

The blade shape, impeller profile and flow channel was then changed for the other models to develop better circulation and regeneration and to minimize losses.

6.5 Results of Modifications done to Improve Performance

6.5.1 Effect of changing Flow Channel and Impeller Profile

For the six successive models the flow channel is changed to semi-circular and the impeller / blade profile is changed to semi-elliptic. To this modified geometry the blades are changed from a straight radial profile for the base machine to airfoil shape with blade angles of 135^{O}, 145^{O}, 150^{O}, 160^{O} and 180^{O}. As shown in the figures above by doing those modifications regeneration is well promoted and the path line of fluid particle is obtained at low speeds. Turbulence and mismatch between the blade and flow angle are minimized, hence better

performance is obtained. As can be shown in Table 6.1 and Figure 6.2 a maximum efficiency of 34.17% and a pressure ratio of 1.26 is obtained for blades angle $\beta = 145^{O}$.

Maintaining the blade angle to this optimum value ($\beta = 145^{O}$) and the impeller / blade profile to semi-elliptic shape the flow channel depth is decreased (made semi-elliptic) to investigate its effect on turbulence and fluid friction. As can be seen in the table the efficiency is improved to 37.77% with very close pressure ratio (1.255). Therefore changing the flow channel area to semi-elliptic reduces the flow turbulence and optimum cross sectional area can be obtained by investigating other dimensions.

6.5.2 Effect of changing Blades Angle

Blades angle were varied from purely radial 90^{O} to chevroned blade with an angle of 135^{O}, 145^{O}, 150^{O}, 160^{O} and 180^{O}. This angle variations / chevroning are also responsible to establish circulatory flow pattern and regeneration. Many authors suggest that changing the blades angle / chevroning reduce losses and increases the pressure ratio in RFCs [3] [4] [5]. The advantage of changing blade angles on performance is shown in Table 6.1. The blade angle variation from straight radial to aerodynamic shape results in an improved performance and pressure ratio. By varying the blade angle for the first modified geometry i.e. semi-circular flow channel and semi-elliptic impeller / blade profile a maximum efficiency of 34.17% and pressure ratio of 1.26 are obtained for blade angle $\beta = 145^{O}$.

It must however be noted that the chevron angle should not deviate more from 145^{O}, because doing that might bring in excessive slow down to the flow. And this results in a lower efficiency and pressure ratio. As shown in Table 6.1 an efficiency of 28.23% and pressure ratio of 1.224 are obtained for $\beta = 180^{O}$.

6.5.3 Effect of adding a Core

For the above optimum blade angle ($\beta = 145^{O}$) adding a core in between a semi-circular flow channel and impeller / blade profile maximizes both the efficiency and pressure ratio. The core guides the flow properly and avoids local vortices in the blade and flow channel region. At lower running speed addition of core promotes a well developed continuous cork screw flow pattern which is shown in Figure 6.18 for the starting speed of 2891 rpm. As shown in Figure 6.19 also the pressure ratio is increased and a maximum pressure ratio of 1.47 is obtained at the design point with an efficiency of 42.24%.

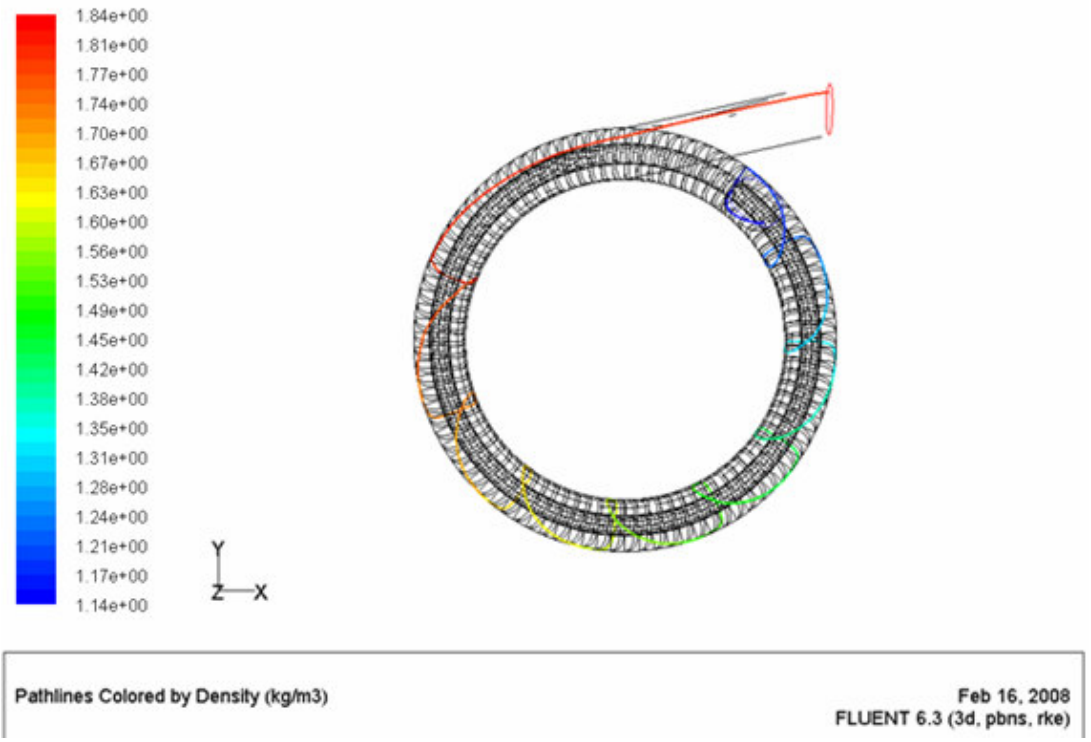

Figure 6.15: Plot of a particle path line from inlet to exit port for Model **RFCCA-145** (*at starting running speed, 2891 rpm*)

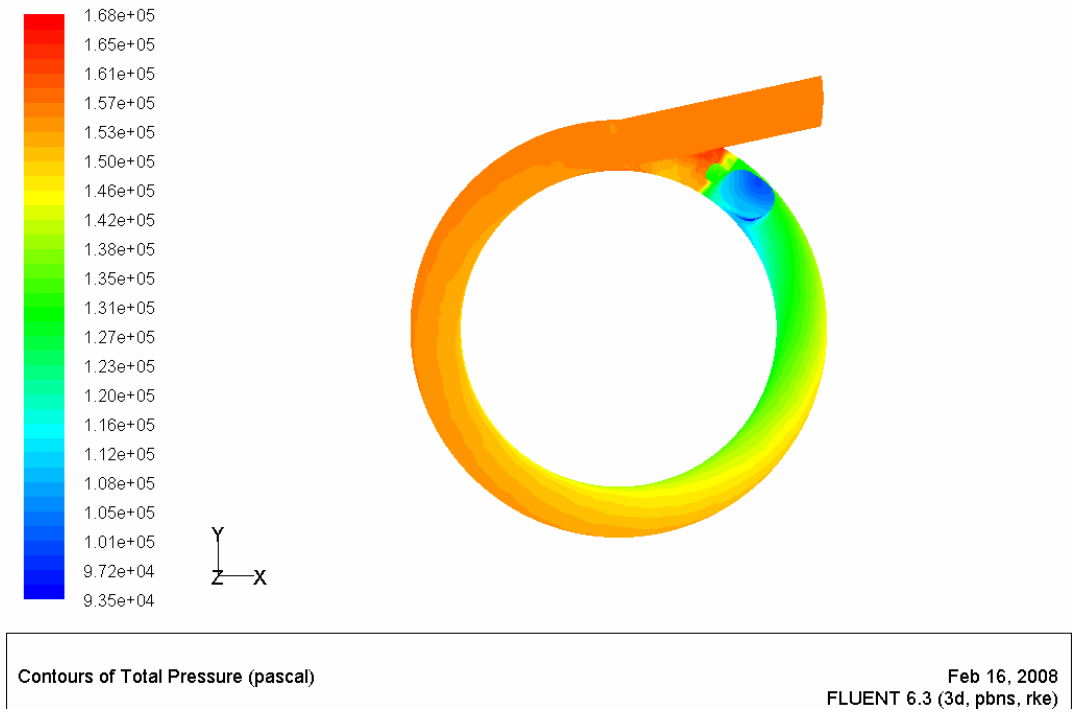

Figure 6.16: Plot of total pressure contours over the entire flow field for Model **RFCCA-145** (*at design point running speed, 28910 rpm*)

6.5.4 Effect of changing the Working Fluid

The base machine was tested by using air as a working fluid [4]. But the actual working fluid is natural gas, hence the model (semi-circular channel, semi-elliptic impeller / blade profile and airfoil blade angle, $\beta = 145^0$) is simulated using both air and natural gas. As shown in the table an efficiency of 39.19% and a pressure ratio of 1.267 are obtained for natural gas. Even though these values slightly deviates from using air, it is reasonable to use air as a working fluid for the actual lab testing purpose which is cheaper as compared to natural gas.

CHAPTER SEVEN

CONCLUSIONS AND RECOMMENDATIONS

RFC has a wide application especially for duties requiring high head at low flow rate, but unfortunately it has low efficiency. This research was started with an objective of improving the performance of the machine by modifying its geometry to aerodynamic shape. Attempt was made to investigate the flow characteristic using FLUENT and the results obtained from the analysis motivate to use CFD software's for further study of these machines.

In this section, based on the results, conclusions will be given and recommendation will be presented in regard to the long-term objectives.

7.1 Conclusions

The following conclusions are drawn from the CFD results:

a. Aerodynamically designed geometries give better performance. The flow channel and impeller / blade geometries of the base machine are changed to aerodynamic shape so that regeneration effect is highly facilitated at lower speeds and better efficiency is obtained in all speed range.

b. The addition of a core in the flow field further increases the performance of RFCs. This merit is investigated by adding a core for a selected blade angle ($\beta = 145^{O}$) and an improved pressure ratio and efficiency is obtained.

c. Flow characteristics in RFC are examined. On the graphical display of FLUENT the three-dimensional continuous cork screw flow patterns are illustrated for lower running speeds; however this regeneration effect diminishes as the running speed of the machine increases. This same phenomenon is also confirmed by

investigating the isothermal power gained by the fluid particle in its passage from inlet to the exit port where at higher speeds no regenerative energy gain is observed.

d. Performance characteristic of RFC that is capability of producing a pressure ratio at low specific mass flow rate is also investigated. As can be shown in Table 6.1 the pressure ratio obtained are at lower specific mass flow rate.

e. High efficiency and pressure ratio is obtained as the blade angle increases from radial straight to aerodynamic shape; however after a certain point where peak efficiency is achieved its value starts to go down with blade angle.

f. Agreement between test data's and those experimental values is observed. This motivates to carry out extensive design analysis on RFC using commercially available CFD software's.

7.2 Recommendations

In this research the design changes focus on the flow channel geometry and impeller / blade profile. The blade angles are also selected randomly from the recommended range. Therefore further design changes can also be considered on the other geometries for improving the performance of the machine.

a. The inlet port is responsible to set up circulatory flow pattern in regenerative flow machine by projecting the fluid towards the inlet edge of the blade with the velocity and direction needed to ensure smooth entry. Hence inlet ports can be further optimized for generating such flow pattern and to ensure smooth entry to the blades. The same is true for outlet ports where they can be designed further to exploit the kinetic energy of the flow for pressure rise.

b. The blade angle can also be varied to obtain other optimum value in the range $135^{O} < \beta < 150^{O}$.

c. For RFC the maximum blade number suggested by many authors is $Z_b = 90$, hence the number of blades can be reduced for the optimum blade angle to check for better performance.

d. Geometry of the stripper, just like the inlet port, is also responsible for generating circulatory flow pattern. Hence various stripper geometries can be considered together with inlet and outlet ports for upgrading the performance of the machine.

Generally a complete analysis of various geometric parameters is very much needed to establish design criteria's for regenerative flow compressors.

REFERENCES

1. Andrew D.N.: **The Calculation of flow in regenerative turbomachines by a streamline curvature method,** Whittle Laboratory, University of Cambridge, 1990.
2. Engda A. and Raheel M.: **Theory and design of the regenerative flow compressor**, Proc. International Gas Turbine Congress – TS050, 2003.
3. Engda A., Song J.W. and Raheel M.: **A Compressible Flow Theory for Regenerative Compressor with Aerofoil Blades**, Proc. Instn Mech. Engrs- 2003.
4. Raheel M.: **A Theoretical, Experimental and CFD Analysis of regenerative flow compressors and regenerative flow pumps for microturbine and automotive fuel applications**, Ph.D. thesis, Michigan State University, USA, 2003.
5. Sixsmith H.: **The theory and design of a regenerative compressor,** Research paper for Institute of Refrigeration, Institute of Marine Engineers, 1981, 69-77.
6. Sixsmith H. and Altmann H.: **A regenerative Compressor**, Trans. ASME Journal of Eng'g for Industry, 1977, 637-647.
7. Song J.W., Engda A. and Chung M. K.: **A modified theory for the flow mechanism in regenerative flow pump**, Proc. Instn Mech. Engrs – A05202, 2003.
8. Dixon S.L.: **Fluid Mechanics and Thermodynamics of Turbomachines**, Fourth Edition, University of Liverpool, 2005.
9. Wilson W.A., Santalo M.A. and Oelrich, J.A.: **A Theory of the Fluid Dynamic Mechanism of Regenerative Pumps**, ASME Journal of Eng'g for Industry, 54-A59/60, August 1954.
10. Meakhail T. and Park S. O.: **An improved theory for regenerative pump performance**, Proc. Instn Mech. Engrs - A05604, Korea Advanced Institute of Science and Technology, 18 October 2004.
11. Fluent Inc.: **FLUENT 6.3.26 Documentation** – User's Guide, 2006.
12. http://en.wikipedia.org/wiki/gas compressors

APPENDIX

OUTPUT RESULTS FOR RFC MODELS

** All the figures are at the design point except for the particle path line, which is taken at 2891 rpm.*

1. Output results for model RFCR-90

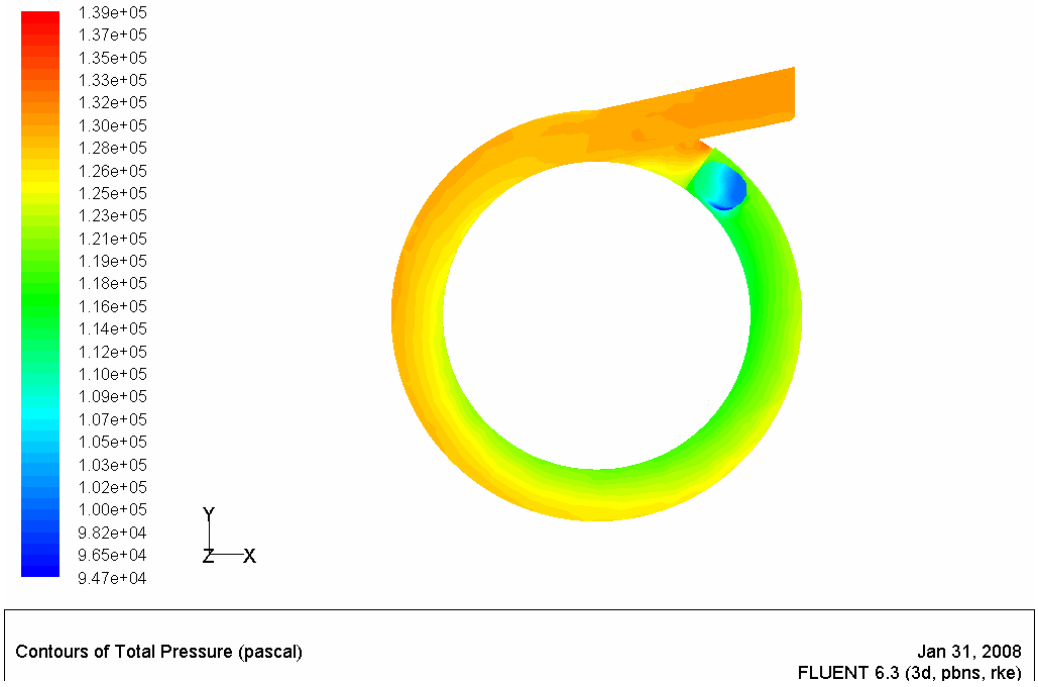

Figure 6.17: Plot of total pressure contours over the entire flow field for Model **RFCR-90**

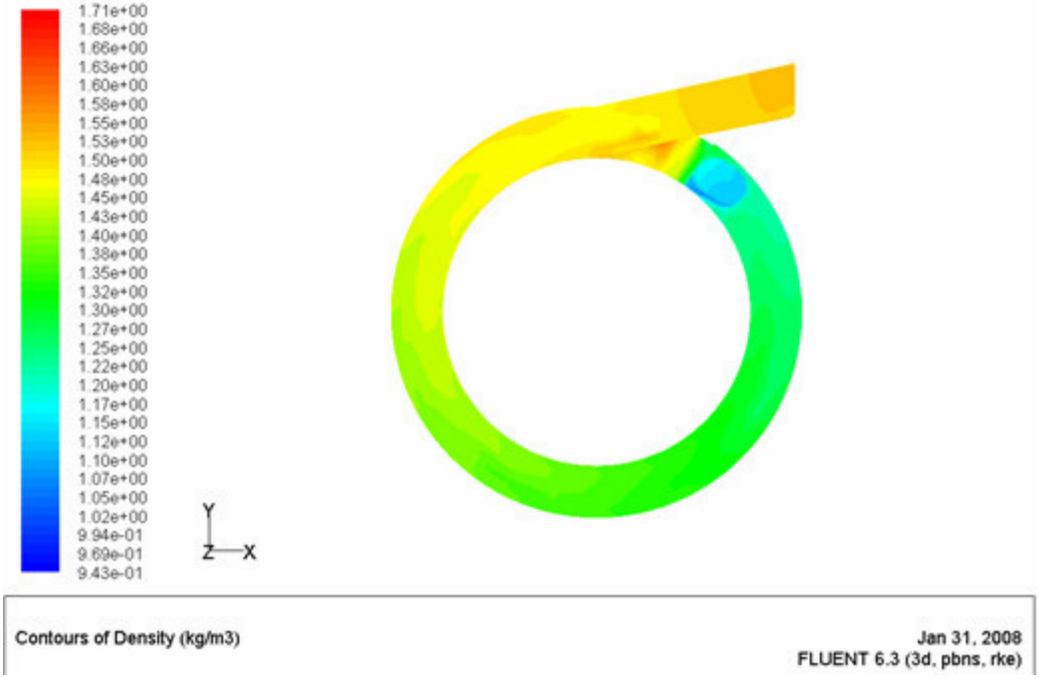

Figure 6.18: Plot of density contours over the entire flow field for Model **RFCR-90**

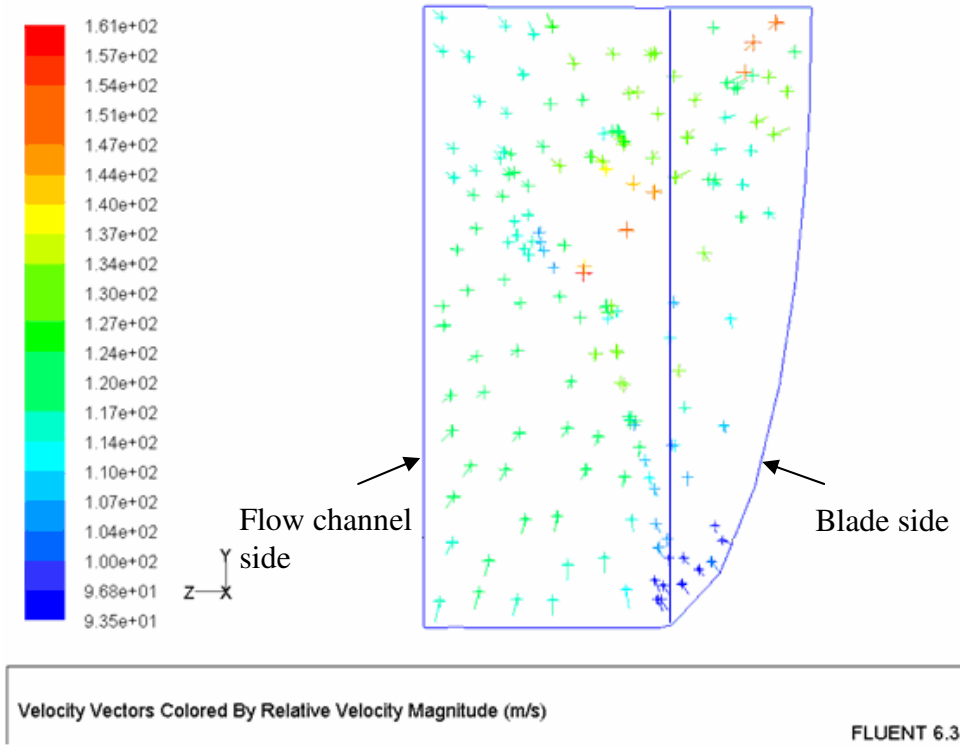

Figure 6.19: Plot of relative velocity vectors on a cross-sectional surface in the flow field for Model **RFCR-90**

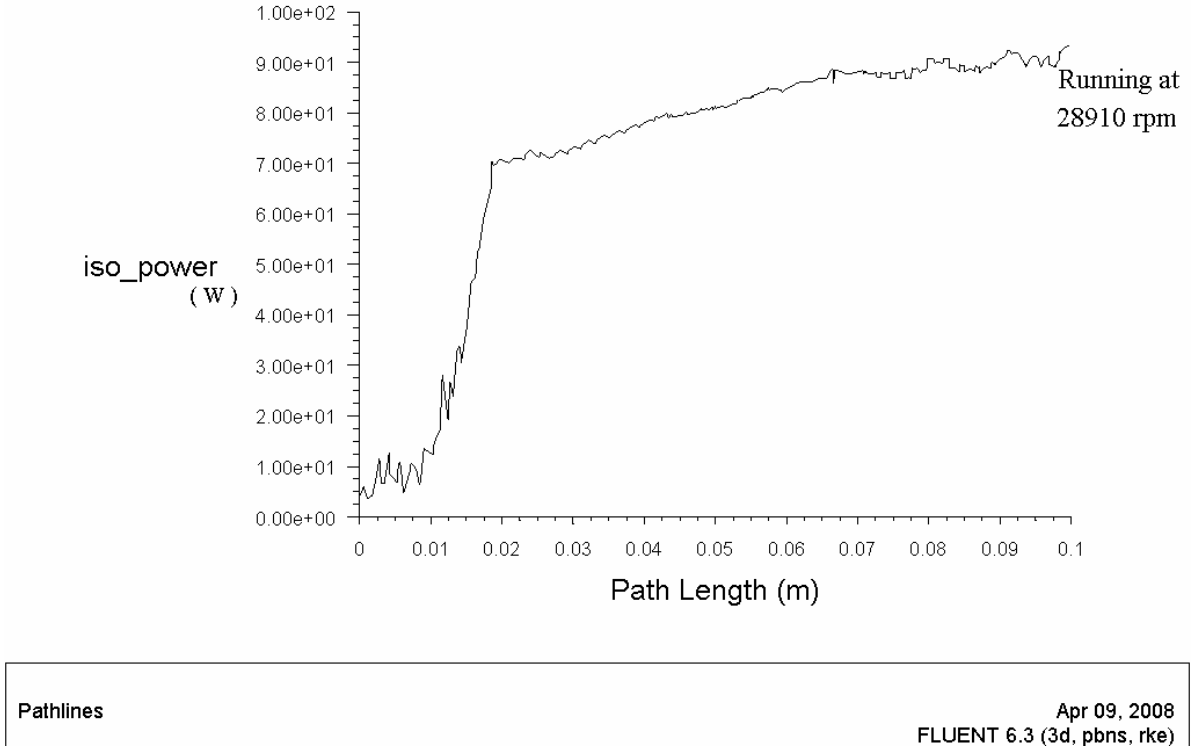

Figure 6.20: Plot of Isothermal power gained by a particle along its path line from inlet to exit port for Model **RFCR-90**

2. Output results for model RFCS-135

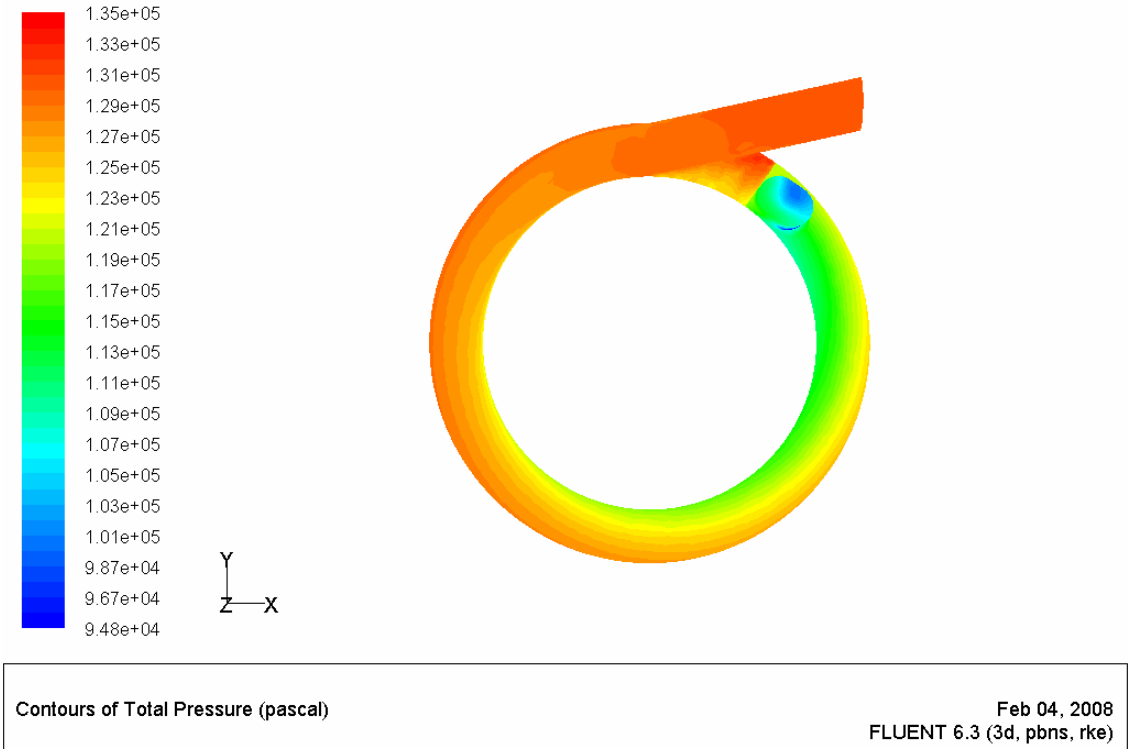

Figure 6.21: Plot of total pressure contours over the entire flow field for Model **RFCS-135**

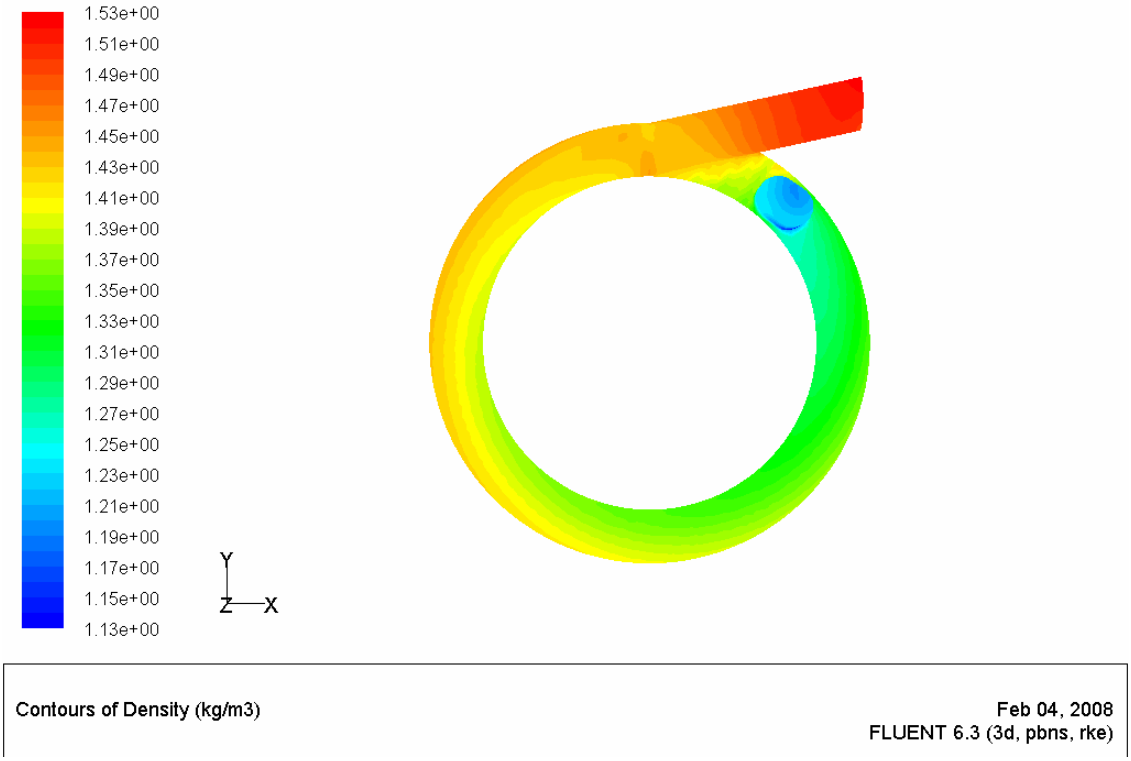

Figure 6.22: Plot of density contours over the entire flow field for Model **RFCS-135**

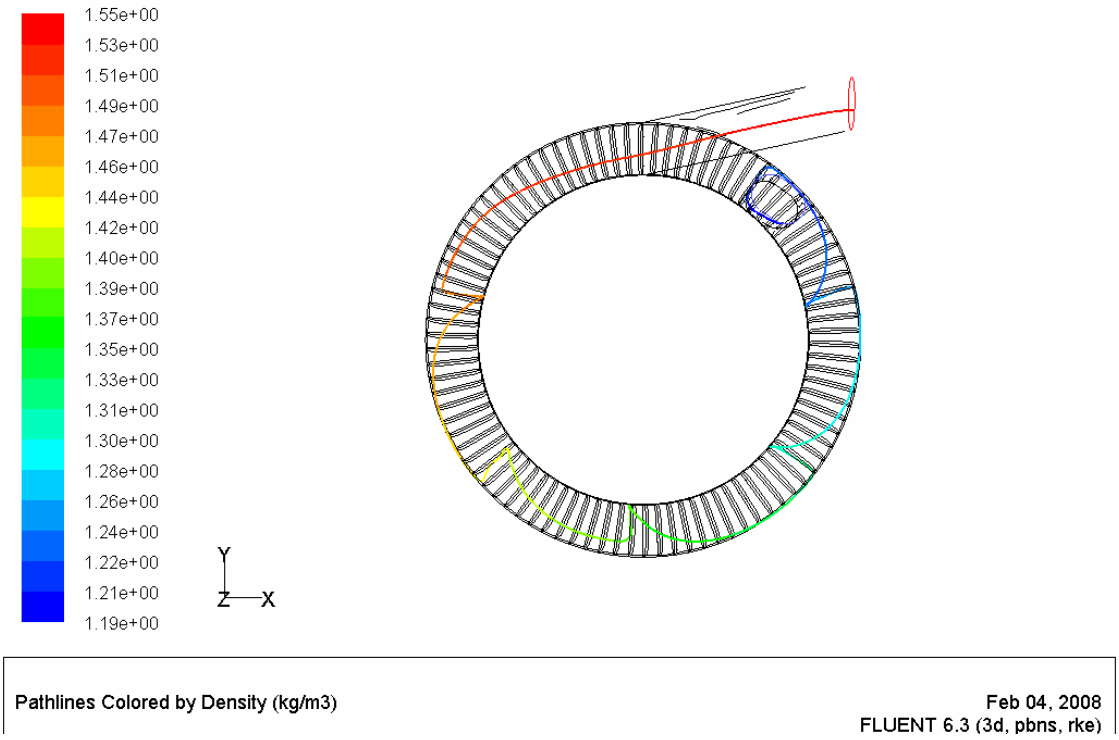

Figure 6.23: Plot of a particle path line from inlet to exit port for Model **RFCS-135** (*at starting running speed, 2891 rpm*)

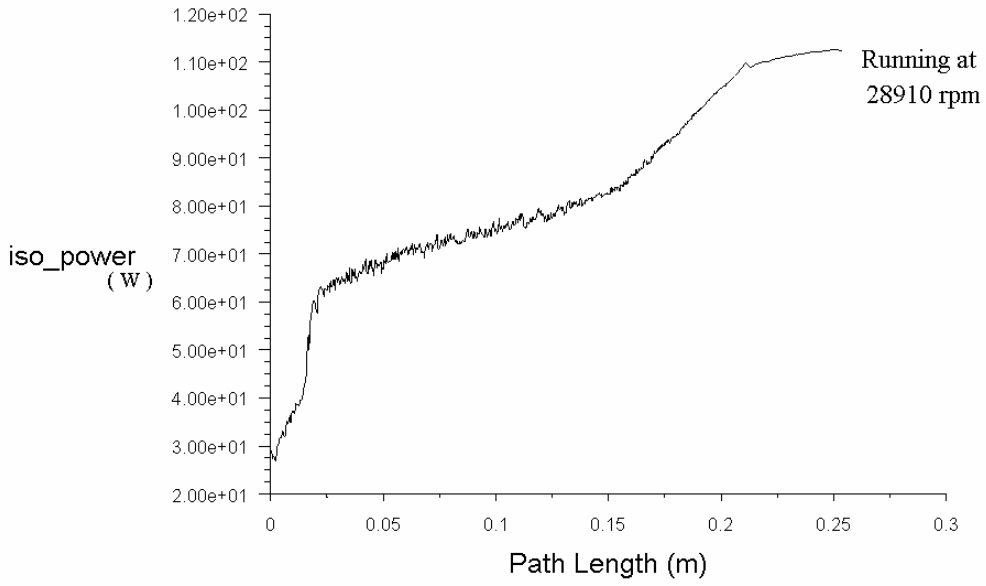

Figure 6.24: Plot of Isothermal power gained by a particle along its path line from inlet to exit port for Model **RFCS-135**

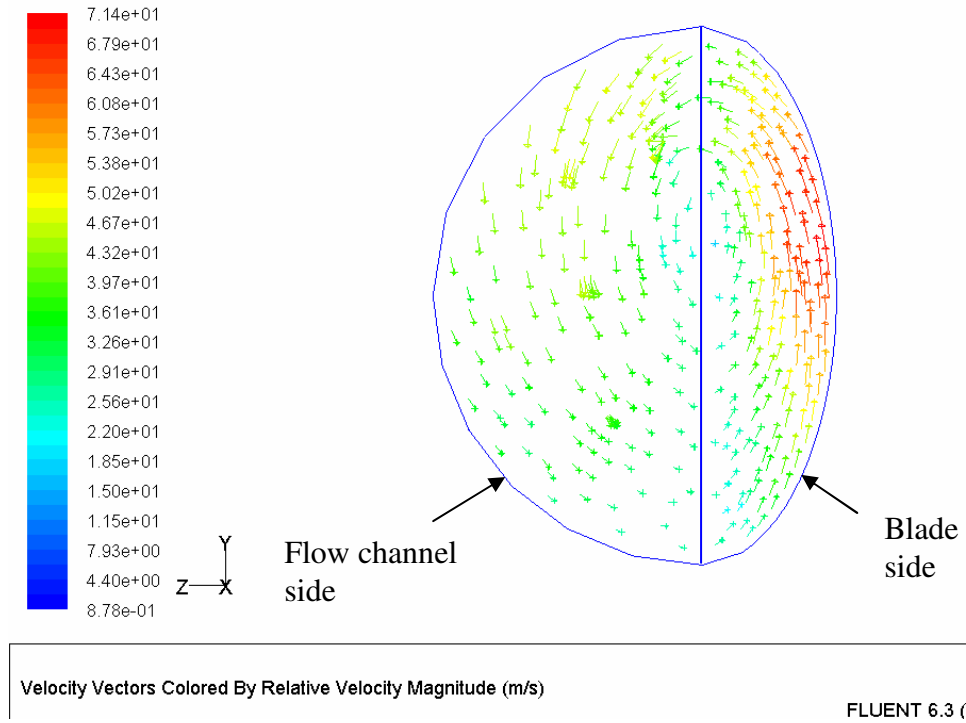

Figure 6.25: Plot of relative velocity vectors on a cross-sectional surface in the flow field for Model **RFCS-135**

3. Output results for model RFCA-135

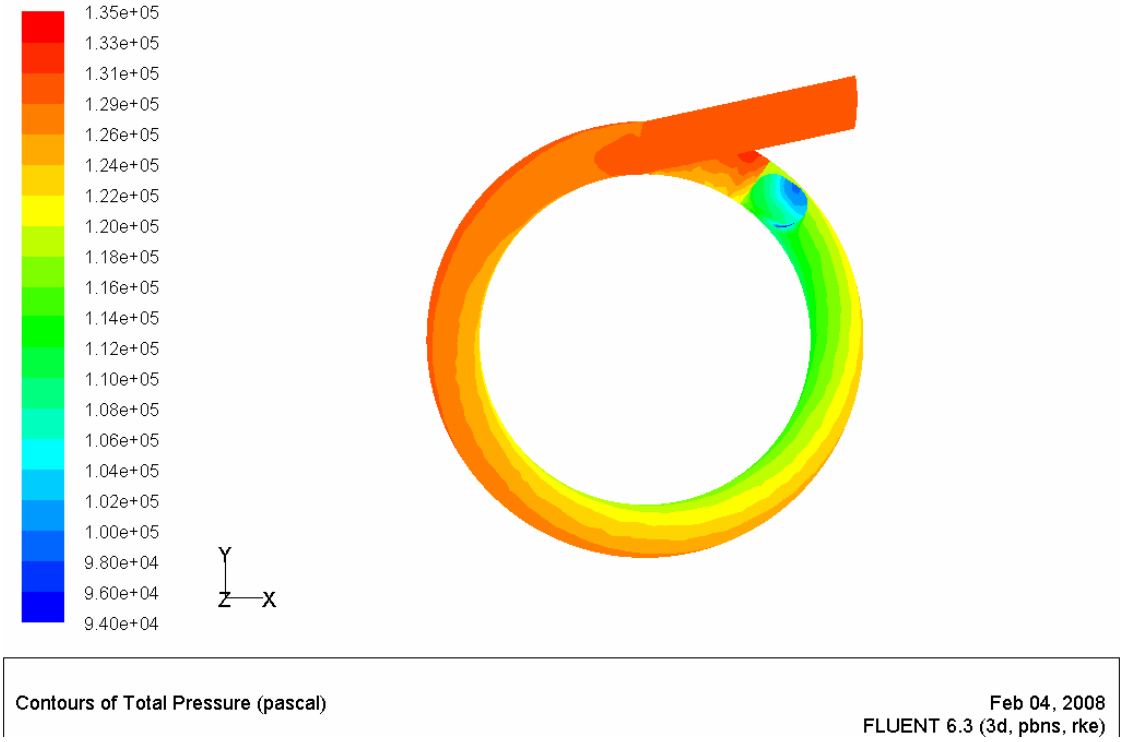

Figure 6.26: Plot of total pressure contours over the entire flow field for Model **RFCA-135**

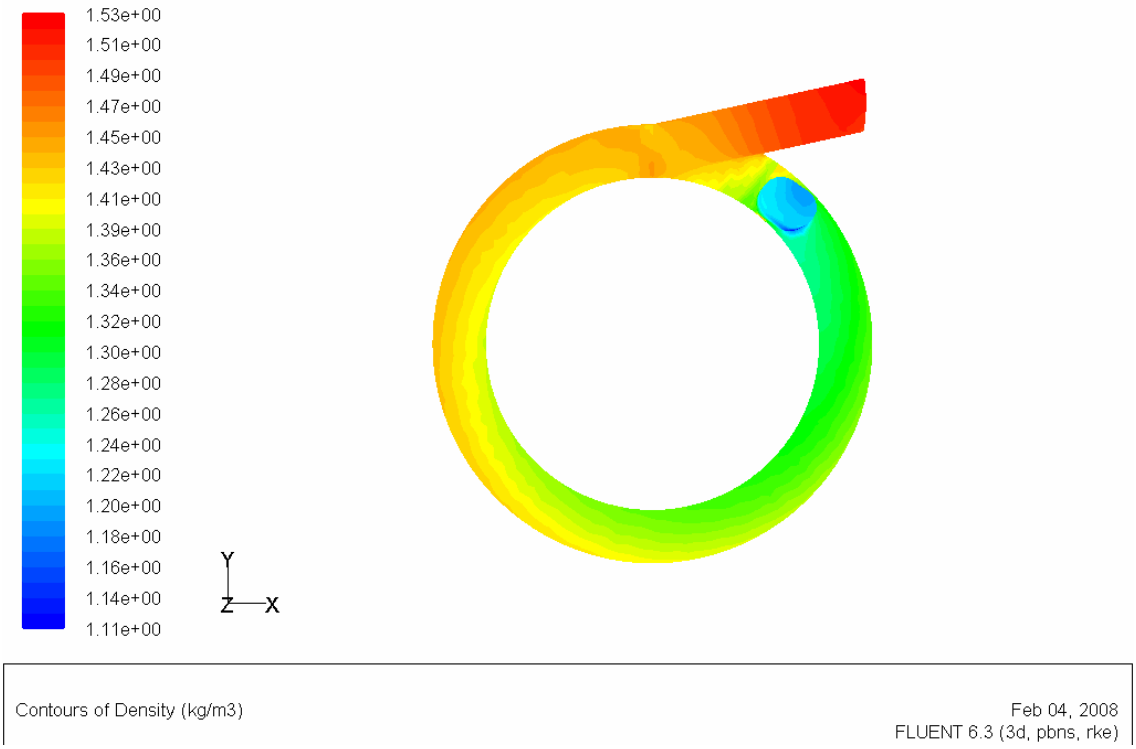

Figure 6.27: Plot of density contours over the entire flow field for Model **RFCA-135**

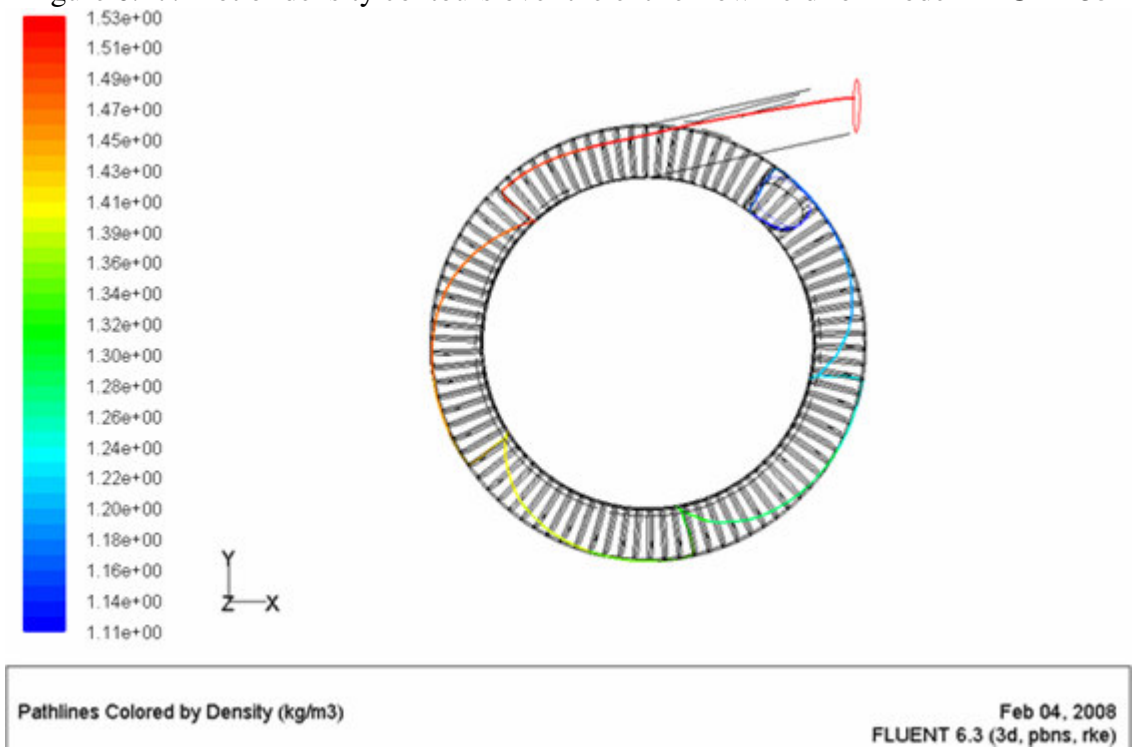

Figure 6.28: Plot of a particle path line from inlet to exit port for Model **RFCA-135** (*at starting running speed, 2891 rpm*)

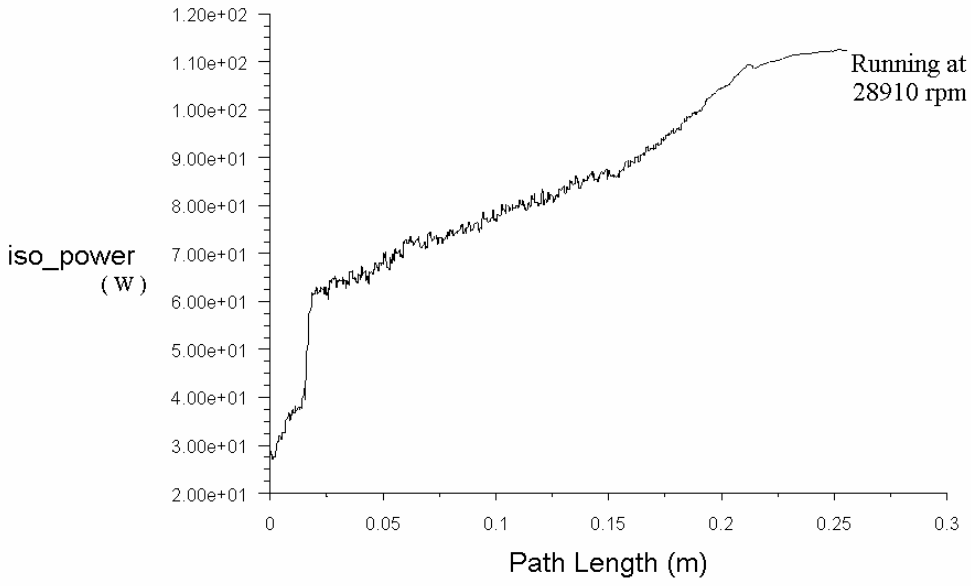

Figure 6.29: Plot of Isothermal power gained by a particle along its path line from inlet to exit port for Model **RFCA-135**

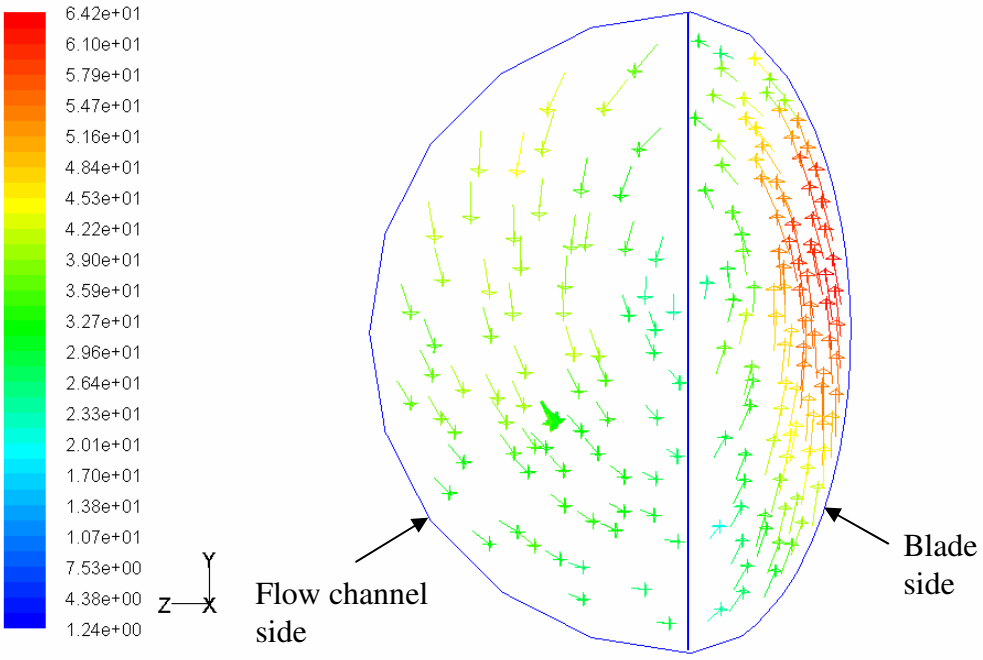

Figure 6.30: Plot of relative velocity vectors on a cross-sectional surface in the flow field for Model **RFCA-135**

4. Output results for model RFCA-145

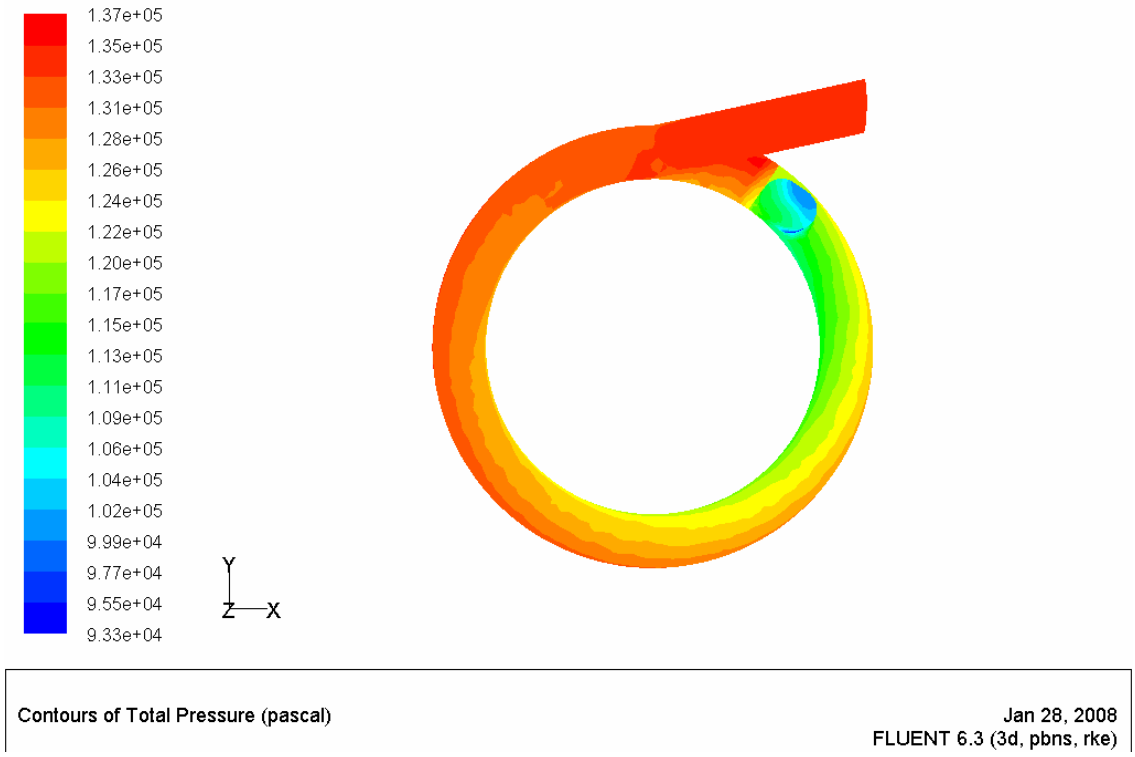

Figure 6.31: Plot of total pressure contours over the entire flow field for Model **RFCA-145**

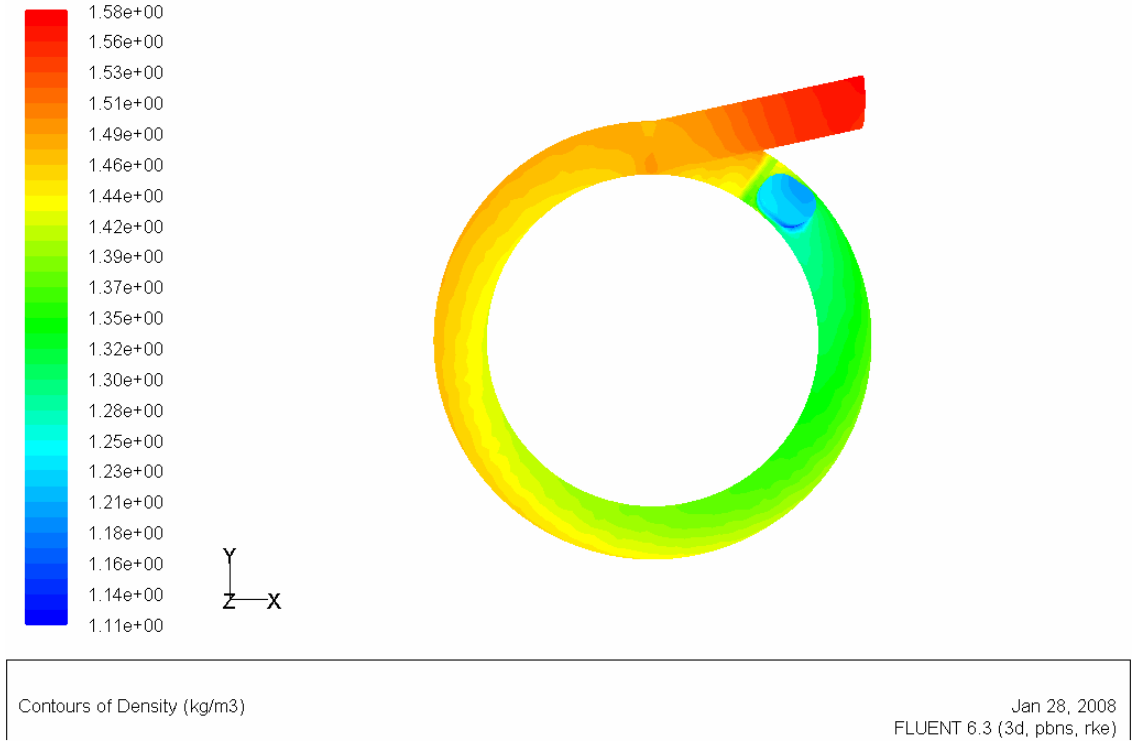

Figure 6.32: Plot of density contours over the entire flow field for Model **RFCA-145**

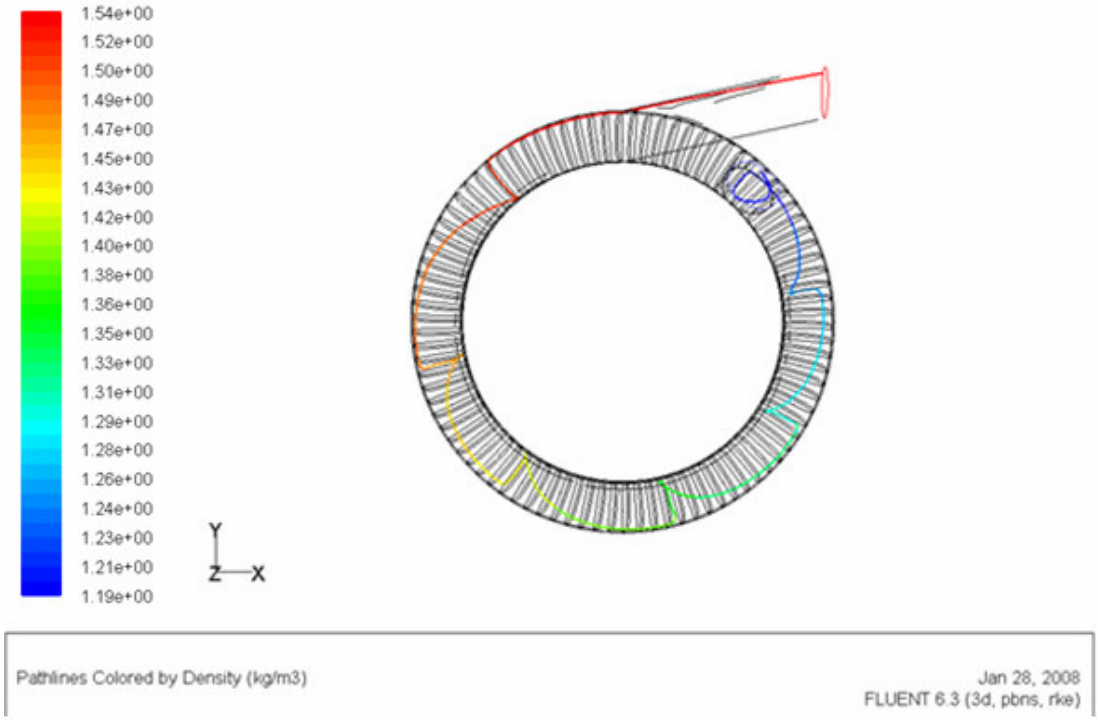

Figure 6.33: Plot of a particle path line from inlet to exit port for Model **RFCA-145** (*at starting running speed, 2891 rpm*)

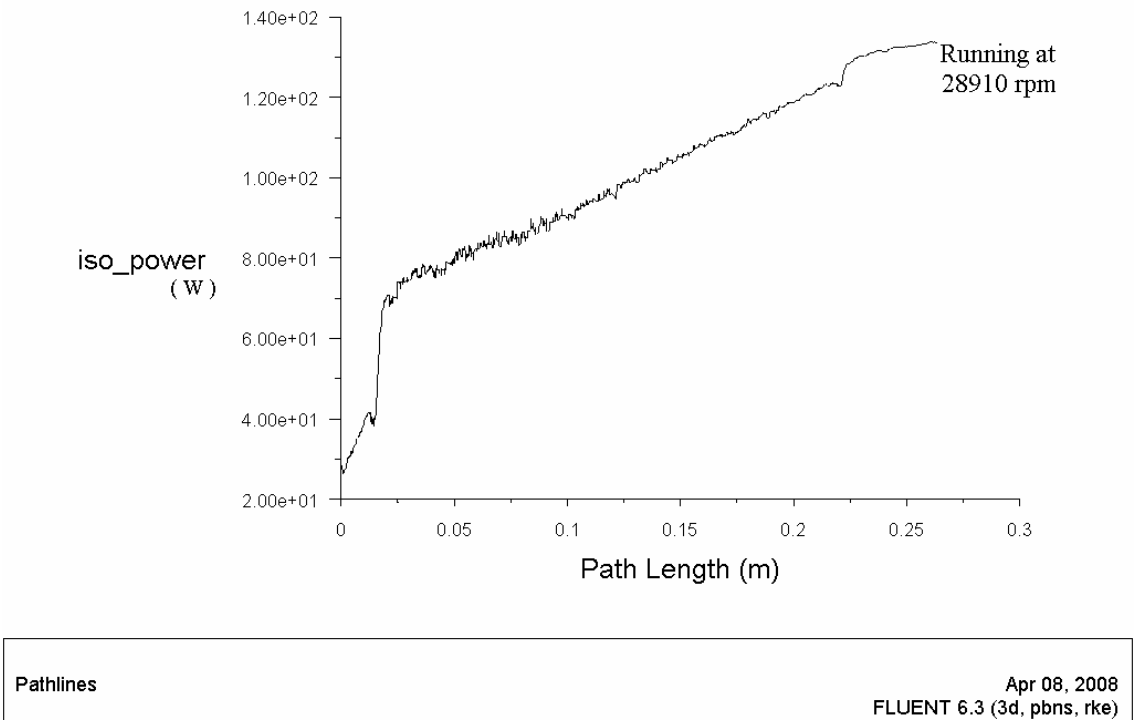

Figure 6.34: Plot of Isothermal power gained by a particle along its path line from inlet to exit port for Model **RFCA-145**

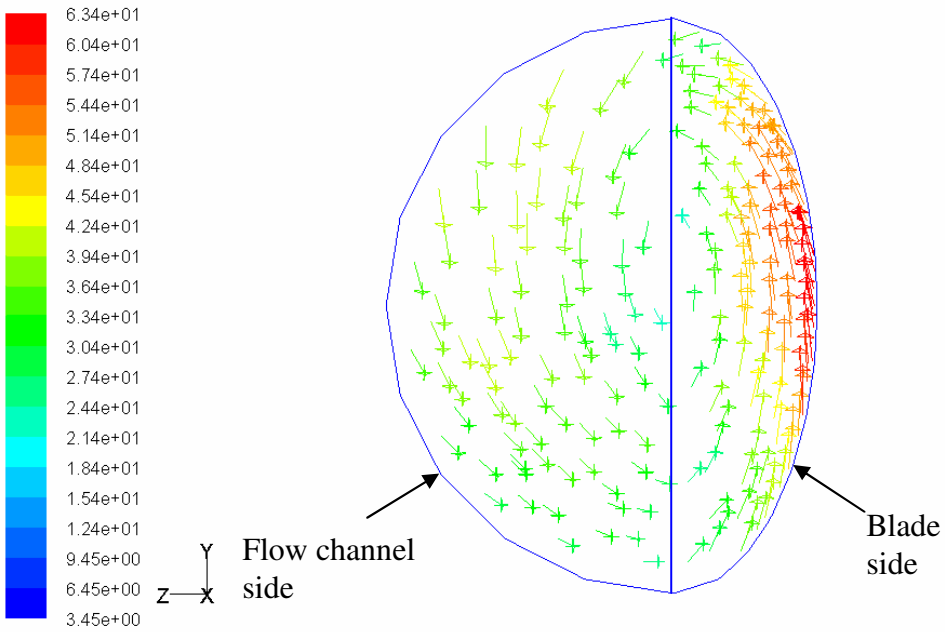

Figure 6.35: Plot of relative velocity vectors on a cross-sectional surface in the flow field for Model **RFCA-145**

5. Output results for model RFCA-150

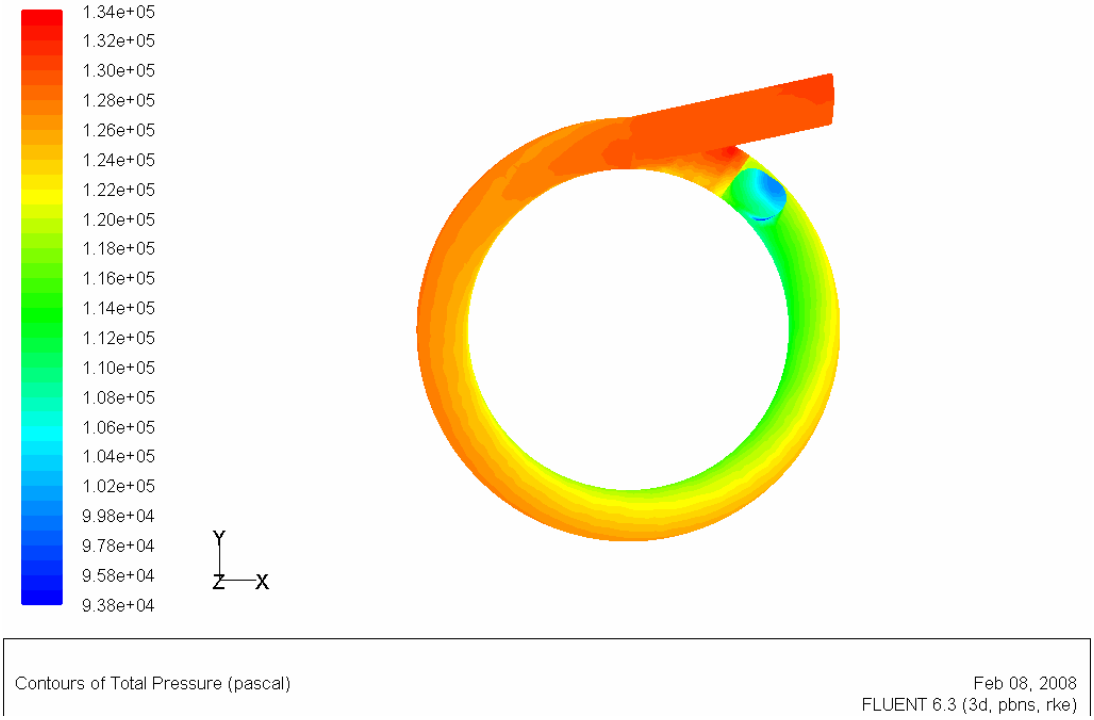

Figure 6.36: Plot of total pressure contours over the entire flow field for Model **RFCA-150**

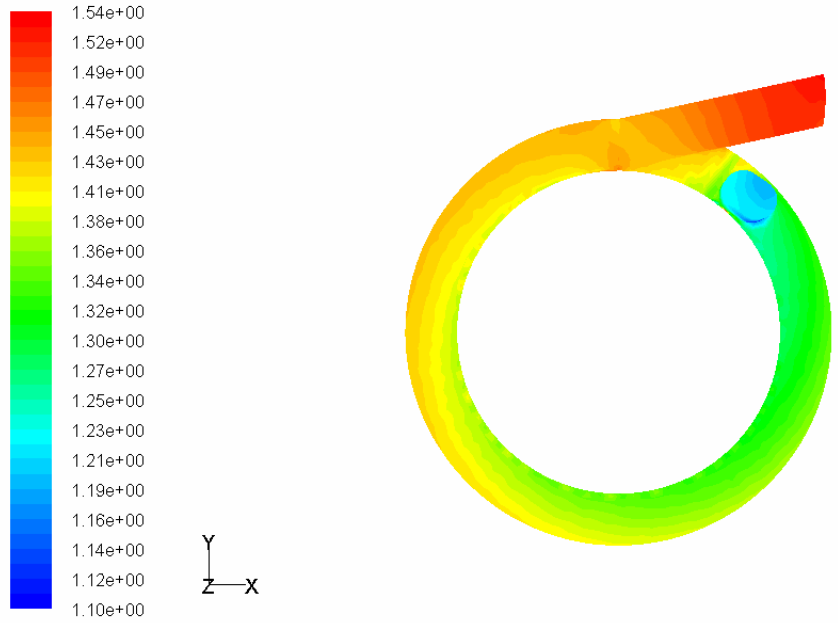

Figure 6.37: Plot of density contours over the entire flow field for Model **RFCA-150**

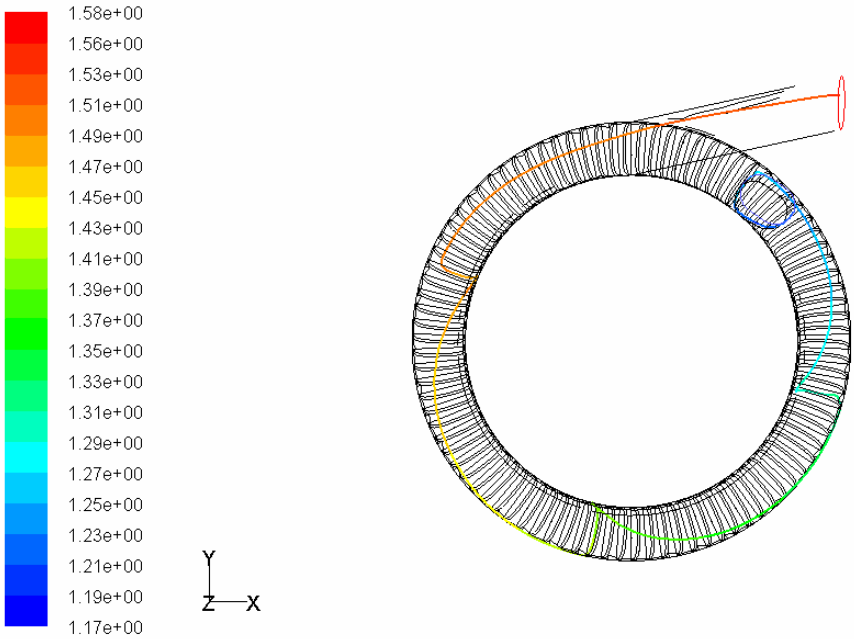

Figure 6.38: Plot of a particle path line from inlet to exit port for Model **RFCA-150** (*at starting running speed, 2891 rpm*)

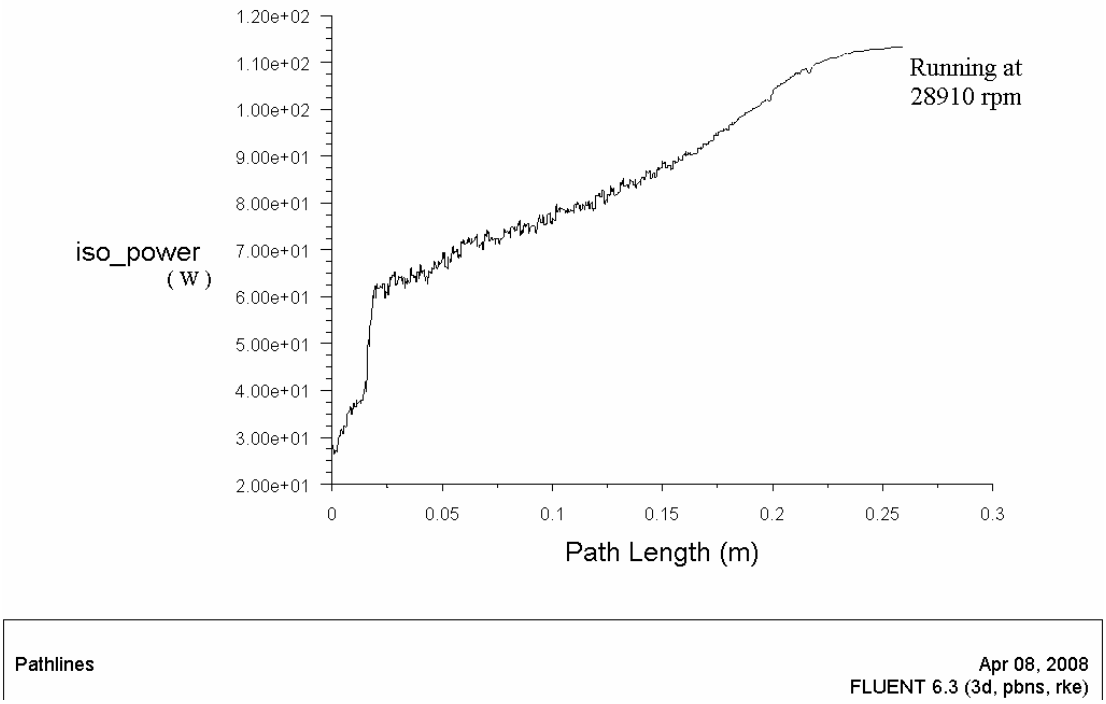

Figure 6.39: Plot of Isothermal power gained by a particle along its path line from inlet to exit port for Model **RFCA-150**

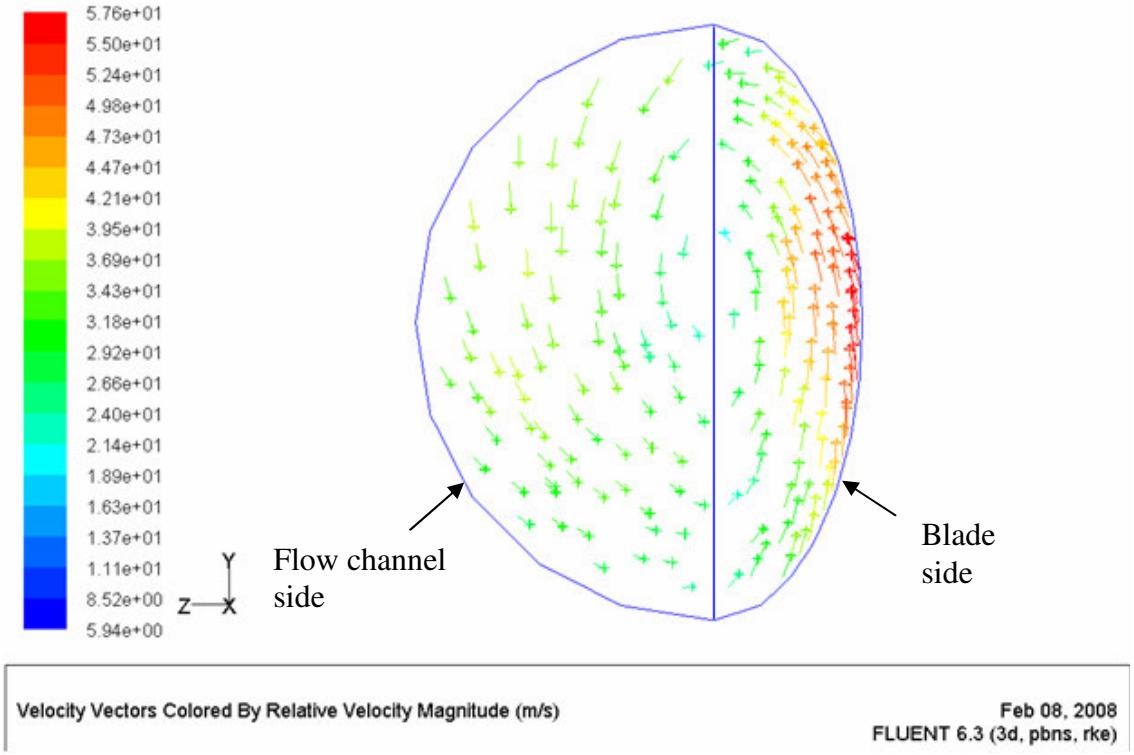

Figure 6.40: Plot of relative velocity vectors on a cross-sectional surface in the flow field for Model **RFCA-150**

6. Output results for model RFCA-160

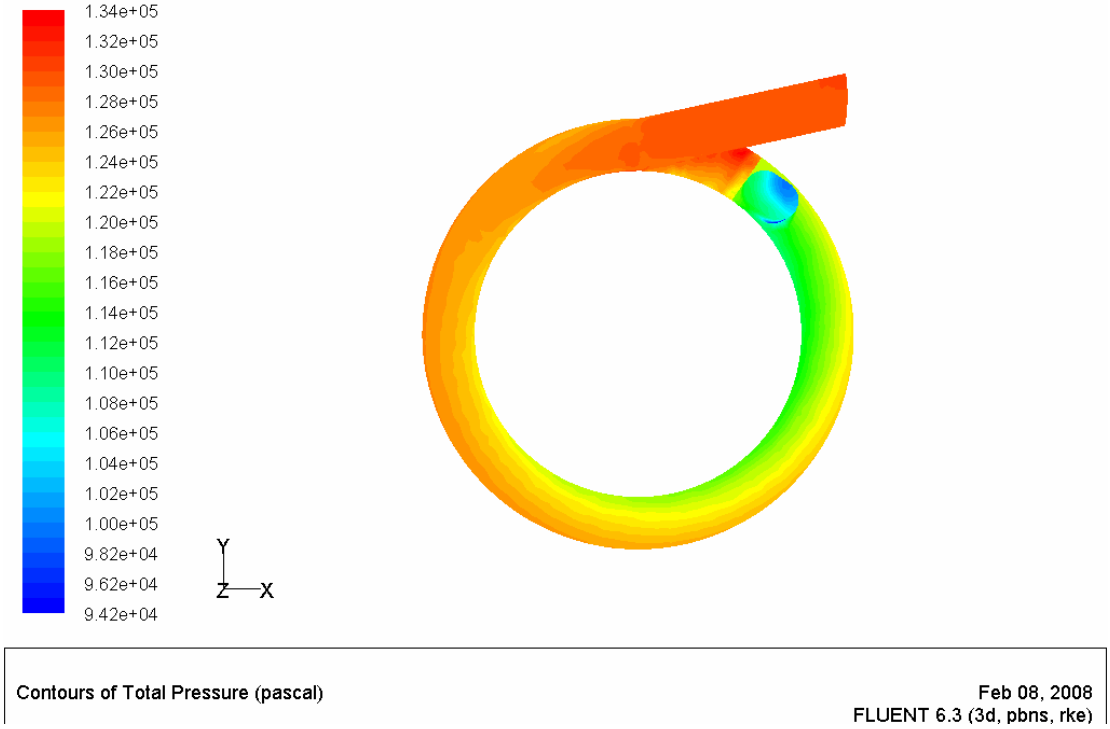

Figure 6.41: Plot of total pressure contours over the entire flow field for Model **RFCA-160**

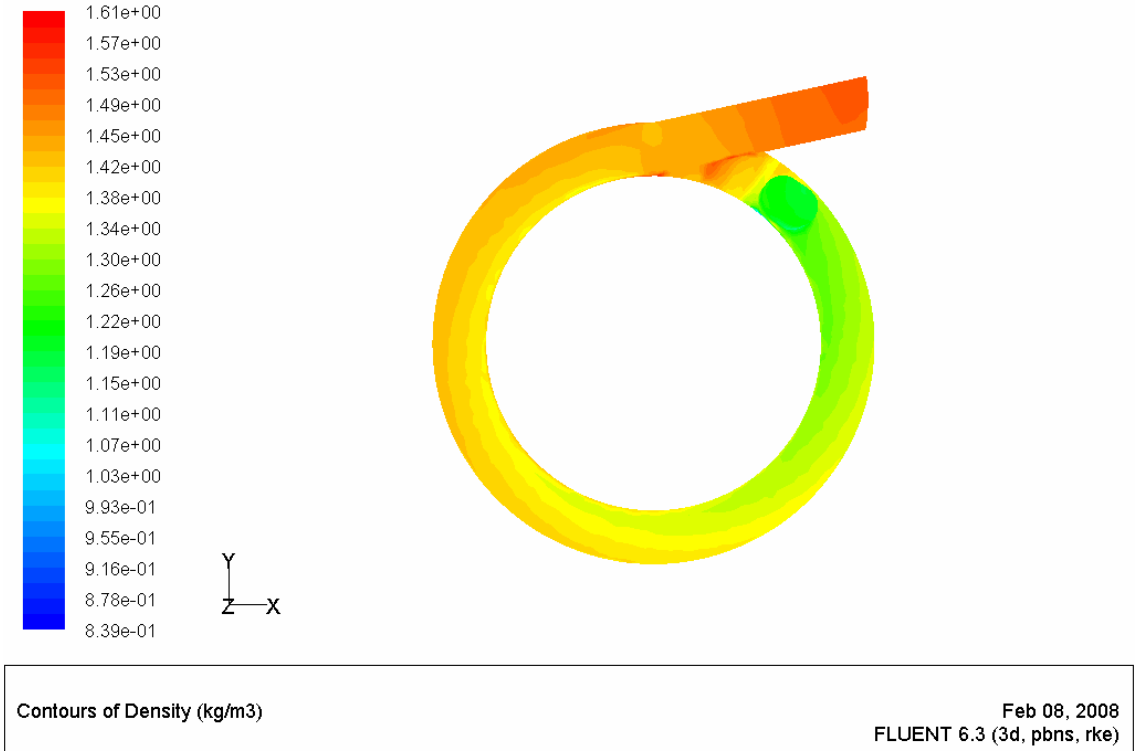

Figure 6.42: Plot of density contours over the entire flow field for Model **RFCA-160**

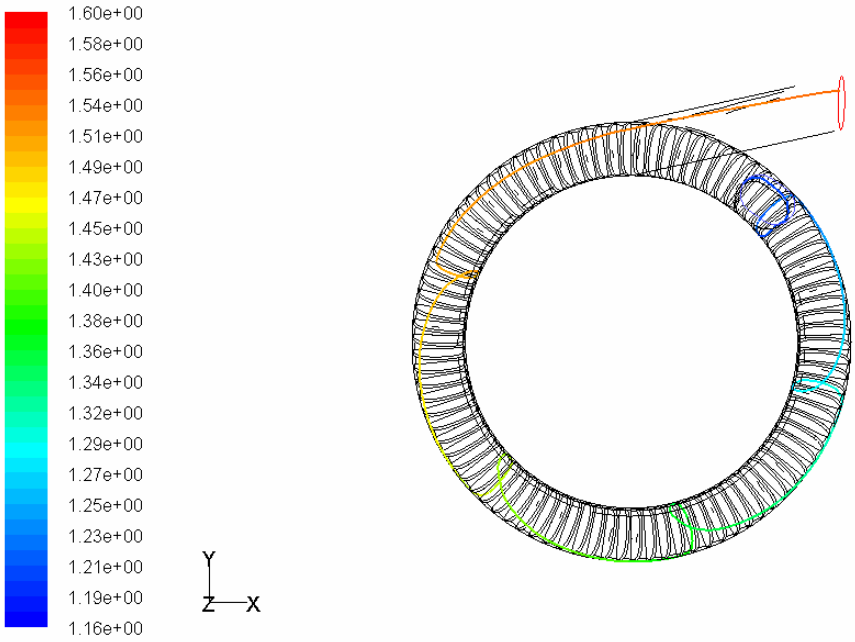

Figure 6.43: Plot of a particle path line from inlet to exit port for Model **RFCA-160** (*at starting running speed, 2891 rpm*)

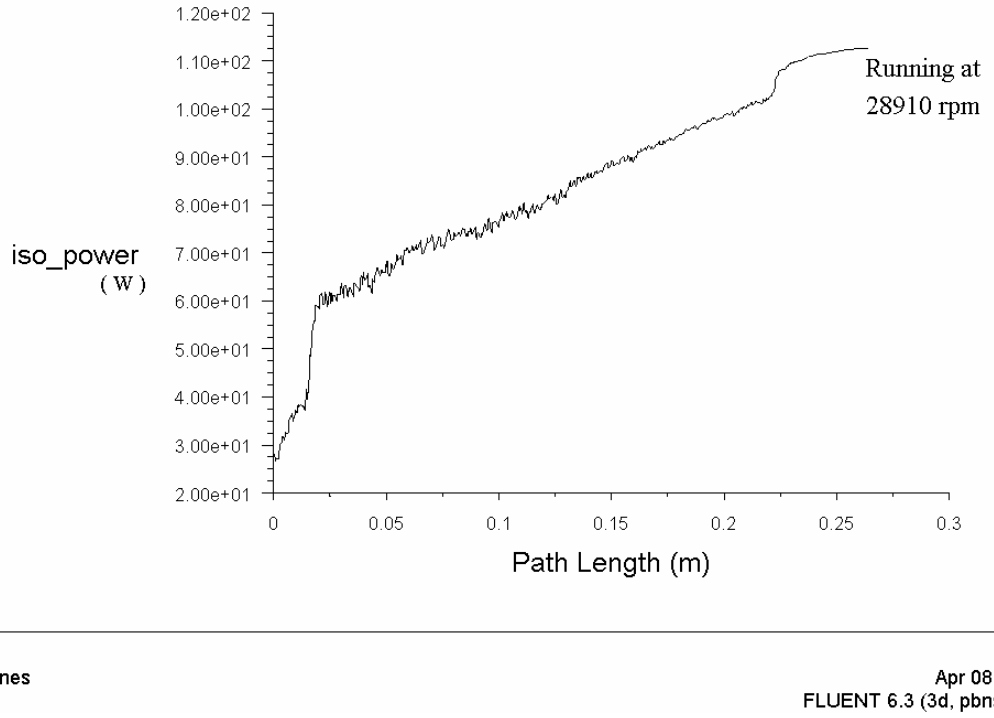

Figure 6.44: Plot of Isothermal power gained by a particle along its path line from inlet to exit port for Model **RFCA-160**

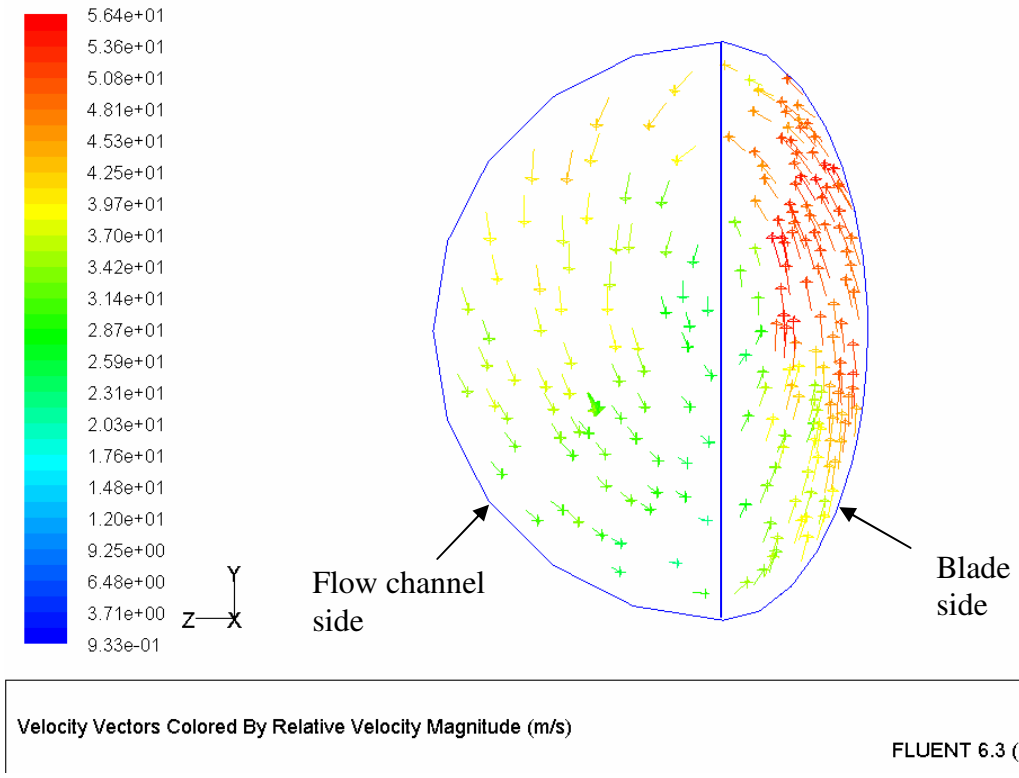

Figure 6.45: Plot of relative velocity vectors on a cross-sectional surface in the flow field for Model **RFCA-160**

7. Output results for model RFCA-180

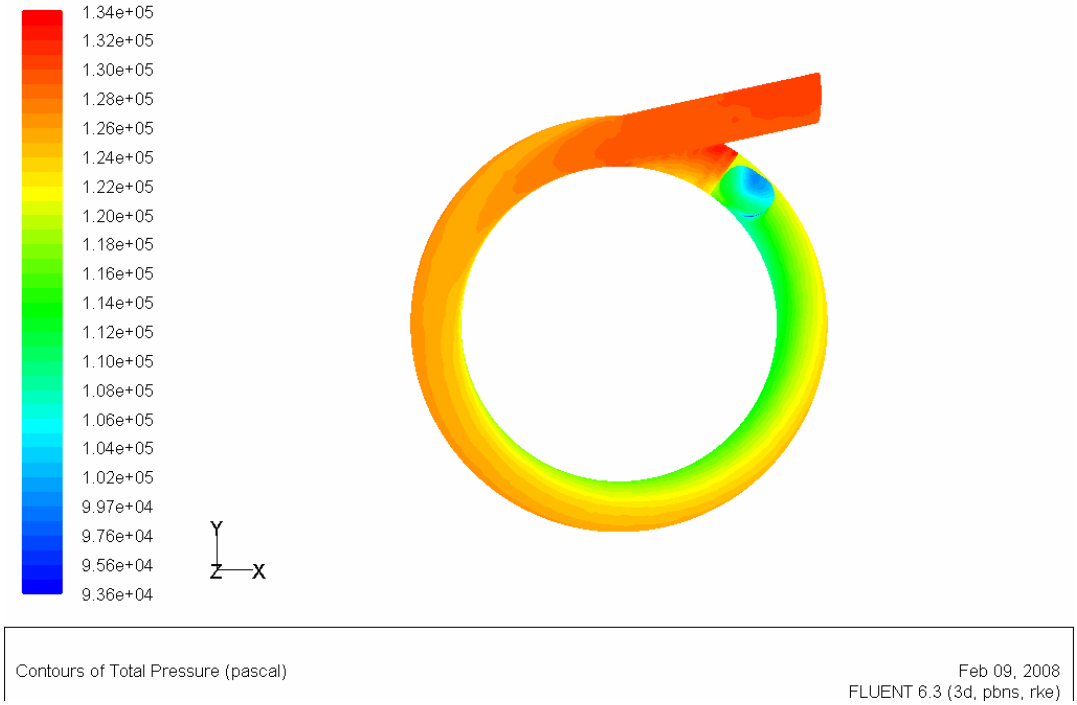

Figure 6.46: Plot of total pressure contours over the entire flow field for Model **RFCA-180**

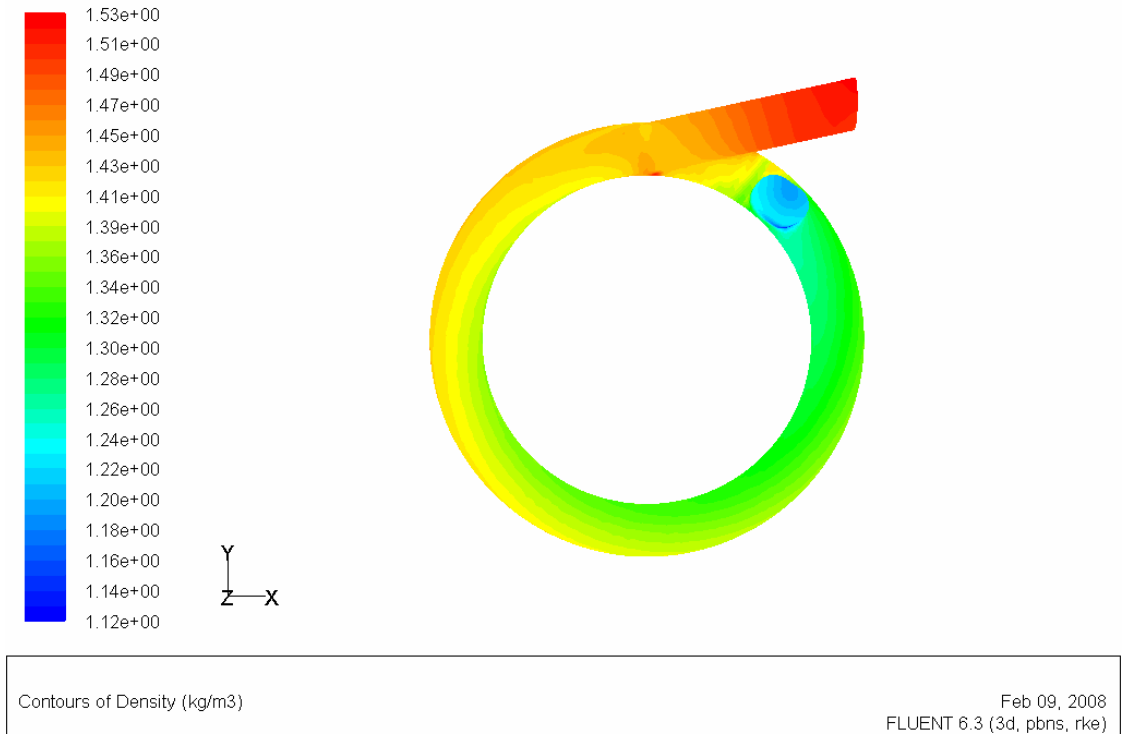

Figure 6.47: Plot of density contours over the entire flow field for Model **RFCA-180**

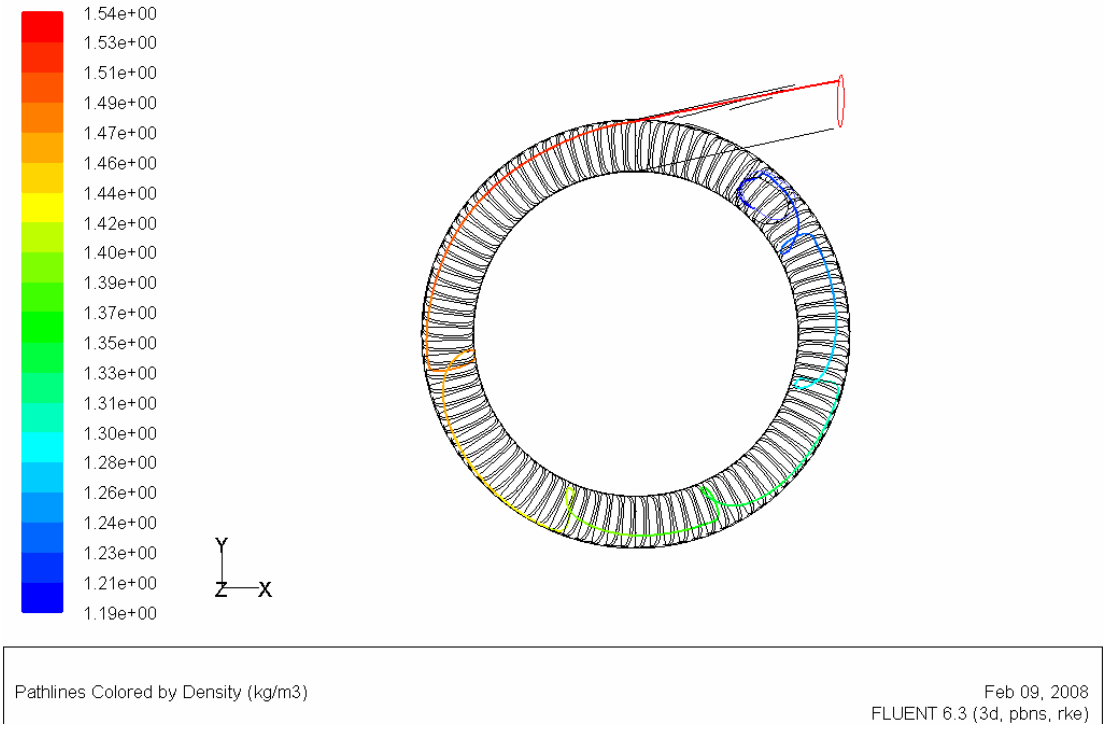

Figure 6.48: Plot of a particle path line from inlet to exit port for Model **RFCA-180** (*at starting running speed, 2891 rpm*)

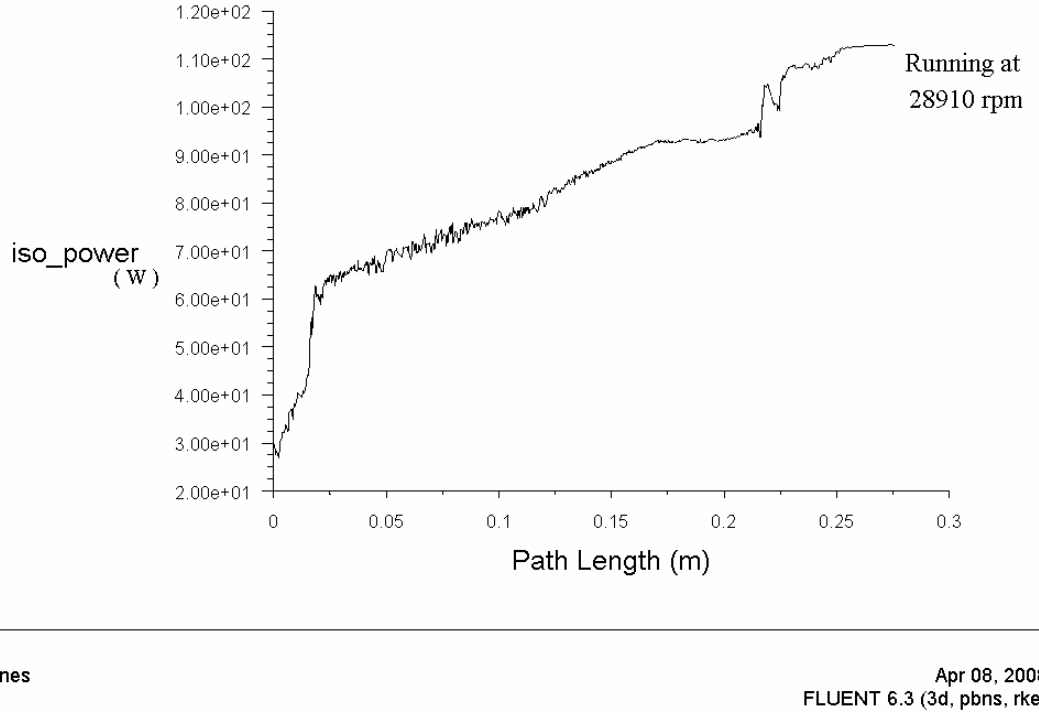

Figure 6.49: Plot of Isothermal power gained by a particle along its path line from inlet to exit port for Model **RFCA-180**

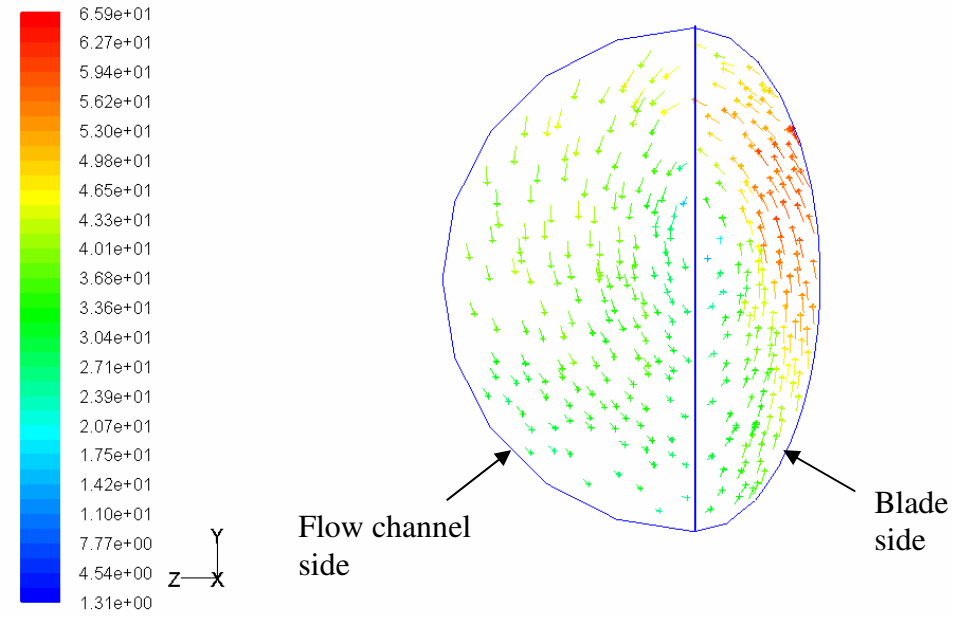

Figure 6.50: Plot of relative velocity vectors on a cross-sectional surface in the flow field for Model **RFCA-180**

8. Output results for model RFCSEA-145

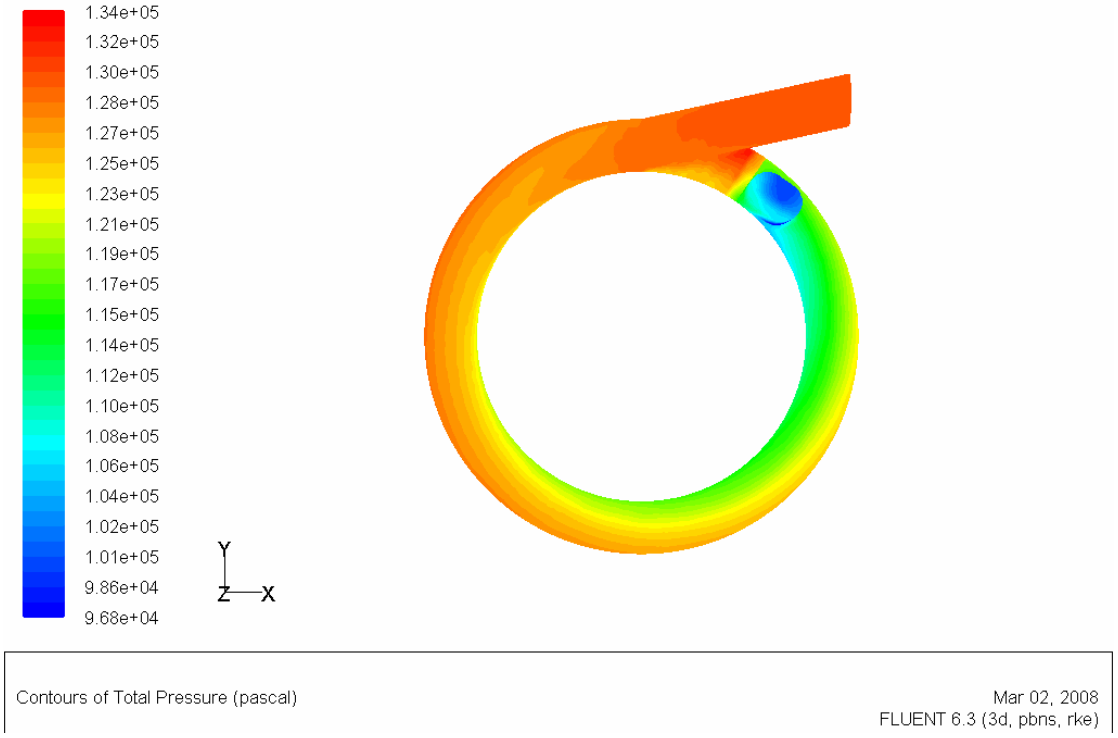

Figure 6.51: Plot of total pressure contours over the entire flow field for Model **RFCSEA-145**

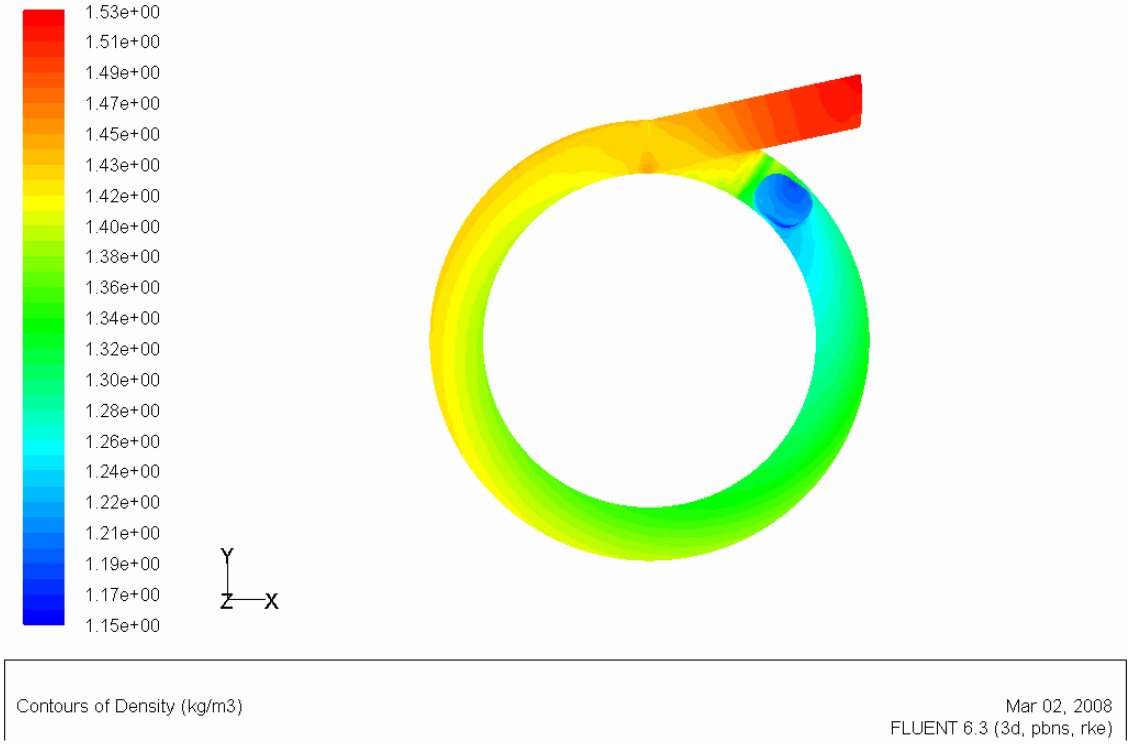

Figure 6.52: Plot of density contours over the entire flow field for Model **RFCSEA-145**

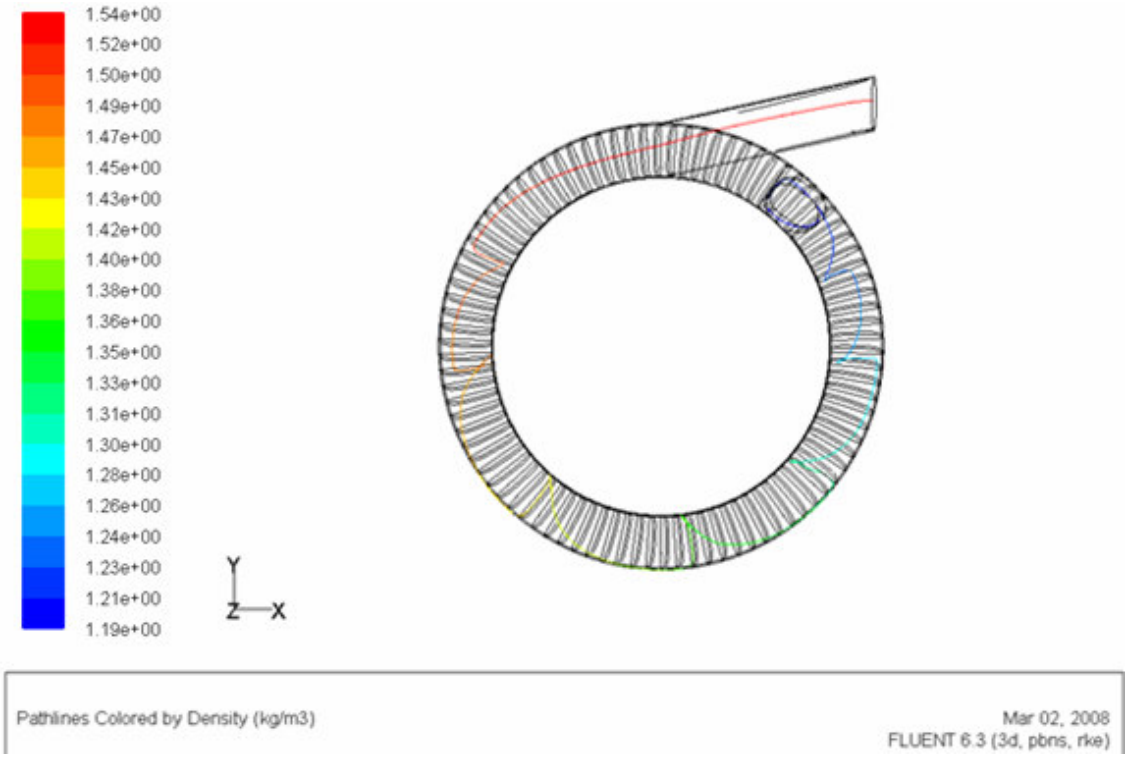

Figure 6.53: Plot of a particle path line from inlet to exit port for Model **RFCSEA-145** (*at starting running speed, 2891 rpm*)

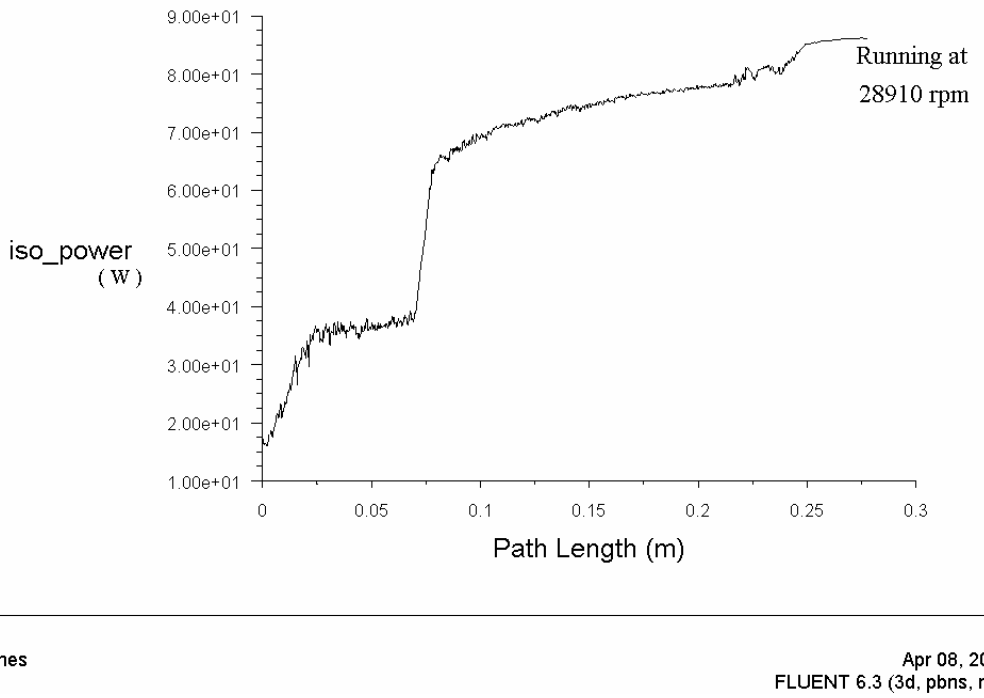

Figure 6.54: Plot of Isothermal power gained by a particle along its path line from inlet to exit port for Model **RFCSEA-145**

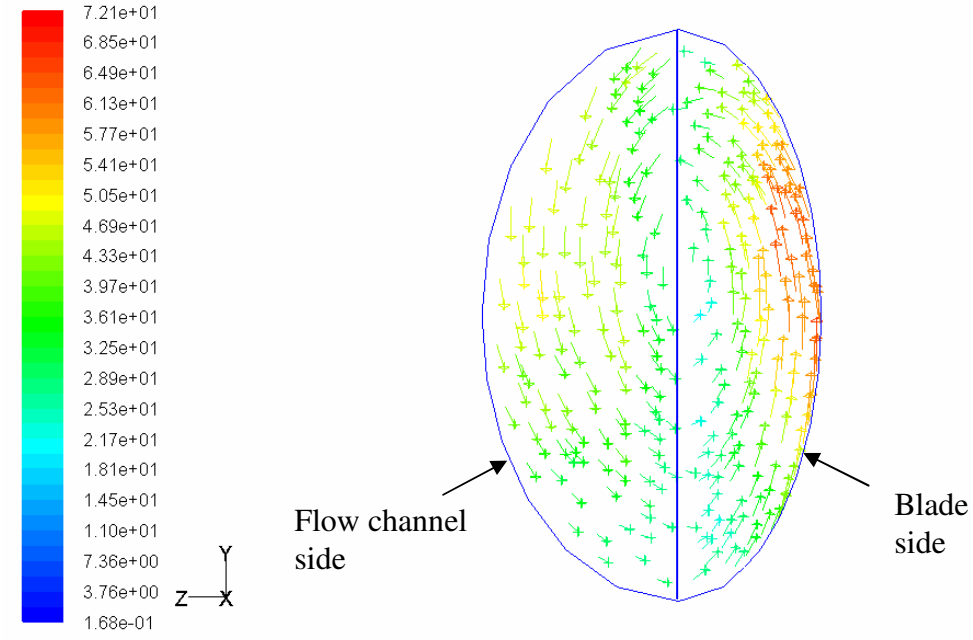

Figure 6.55: Plot of relative velocity vectors on a cross-sectional surface in the flow field for Model **RFCSEA-145**

9. Output results for model RFCNGA-145

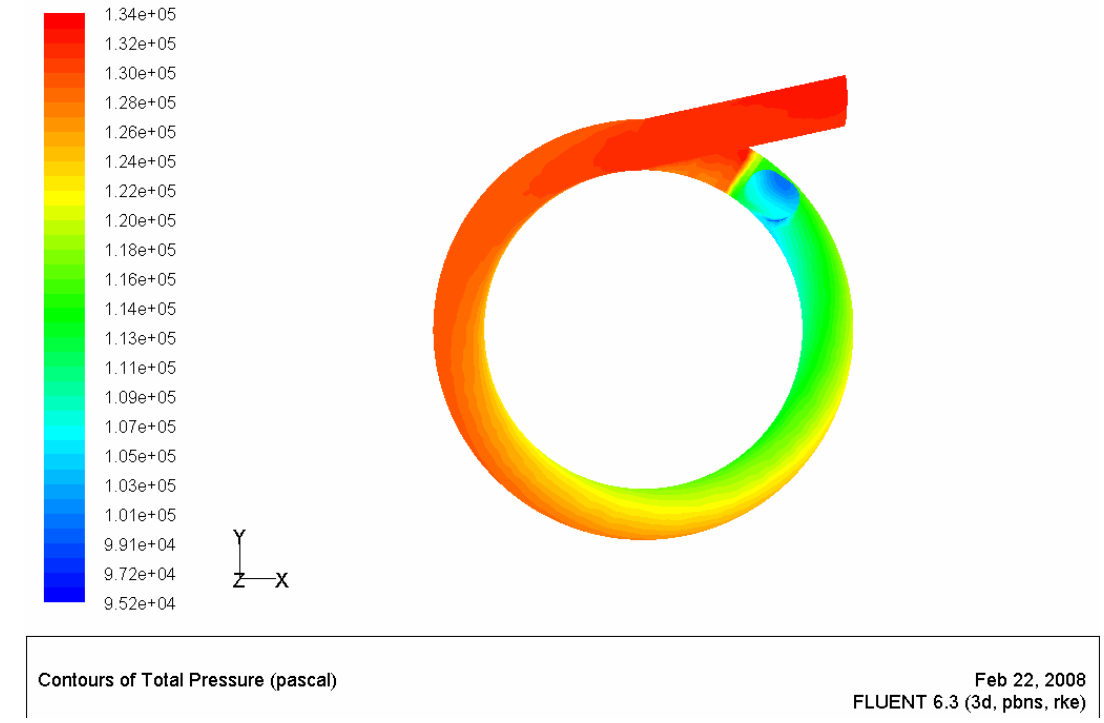

Figure 6.56: Plot of total pressure contours over the entire flow field for Model **RFCNGA-145**

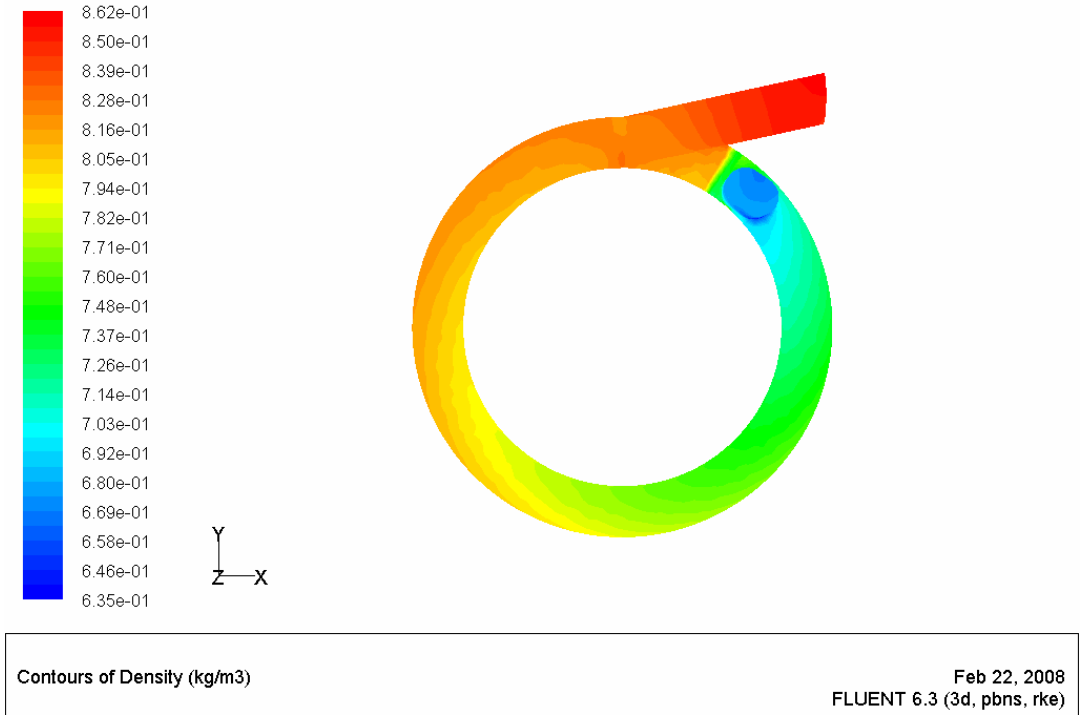

Figure 6.57: Plot of density contours over the entire flow field for Model **RFCNGA-145**

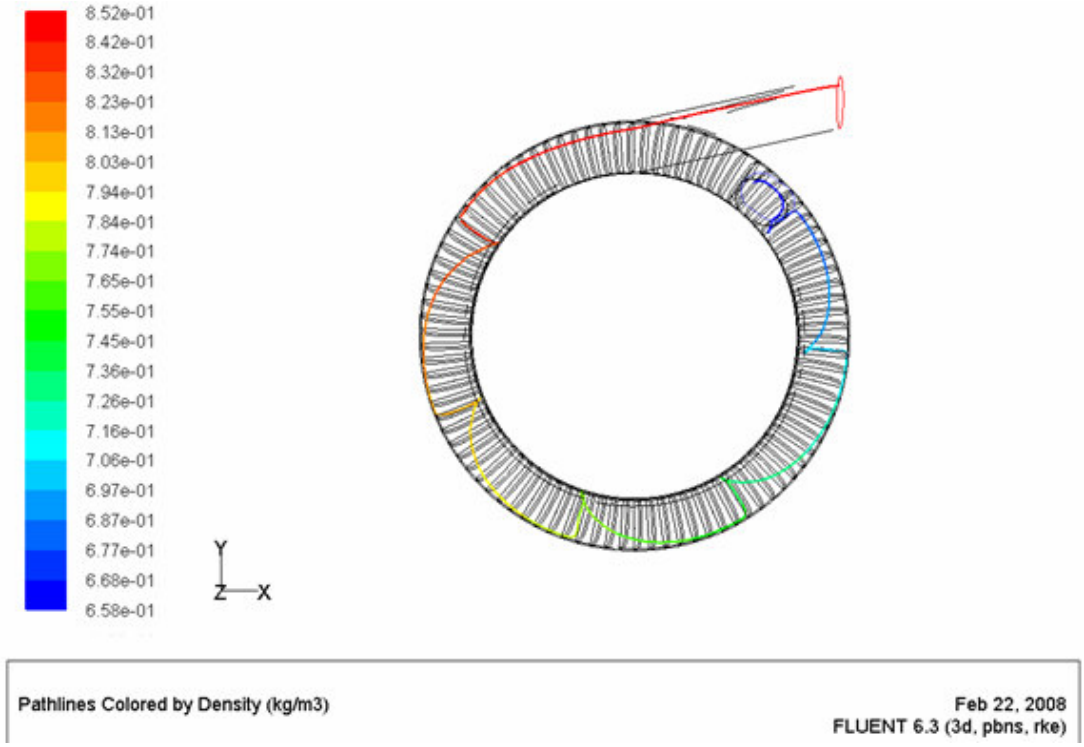

Figure 6.58: Plot of a particle path line from inlet to exit port for Model **RFCNGA-145** (*at starting running speed, 2891 rpm*)

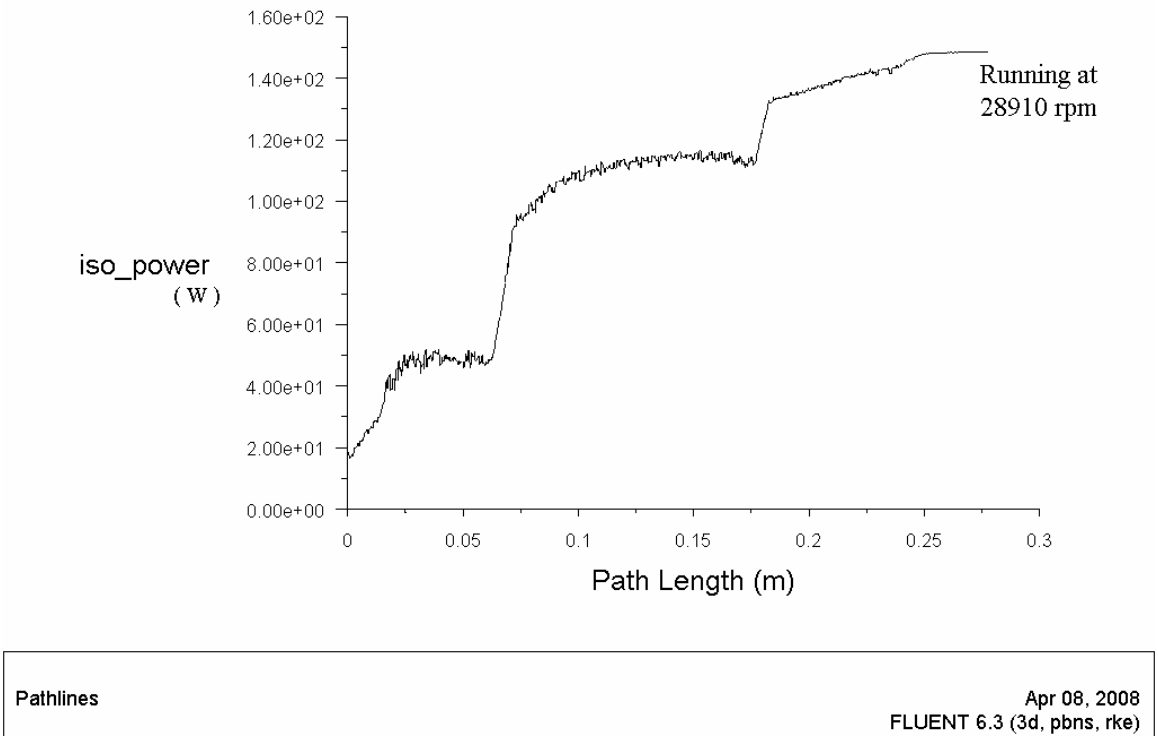

Figure 6.59: Plot of Isothermal power gained by a particle along its path line from inlet to exit port for Model **RFCNGA-145**

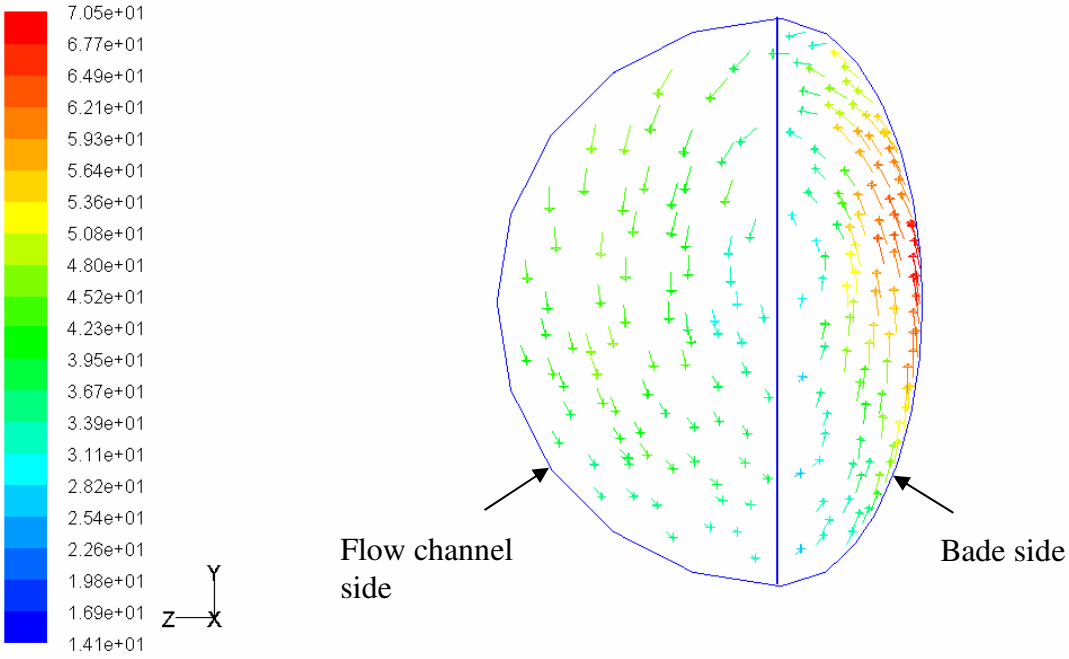

Figure 6.60: Plot of relative velocity vectors on a cross-sectional surface in the flow field for Model **RFCNGA-145**

10. Output results for model RFCCA-145

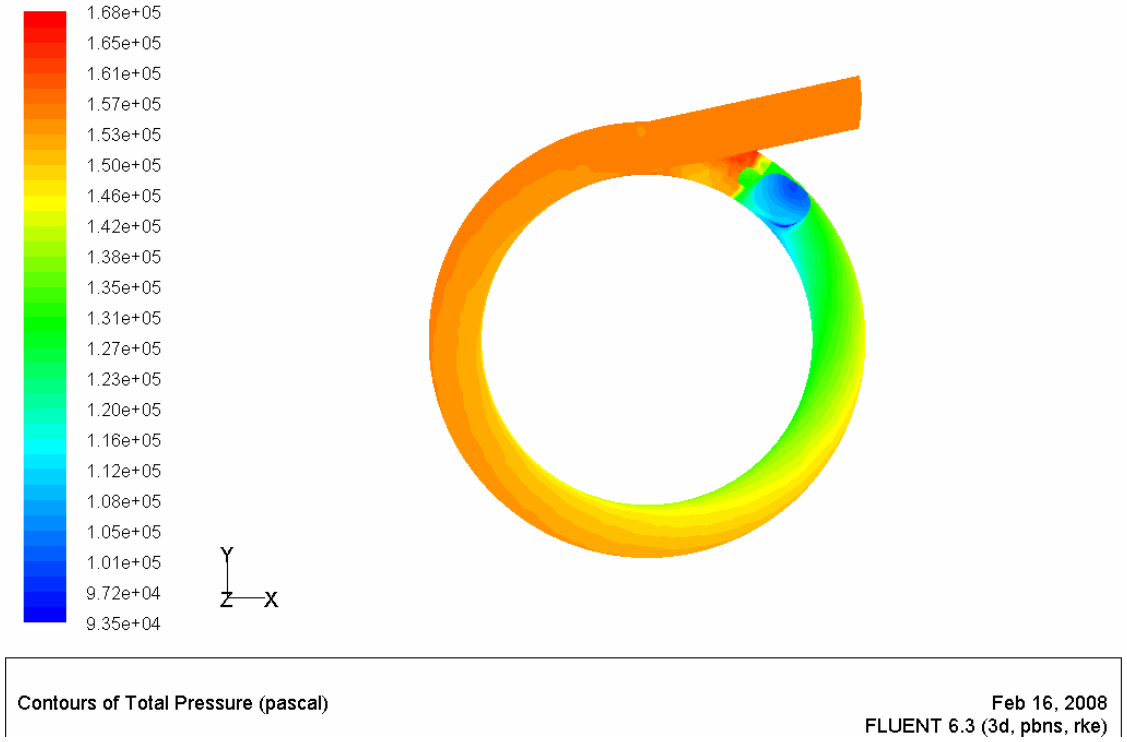

Figure 6.61: Plot of total pressure contours over the entire flow field for Model **RFCCA-145**

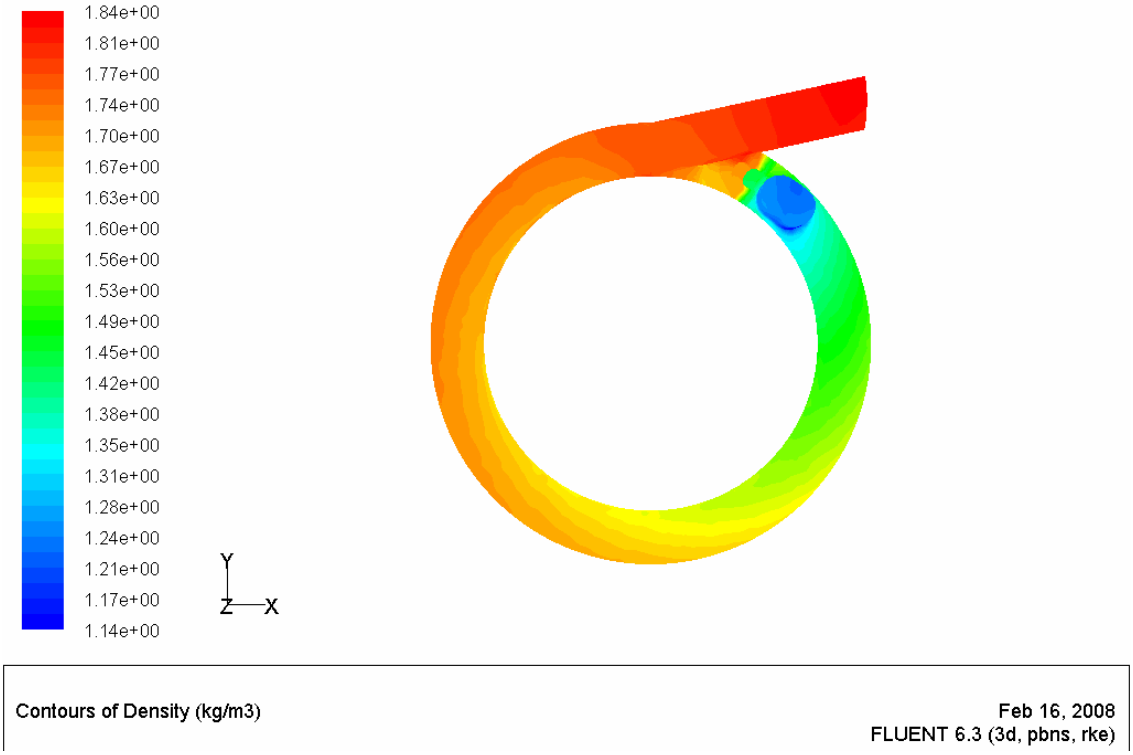

Figure 6.62: Plot of density contours over the entire flow field for Model **RFCCA-145**

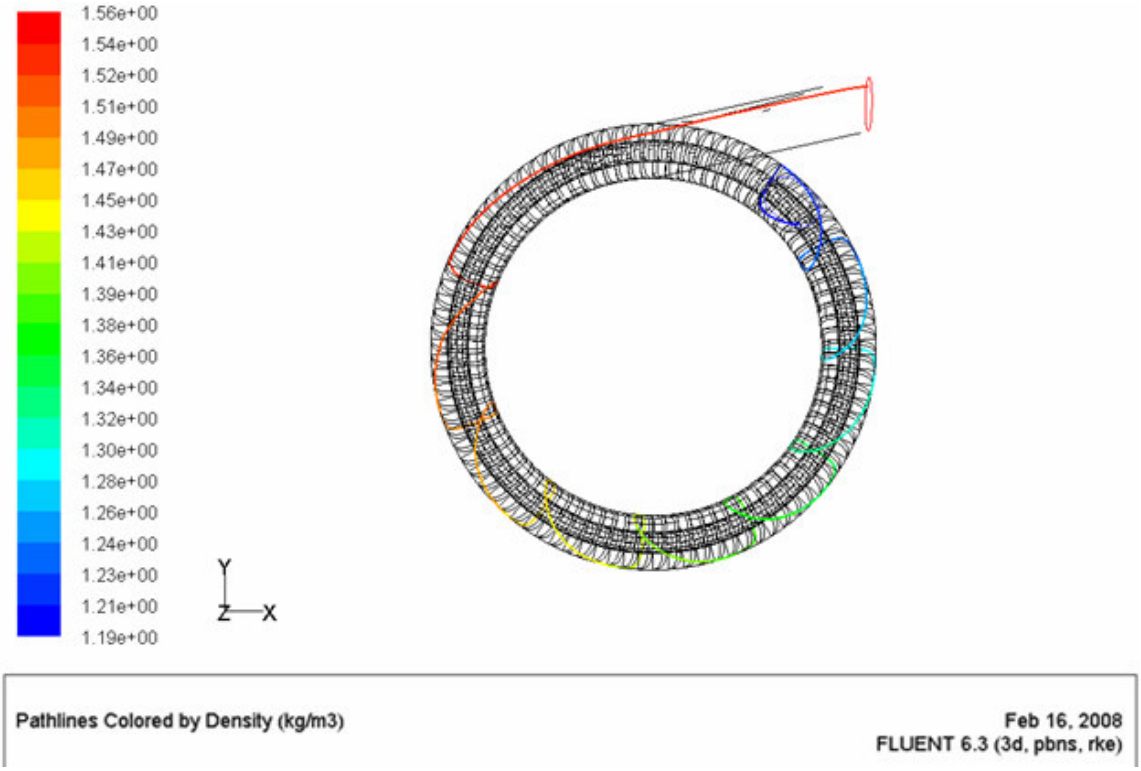

Figure 6.63: Plot of a particle path line from inlet to exit port for Model **RFCCA-145** (*at starting running speed, 2891 rpm*)

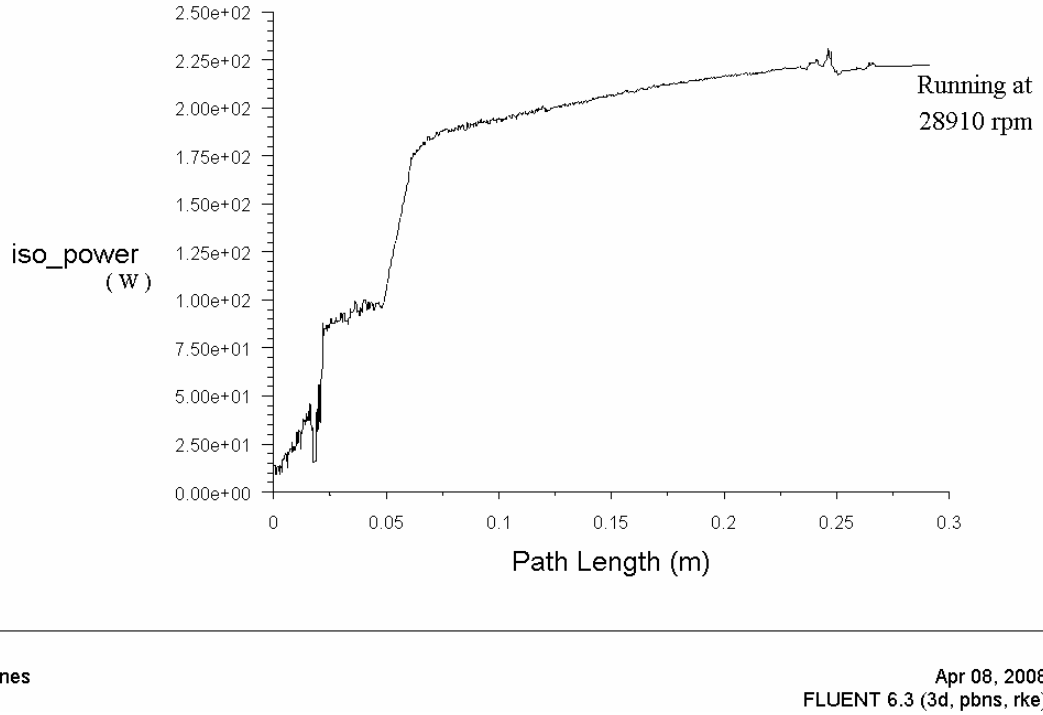

Figure 6.64: Plot of Isothermal power gained by a particle along its path line from inlet to exit port for Model **RFCCA-145**

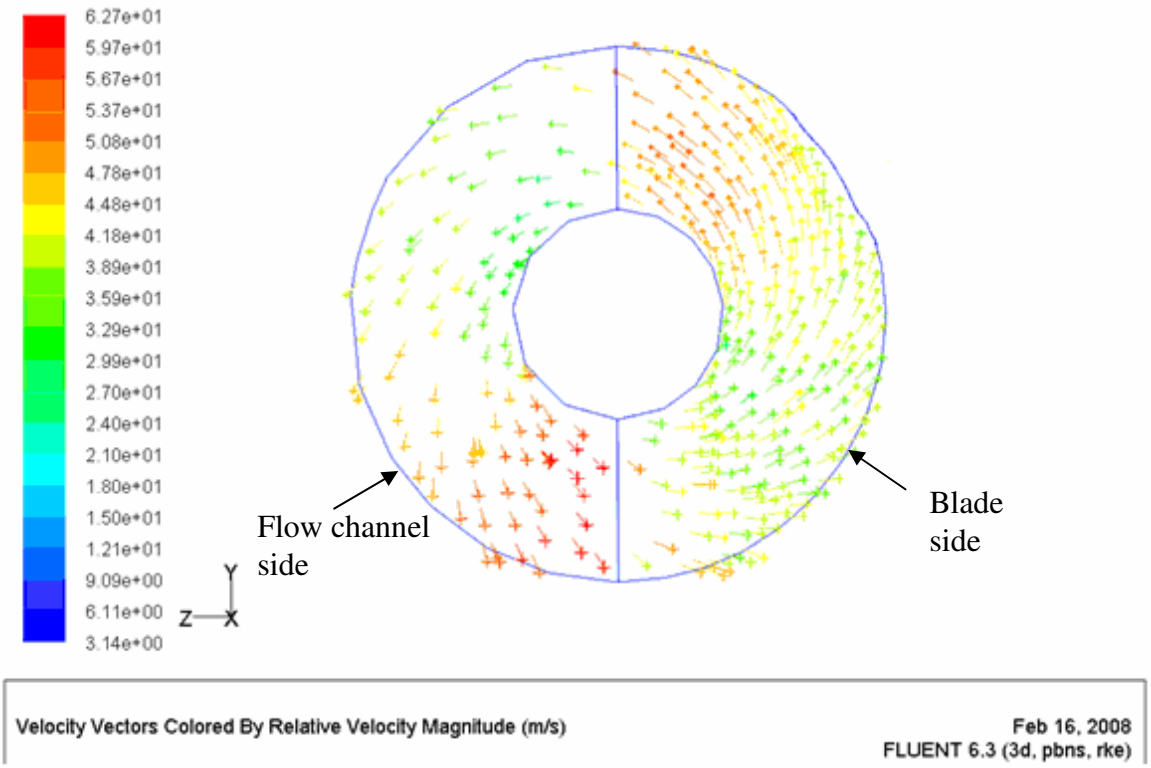

Figure 6.65: Plot of relative velocity vectors on a cross-sectional surface in the flow field for Model **RFCCA-145**

DECLARATION

I hereby declare that the work which is presented in this thesis entitled "**ANALYSIS OF FLUID FLOW AND LOSSES IN REGENERATIVE FLOW COMPRESSORS USING CFD**" is original work of my own, has not been presented for a degree in any other university and that all sources of material used for the thesis have been duly acknowledged.

Kassa Teferi — **Date** May 10, 2008

This is to certify that the above declaration made by the author is correct to the best of my knowledge.

Dr. - Ing Edessa Dribsa
(Thesis Advisor) — **Date** 10/05/2008